TAMPEREEN TEKNILLINEN YLIOPISTO
TAMPERE UNIVERSITY OF TECHNOLOGY

ADEYEMI ADELEKE

ADAPTIVE BACKLASH INVERSE COMPENSATED VIRTUAL DECOMPOSITION CONTROL OF A HYDRAULIC MANIPULATOR WITH BACKLASH NON-LINEARITY

Master of Science Thesis

Examiner: Professor Jouni Mattila
Examiner and topic approved by Faculty Council of the Faculty of Engineering Sciences on 1st March 2017.

ABSTRACT

ADEYEMI ADELEKE: Adaptive Backlash Inverse Compensated Virtual Decomposition Control of a Hydraulic Manipulator with Backlash Nonlinearity
Tampere University of technology
Master of Science Thesis, 75 pages, 19 Appendix pages
March 2017
Master's Degree Programme in Automation Engineering
Major: Fluid Power
Examiner: Professor Jouni Mattila

Keywords: Virtual Decomposition Control, Backlash, Virtual Stability, Adaptive Control, Hydraulic Manipulator, Parameter Adaptation, Rotary Actuator.

Virtual decomposition control is a new non-linear model-based (that is, based on the kinematics and dynamics of rigid bodies) control approach for controlling multiple degrees of freedom robots. It has been successfully applied to control several different hydraulic robots. On the other hand, hydraulic rotary actuators are types of actuator used when high power-to-size ratio and compact space utilization are required. They come in different types; the helical spline type often introduces backlash nonlinearity into control systems because of gear the transmission involved. Therefore, in order to achieve good reference tracking performance and guaranteed stability of systems in which they are applied, their backlash has to be somewhat accounted for by incorporating backlash compensation into their main controller structure.

Thus, the essence of this research was to design a virtual decomposition controller with the capability to reduce or eliminate the effect of backlash in an application where helical type hydraulic rotary actuators is applied and compare the system performance with that obtained by applying the traditional Proportional- Integral- Differential controller.

A general overview of robot control is presented, followed by the definition of basic terms related to virtual decomposition control. Thereafter, hydraulic rotary actuator is described, focusing on the helical gear type. Finally, backlash and its inverse are presented in graphical and mathematical forms to show their characteristics. A combination of the aforementioned concepts was used in the development and implementation of effective control approach for a manipulator actuated by a hydraulic rotary actuator.

Based on recently proposed normalizing performance indicator μ, comparison of the three different controller algorithms presented were made. The results obtained indicated that the designed nonlinear model based controller, without and with backlash compensation significantly outperformed the classical Proportional-Integral-Derivative controller. However, the experimental results show that much work still need to be done in the future to implement parameter adaptation algorithm portion of the control equations.

PREFACE

This thesis has been prepared in partial fulfilment of the requirements for the completion of a Master's degree programme in Automation Engineering at Tampere University of Technology, Finland.

I wish to express my sincere gratitude to God almighty for giving me the opportunity to be at this juncture in my academic career. I also express my appreciation to Professor Jouni Mattila for giving me the opportunity to work on this challenging topic at the laboratory of Automation and Hydraulics of the university; he was indeed helpful as a great Manager that everyone would wish to have. In addition, I recognize the support granted to me by the seating *head of laboratory*- Professor Kalevi Huhtala- before and during the course of this research project.

Furthermore, I want to appreciate the support I received from my colleagues in room K2442B, and later K2305 of the university. Their cooperation was quite essential during the period of conducting this research.

Finally, I deeply appreciate the moral support granted to me by my family during the duration of my studies in a foreign land far away from home. Indeed, your encouragements and pieces of advice were immensely useful in handling many challenges that came along the way.

Tampere, 28.3.2017.

Adeyemi Adeleke

CONTENTS

LIST OF SYMBOLS AND ABBREVIATIONS

Some of the most predominantly used notations in this thesis are defined here.

AUT/ TUT	Laboratory of Automation and Hydraulic, Tampere University of Technology
CT	Continuous-Time
DOF	Degree of Freedom
DT	Discrete-Time
PID	Proportional-Integral-Derivative
TUT	Tampere University of Technology
VDC	Virtual Decomposition Control
VCP	Virtual Cutting Point
VPF	Virtual Power Flow

A_A	Area of actuator chamber A
A_B	Area of actuator chamber B
${}^{\mathbf{A}}\mathbf{R}_{\mathbf{B}} \in \mathbb{R}^{3\times 3}$	Rotation matrix between frame $\{\mathbf{B}\}$ and $\{\mathbf{A}\}$
${}^{\mathbf{B}}\mathbf{F} \in \mathbb{R}^{6}$	Force/ moment vector of frame $\{\mathbf{B}\}$
${}^{\mathbf{B}}\mathbf{F}^{*} \in \mathbb{R}^{6}$	Net force/ moment vector of frame $\{\mathbf{B}\}$
${}^{\mathbf{B}}\mathbf{F}_{\mathrm{r}} \in \mathbb{R}^{6}$	Required force/ moment vector of frame $\{\mathbf{B}\}$
$\{\mathbf{B}\}$	Coordinate system (frame) $\mathbf{B}$
$\mathbf{B}^{\mathrm{T}}$	Transpose of matrix $\mathbf{B}$
$\mathbf{B}^{-1}$	Inverse of matrix $\mathbf{B}$
B	Bulk modulus of hydraulic oil
${}^{\boldsymbol{B_2}}\mathbf{V} \in \mathbb{R}^{6}$	Linear/ angular velocity vector of frame $\{\mathbf{B}\}$
${}^{\mathbf{B_2}}\mathbf{V}_{\mathbf{r}} \in \mathbb{R}^{6}$	Required linear/ angular velocity vector of frame $\{\mathbf{B}\}$
$\mathbf{C_B}(\mathbf{B}_{\omega})\mathbb{R}^{6\times 6}$	Centrifugal and Coriolis terms of rigid body related to frame $\{\mathbf{B}\}$
c_l	Left crossing parameter of backlash model
c_n	Tank side valve flow coefficient
c_p	Pressure side valve flow coefficient
c_r	Right crossing parameter of backlash model
Δp	Pressure differential across orifice
$\varepsilon(x)$	A selective function in terms of x
f_p	Pressure induced actuator force
f_f	Friction force of actuator piston
$\boldsymbol{\theta}_{\mathbf{B}}$	Parameter vector of rigid body associated with frame $\{\mathbf{B}\}$
$\mathbf{G_B} \in \mathbb{R}^{6}$	Vector of gravity terms of rigid bodies related to frame $\{\mathbf{B}\}$
$\mathbf{I_0}(t)$	The moment of inertia matrix around the center of mass
$\mathbf{I_3}\mathbb{R}^{3\times 3}$	An identity matrix of dimension 3×3
$\mathbf{K_B} \in \mathbb{R}^{6\times 6}$	Positive definite gain matrix of rigid body related to frame $\{\mathbf{B}\}$
$\mathrm{K_D}$	PID derivative gain
k_{f_p}	Piston force feedback gain of VDC controller
$\mathrm{K_I}$	PID Integral gain
$\mathrm{K_P}$	PID proportional gain
k_{τ_p}	Piston torque feedback gain of VDC controller
k_x	Position feedback gain of VDC controller

l_0	Effective actuator length
L_p	Lebesgue space
$m > 0$	Slope of backlash model
$\mathbf{M_B} \in \mathbb{R}^{6\times6}$	Mass matrix of rigid body Associated with frame $\{\mathbf{B}\}$
μ	Normalizing performance indicator
$p_{\mathbf{B}}$	Virtual power flow at frame $\{\mathbf{B}\}$
p_r	Return line pressure
p_s	Supply line pressure
p_{B}	Actuator chamber B pressure
Q_A	Flow rate into chamber A of actuator
Q_{B}	Flow rate into chamber B of actuator
T_{c}	Oscillation frequency of critically stable PID controller
$\widehat{\boldsymbol{\theta}}$	Estimate of $\boldsymbol{\theta}$
$\boldsymbol{\theta}_v \in \mathbb{R}^4$	Parameter vector of servo valve control equation
θ_b^*	Backlash Parameter vector
θ_b	Estimate of backlash parameter vector
u	Servo valve control voltage
u_f	Servo valve control term
u_1	Gear ratio between piston and the ring (housing)
u_2	Gear ratio between shaft and the piston
u_d	Signal to achieve control objective in the absence of backlash
$\mathcal{V}(x)$	Pressure differential related function in terms of x
$v(t)$	Non-negative accompanying function of VDC
ω	Angular velocity of manipulator
$\omega_b(t)$	Backlash regressor
$\chi\,[Y]$	Indicator function for backlash model
$\mathbf{Y_B} \in \mathbb{R}^{6\times13}$	Regressor matrix of rigid body related to frame $\{\mathbf{B}\}$
$\mathbf{Y}_v \in \mathbb{R}^{1\times4}$	Regressor matrix of servo valve control equation
$\mathbf{Y}_f \in \mathbb{R}^{1\times7}$	Regressor matrix of friction model
$\dot{}$	The derivative operator
$\int$	The integral operator

1. INTRODUCTION

Control systems are very important to robots. Hence, their selection and implementation from a constantly increasing number of available control approaches require special considerations. The Virtual Decomposition Control (VDC) is a relatively new control approach designed especially for controlling multiple degrees of freedom (DOF) robots. It permits the independent control of a subsystem from an entire system (for example, the hydraulic actuator may be independently controlled from an entire robotic system), provided *virtual stability* (a concept to be defined in subsequent chapter) is ensured. VDC has been successfully applied to control hydraulic robots, just as it has recorded significant success in controlling other types of non-hydraulic robotic systems (Zhu et al. 1998; Zhu and De Schutter 1999; Zhu and De Schutter 2002, Zhu et al. 2013). (Zhu 2010.)

Hydraulic rotary actuators represent a class of actuator used when high power-to-size ratio and compact space utilization are important, and this makes them gain application in modern robotics systems. They come in different types, and they require less space compared to hydraulic cylinders in applications. The helical spline type often introduces backlash nonlinearity into control systems because of the presence of gear connections. This backlash, being a nonlinearity that it is, has to be somewhat suitably eliminated in order to achieve good reference tracking performance, and thus, requires special types of control approach such as the adaptive backlash inverse control presented in (Tao and Kokotovic 1996). Thus, in addition to the traditional heavy nonlinearities associated with hydraulic systems controlled by an electrohydraulic valve (Alleyne and Liu 1999; Edge 1997; Yao et al. 2001), the challenges involved in the control of systems actuated by hydraulic rotary actuator include backlash characteristic.

The most applied control scheme for industrial robots is built around the joint Proportional-Integral-Derivative (PID) servo control. It employs the inverse kinematics of the robot to convert end-effector position into the desired joint positions, before finally applying the PID to control the joint positions. The PID controller is however only capable of controlling regulation tasks. That is, tasks demanding precision only at the steady state. For other tasks that require dynamic accuracies and involving nonlinearities (such as backlash), the capability of the PID becomes clearly insufficient to provide good tracking accuracies. Thus, this scenario places considerable limitations on the applicability of the PID control algorithm. Zhu (2010) gives a detail explanation of this approach and its challenges.

To improve on the performance of the joint PID controller, other control approaches in common use include a combination of a dynamics based feedforward term with the normal PID feedback control (this is simply referred to as the *dynamics based control*) as illustrated in Figure 1.1. P(s) is the controlled plant, C(s) is the feedback compensator and F(s) is the feedforward controller. The feedforward term essentially improves control accuracies, while the PID feedback part ensures good disturbance rejection, deals with the transition problems and maintains stability. The benefit of this scheme is that it is possible to achieve infinite bandwidth with it; so far proper feedforward control is constructed. This implies that accurate execution of some dynamically involving tasks as well as the fast executions of tasks earlier performed slowly by PID-controlled robots becomes possible with the use of dynamics based control. Thus, based on these benefits of the dynamics based control architecture, the original theory of VDC relies on the control structure presented in Figure 1.1. (Zhu 2010).

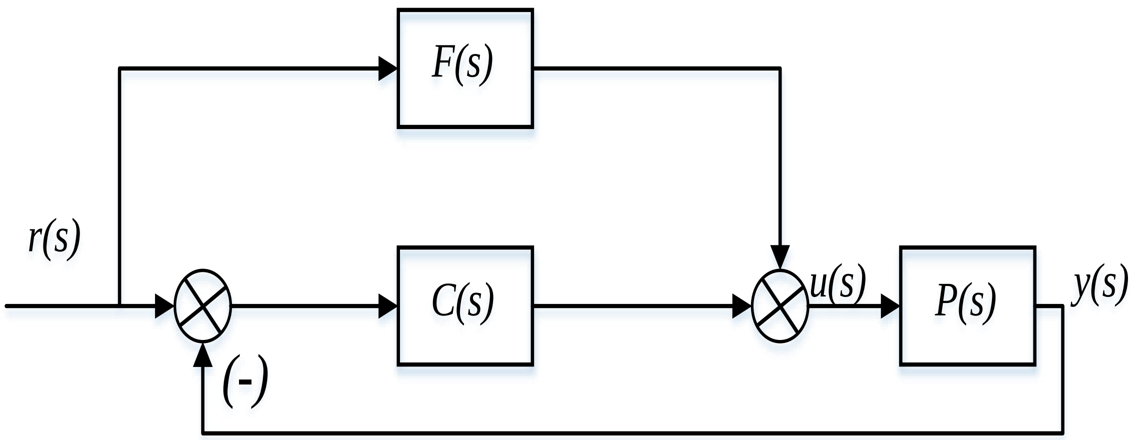

Figure 1.1. *Dynamics based feedforward and PID feedback control system.*

As stated earlier, the VDC is a subsystems dynamics based control approach, which is an efficient and powerful tool for conducting full-dynamics-based control. It greatly simplifies the complexity of robotics control to that of the subsystem dynamics. However, no studies have hitherto been conducted to incorporate backlash control into the VDC algorithm, as it is required when the virtual decomposition control of a robotic manipulator employing a helical type hydraulic rotary actuator is performed.

1.1 Objectives

Thus, the objectives of this thesis shall be to:

i) Design a VDC controller for a hydraulic manipulator actuated by helical type hydraulic rotary actuator.

ii) Incorporate the adaptive backlash inverse control algorithm into that of the VDC.

iii) Mathematically establish the stability of the entire robotic system under the designed control algorithm.

iv) Conduct experiment(s) to show the possibility to implement the resulting control algorithm and compare the control performance with that of the conventional PID controller under idem conditions.

1.2 Scope

The scope of this work is to apply VDC approach to the control of a hydraulic manipulator shown in Figure 1.2 (and discussed subsequently). As existing literature reveal, this task has never been previously conducted. In addition, due to the presence of backlash nonlinearity in the target system, application of VDC to this kind of system offers an opportunity to extend the scope of the VDC theory itself (that is, to cover a case where backlash nonlinearity exists in a system). In view of the extent of a master's degree thesis, although parameter adaptation laws are included in the control law design, the VDC parameter adaptation law was not included in the experimentations performed and presented in Chapter 4, but has been left for future studies. The target system is discussed below.

1.3 Target System

The target system of this thesis is a hydraulic manipulator shown in the Figure 1.2. It consists of a vertical frame, which rigidly supports a hydraulic rotary actuator from its base in a horizontal position. To the output shaft of the horizontally suspended actuator is then attached a vertically hanging lever arm, which has an adjustable inertia load coupled to its free end. The lever arm weighs 18.45 kg, and a total of 147 kg (that is, 6×24.5 kg) external inertial load was rigidly bolted to its free end throughout the experimentation phase of this research. The assembly is installed in the heavy machinery laboratory of Automation and Hydraulics Engineering Unit of Tampere University of Technology (AUT/ TUT).

The hydraulic rotary actuator is Eckart E3.150-360°/ M type with maximum operating pressure and maximum output torque of 210 bar and 2500 Nm, respectively. It has the capacity to rotate through 360° and weighs 57.675 kg.

1.4 Structure of the Thesis

The thesis has five chapters. The remaining chapters are arranged in the following order. Chapter 2 delves into existing literature, to review the foundational mathematical concepts required for presents the virtual decomposition of the target system, presenting the kinematics and dynamics, as well as the control equations. In addition, the virtual stability of the system, in the absence of backlash as well as in view of the presence of backlash, is proven.

Chapter 4 presents the experimental set-up used in the implementation of the developed controller. Furthermore, the results obtained by driving the manipulator with PID controller is compared with those obtained by applying VDC with and without backlash incorporation, respectively. In addition, the chapter discusses and analyses the obtained results and makes appropriate inferences. The last chapter makes conclusion on the study and presents recommendations for future work.

There are four appendages. Appendix A contains the rigid body regressor matrix and parameter vector, Appendix B presents the used parameter vectors of the studied system. Appendix C gives some of the measured signals when the manipulator was controlled with PID and VDC controllers, respectively. Finally, The fourth appendix, D, contains the C- code used in implementing the backlash compensation in Simulink and dSpace simulation environments.

Figure 1.2. *Target system.*

2. LITERATURE SURVEY

This chapter presents, in general terms, an overview of robot control and associated challenges, followed by a description of hydraulic rotary actuators and a review of the most important mathematical concepts and tools to be used throughout the work. The mathematical concepts are essential for formulating and establishing the VDC objectives and proving virtual stability, as well as for the description of backlash non-linearity and its inverse as multi-region functions.

Therefore, spaces and coordinate systems are presented, followed by an introduction of vectors and their orientation by using orientation matrix. Subsequently, linear/ angular velocity and force/ moment vectors expressed in body-frames are defined without omitting their duality. These led to the development of rigid body dynamics and their linear parameterization. Thereafter, the concept of *virtual cutting points (VCP)* - a key idea to the VDC approach- and *oriented graphs* are presented. Finally, virtual stability concept is explored, and backlash non-linearity and its inverse are described.

2.1 Summary of Robot Control

Control systems are important in robotics. They are used to achieve desired trajectory, obtain satisfactory accuracy, and optimize performance potentials of robots, subject to robustness requirements.

The joint Proportional-Integral-Derivative (PID) servo controller is the most commonly applied industrial robot controller. It is based on the inverse kinematics of robot systems. According to Zhu, it is easy to implement and have good steady state characteristics, but its dynamic behaviours are generally unsatisfactory. Thus, they are limited to some categories of applications, which require only static accuracies. (Zhu 2010.)

The other control approaches used in robotics include the dynamics based control (a combination of dynamics based feedforward and PID feedback control), nonlinear feedback linearization, model based adaptive control etc. In Contrast to pure PID controller, the dynamics based control method is appropriate for extremely coupled nonlinear systems typical in robotics. This is possible because they are capable of achieving significant bandwidth control without depending on feedback multipliers. The VDC approach, which is the core concept of this work, is based on this control approach. (Slotine and Li 1991; Zhu 2010, p.7.)

Furthermore, nonlinear feedback linearization control technique has been widely accepted in the discipline of robotics control, as can be deduced from the works of An et al. (1988)**,** Bonitz and Hsia (1994), Spong and Vidyasagar (1987), and Yoshikawa (1990). It relies on the use of special feedbacks that perfectly neutralize nonlinearities in a system, so that the resulting linearized system may be controlled by conventional PID scheme. According to Zhu, the limitations of this approach include requirement of precise models, availability of some state variables, and limited region of applicability. In addition, early form of model-based adaptive control introduced by Slotine and Li for robotic system comprises feedforward and feedback parts, comparable to the dynamics-based control Slotine and Li (1987, 1988). However, unlike the case in nonlinear feedback linearization techniques, there is no need for the mass matrix inverse, a feature which allows the implementation of a direct adaptive control that results in asymptotic motion stability with convergent parameter error. (Zhu 2010; Slotine and Li 1991.)

2.1.1 Practical Issues in Control of Compound Robots

In the development of concepts and simulations found in existing literature on robot control, only systems with two or three DOF are typically used as illustrations **(**An et al. 1988; Canudas de Wit 1996; Gorineysky et al. 1997**)**. Moreover, the control designs are based on overall dynamic models of the robots. However, significant practical difficulties ensue when the DOF number exceeds six, since the computational burden of robot dynamics is directly relational to the fourth exponent of the number of DOF. These difficulties become almost insurmountable, that the application of dynamics based control on a sole processor appears impossible when the DOF is 30 or more. (Zhu, 2010.)

Therefore, an efficient and powerful control approach called *Virtual Decomposition Control- VDC-* has been recently developed to handle such difficulties encountered in the complete dynamics-based control of complex robots. The basic approach in VDC is to develop control of multipart robots directly on subsystems dynamics (while maintaining the L_2 and L_∞ stability and convergence of the whole system), instead of on the complete system dynamics. This is possible because the dynamics of robotic subsystems remain comparatively simple and static in structure regardless of the complexity of the entire robot. Thus, after the subsystem dynamics based control has been achieved for a complex robot, the remaining concerns reduce to addressing interactions among the subsystems. (Zhu 2010.)

2.2 Hydraulic Rotary Actuator

According to Atkins and Escudier, ‘‘Rotary hydraulic actuator is a device that converts hydraulic power into rotational mechanical power’’. It is a portable device for generating torque from hydrostatic pressure. It is a self-contained component, which may provide partial revolution or complete (360°) revolution of an inertia load, and it can generate oscillating motion in addition to large, constant torque. (Atkins and Escudier 2013.) Hydraulic rotary actuators find usual application in rotational applications found in aircraft, machine tools, robots and manipulators, heavy machinery, etc. (Yao et al. 2014). They come in different types as discussed next.

2.2.1 Types of Hydraulic Rotary Actuator

There are three common types (vane, rack and pinion, and helical spline) of design, each with its own strengths and drawbacks. The helical design type used on the studied manipulator in this thesis essentially consists of a piston sleeve, that works in a similar manner to a cylinder piston (but with additional rotational motion), and a revolving output shaft enclosed in a cylinder-like housing (Figure 2.1).

The output shaft obtains its rotary motion from the linear motion of the piston sleeve effected through a male helix cut on the shaft, and a fixed helical ring attached to the cylinder housing. The output torque of the shaft is proportionate to the twist angle, operating pressure, piston area, and the mean pitch radius of the shaft (Parker, 2015).

The helical type designs are generally preferred for their compactness, while double helical designs, which help in reducing the overall unit length or double the output torque, are also available. However, they are generally the costliest. The helical gear type actuators have inherent backlash and can be made as self-locking type with distinctive spline construction. They are available from 2.3 to 450 kN-m of torque and are generally leakage-free because of their effective sealing. (Parker, 2015.)

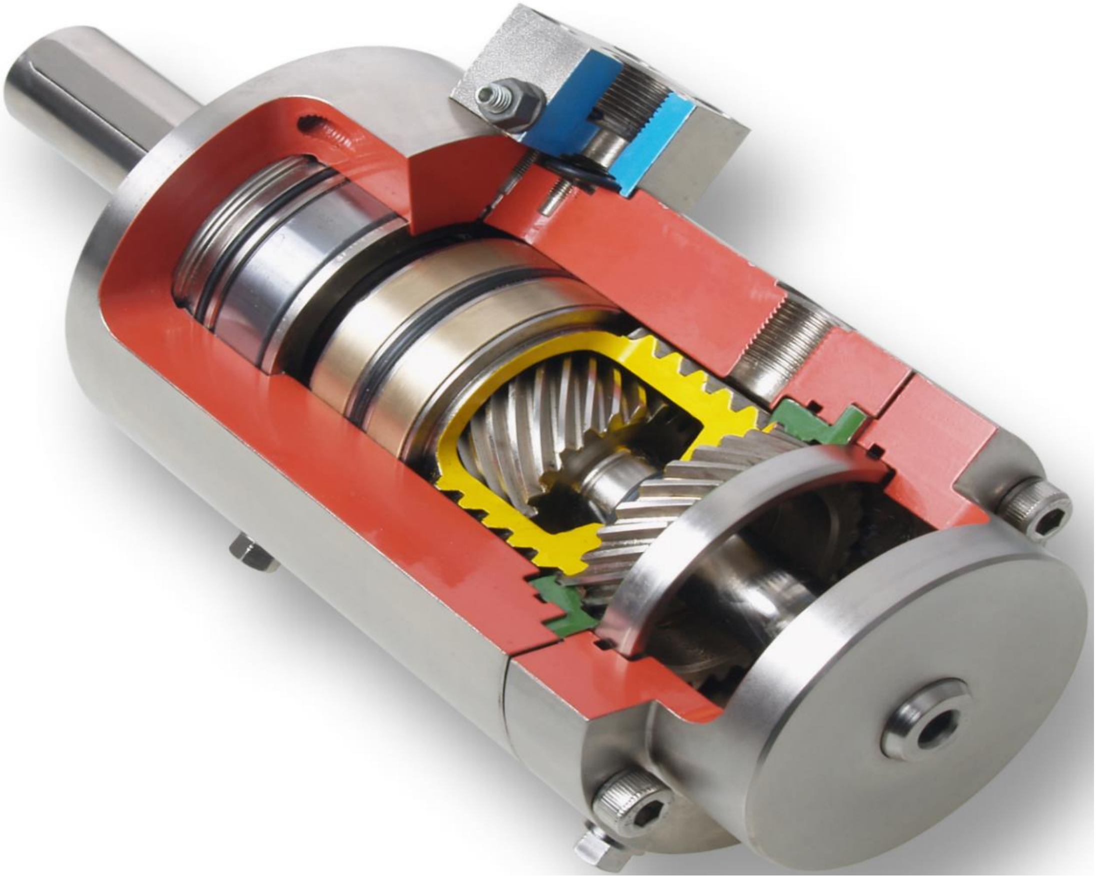

Figure 2.1. *Helical type hydraulic rotary actuator. Source: icfluid.com*

2.3 Frames and Orientation Expressions

In a simplified form, coordinate systems applied in this Master's degree thesis are referred to as frames. The frames are generated by using three mutually orthogonal three-dimensional unit vectors as bases. Example of such frames can be written as $\{\mathbf{A}\} = [\overrightarrow{\boldsymbol{a}_x}, \overrightarrow{\boldsymbol{a}_y}, \overrightarrow{\boldsymbol{a}_z}]$. (Zhu 2010, p.24).

In consideration of the fact that different frames used in kinematics and dynamics of bodies require different orientations for convenience, there arises the need to rotate one frame into the other, and likewise some frame into the inertia frame. Therefore, for this purpose, rotation matrices are utilized for transforming a physical vector expressed in one frame into another frame. In line with the rotation matrix that rotates a frame $\{\mathbf{B}\} = [\overrightarrow{\boldsymbol{b}_x}, \overrightarrow{\boldsymbol{b}_y}, \overrightarrow{\boldsymbol{b}_z}]$ about the $\overrightarrow{\boldsymbol{b}_z}$ axis so that the frame $\{\boldsymbol{B}\}$ coincides with the frame $\{\mathbf{A}\}$ is generally represented, according to (Jazar 2010; Sciavicco 2001, p.23) as

$$ {}^{\mathbf{A}}\mathbf{R}_{\mathbf{B}} = \begin{bmatrix} c(\theta) & -s(\theta) & 0 \\ s(\theta) & \mathrm{c}(\theta) & 0 \\ 0 & 0 & 1 \end{bmatrix} \tag{2.1} $$

The c and s represent cosine and sine functions, respectively, while θ represents the angle between the respective third bases of frames $\{\mathbf{A}\}$ and $\{\mathbf{B}\}$, and through which the latter frame is rotated in order to take the orientation of the former.

2.4. Spaces and Groups

Here, definitions are given for Euclidean n-space, the special orthogonal group, the special Euclidean groups, and the Lebesgue space according to Zhu (2010), Royden (1988), and Craig (1986).

Definition 1. *Euclidean n-space refers to the space of all n-tuples of real numbers, depicted as* $\in \mathbb{R}^n$, *such that* $\boldsymbol{x} = [x_1, x_2, \dots, x_n]^T \in \mathbb{R}^n$. *The Euclidean norm, denoted as* $||\boldsymbol{x}||$, *is defined as* $\left||\boldsymbol{x}|\right| = \sqrt{\sum_1^n x_i^2}$.

Definition 2.1. *Special orthogonal group of degree 3, depicted as* ***SO** (3), is the group of 3×3 orthogonal matrices. They are used in proving some Lemmas and Theorems throughout the thesis.*

Definition 2.2. *The special Euclidean group is denoted as* ***SE** (3), it is the group of 4×4 matrices obtained from a* $\boldsymbol{SO}(\mathbf{3}) \in \mathbb{R}^{3\times3}$ *and* $\mathbb{R}^3$ *in the form:*

$$ \begin{bmatrix} \mathbf{R} & \mathbf{v} \\ 0 & 1 \end{bmatrix} \epsilon\, \mathbb{R}^{4\times4} \tag{2.2} $$

with $\mathbb{R} \in \mathbf{SO}(\mathbf{3}) \cap \mathbb{R}^{3\times3}$, and $\mathbf{v} \in \mathbb{R}^3$. Space $\mathbf{SE}(\mathbf{3})$ is homomorphic to $\mathbb{R}^{\mathbf{3}} \times \mathbf{SO}(\mathbf{3})$.

Definition 2.3. *Lebesgue Space, denoted as* L_p, *p being a positive integer, is a set of all measurable and integrable functions f (t) subject to equation (2.3)*

$$ \left||f|\right|p \;= \lim_{T\to\infty} \left[\int_0^T |f(t)|^p d\tau\right]^{\frac{1}{p}} < +\infty \tag{2.3} $$

Two specific cases where *p = 2 and* ∞ are of general interest in the development of VDC.

(a) A Lebesgue measurable function *f* (*t*) belongs to L_2 if and only if

$$\lim T \to \infty \ \int_0^T | f(t)|^2 \ d\tau < +\infty. \tag{2.4}$$

(b) A Lebesgue measurable function $f(t)$ belongs to L_∞ if and only if

$$\max_{\mathrm{t}} \in [0, \infty)] \mid \mathrm{f}(\mathrm{t}) \mid < +\infty. \tag{2.5}$$

Definition 2.4. *A vectored Lebesgue measurable function*

$f(t) = [f_1(t), f_2(t), \dots f_n(t)]^T \in L_p, p = 1,2, \dots, \infty, implies\ f_i(t) \in L_p for\ all\ i \in \{1, n\}.$

2.5 Linear/ Angular Velocity and Force/ Moment Vectors

For an arbitrary frame $\{\mathbf{A}\}$, if $\vec{\mathbf{f}}_{\mathbf{A}}\ and\ \overrightarrow{\boldsymbol{m}}_{\boldsymbol{A}}$, are force and moment applied to the origin of $\{\boldsymbol{A}\}$, and if $\vec{\mathbf{v}}_{\mathbf{A}}\ and\ \overrightarrow{\boldsymbol{\omega}}_{\mathbf{A}}$ are two vectors representing the linear and angular velocities of $\{\boldsymbol{A}\}$, reference to the inertial frame $\{\mathbf{I}\}$, then

$$\vec{\mathbf{v}}_{\mathbf{A}} = \{\mathbf{I}\}\ {}^{\mathbf{I}}\mathbf{V}_{\mathbf{A}} = \{\mathbf{A}\}\,{}^{\mathbf{A}}\mathbf{V}_{\mathbf{B}} \tag{2.6}$$

or

$${}^{\mathbf{A}}\mathbf{V}_{\mathbf{A}} = {}^{\mathbf{A}}\mathbf{R}_{\mathbf{I}}\ {}^{\mathbf{I}}\mathbf{V}_{\mathbf{A}} \tag{2.7}$$

where ${}^{A}\boldsymbol{R}_{I} = {}^{\mathbf{I}}\mathbf{R}_{\mathbf{A}}^{-1} = {}^{\mathbf{I}}\mathbf{R}_{\mathbf{A}}^{\mathbf{T}}$

Then, the following expression may be written: $\vec{\mathbf{v}}_{\mathbf{A}} = \{\mathbf{A}\}\,{}^{\mathbf{A}}\mathbf{V}, \overrightarrow{\boldsymbol{\omega}}_{\mathbf{A}} = \{\mathbf{A}\}^{A\omega}, \vec{\mathbf{f}}_{\mathbf{A}} = \{\mathbf{A}\}\,{}^{A}\boldsymbol{f},\ \overrightarrow{\mathbf{m}}_{\mathbf{A}} = \{\mathbf{A}\}\,{}^{A}\boldsymbol{m}$.

These expressions allow writing velocities in body frames rather than in inertia frame. Although that does not simplify the kinematics, but the dynamics becomes more efficient because the inertial matrix of a rigid body becomes independent of time and symmetric positive-definite. (Zhu 2010.)

For convenience in VDC approach, the linear/ angular velocity vector of frame $\{\mathbf{A}\}$ expressed in frame $\{\boldsymbol{A}\}$ is defined as

$${}^{A}\mathbf{V} \stackrel{\text{def}}{=} \begin{bmatrix} {}^{\mathbf{A}}\mathbf{V} \\ {}^{\mathbf{A}}\boldsymbol{\omega} \end{bmatrix} \epsilon\ \mathbb{R}^6. \tag{2.8}$$

This is often used together with force/ moment vector in the computation of *virtual power flow* (VPF) - a concept that is discussed later on- in a rigid body.

Likewise, the force/ moment vectors transmitted in a frame, say $\{\mathbf{A}\}$, can be simply expressed in frame $\{\mathbf{A}\}$ as

$$ {}^{\mathbf{A}}\mathbf{F} \stackrel{\text{def}}{=} \begin{bmatrix} {}^{\mathbf{A}}\boldsymbol{f} \\ {}^{\mathbf{A}}\boldsymbol{m} \end{bmatrix} \epsilon\, \mathbb{R}^{6}. \tag{2.9} $$

As discussed above, this is also useful in the calculation of the virtual power flow in a rigid body whose origin is subjected to these vectors.

2.6 Duality: Linear/ Angular Velocity and Force/ Moment Vectors

For two frames, $\{\mathbf{A}\}$ and $\{\mathbf{B}\}$, attached to a common freely moving rigid body under a duo of physical force and moment vectors, these relations subsist

$$ {}^{\mathbf{B}}\mathbf{V} = {}^{\mathbf{A}}\mathbf{U}_{\mathbf{B}}^{\mathbf{T}}\; {}^{\mathbf{B}}\mathbf{V} \tag{2.10} $$

$$ {}^{\mathbf{A}}\mathbf{F} = {}^{\mathbf{A}}\mathbf{U}_{\mathbf{B}}\; {}^{\mathbf{B}}\mathbf{F} \tag{2.11} $$

where the term ${}^{\boldsymbol{A}}\boldsymbol{U}_{\boldsymbol{B}}$ denote the *constant* force transformation matrix that transforms the force moment vector measured and expressed in frame $\{\mathbf{B}\}$ to its exact equivalence in frame $\{\mathbf{A}\}$. ${}^{\boldsymbol{A}}\boldsymbol{U}_{\boldsymbol{B}}$ is defined as

$$ {}^{\mathbf{A}}\mathbf{U}_{\mathbf{B}} = \begin{bmatrix} {}^{\mathbf{A}}\mathbf{R}_{\mathbf{B}} & \mathbf{0}_{3\times 3} \\ (\mathbf{A}_{\mathbf{r}_{\mathbf{AB}}} \times)\; {}^{\mathbf{A}}\mathbf{R}_{\mathbf{B}} & {}^{\mathbf{A}}\mathbf{R}_{\mathbf{B}} \end{bmatrix} \epsilon\, \mathbb{R}^{6\times 6} \tag{2.12} $$

${}^{\mathbf{A}}\mathbf{R}_{\mathbf{B}} \epsilon\, \mathbb{R}^{3}$ represents a vector directed from the base of $\{\mathbf{A}\}$ to that of $\{\mathbf{B}\}$, and expressed in $\{\mathbf{A}\}$.

The above expressions present the duality between linear/ angular velocities and the force/ moment transformations. It should be noted that this is valid only for a pair of exactly equivalent forces/ moment vectors ${}^{\mathbf{A}}\mathbf{F}$ and ${}^{\mathbf{B}}\mathbf{F}$ measured and expressed in $\{\mathbf{A}\}$ and $\{\boldsymbol{B}\}$ respectively. (Zhu 2010.)

2.7 Rigid Body Dynamics in Body Attached Frames

This section presents the net force and moment vectors acting on a rigid body, followed by the derivation of rigid body dynamics expressed in a body frame. In conclusion, the linear parameterization used later in developing parameter adaptation theory is introduced.

2.7.1 Resultant Forces and Moments

Let frame $\{\mathbf{A}\}$ be attached to a rigid body. The resultant (summation or simply *net*) force and moment vectors applied to the rigid body are given as:

$$\overrightarrow{\mathbf{f}^*}_{\mathbf{A}} \stackrel{\text{def}}{=} \{\mathbf{A}\}\,{}^{\mathbf{A}}\mathbf{f}^* \tag{2.13}$$

$$\overrightarrow{\mathbf{m}^*}_{\mathbf{A}} \stackrel{\text{def}}{=} \{\mathbf{A}\}\,{}^{\mathbf{A}}\mathbf{m}^* \tag{2.14}$$

where $\overrightarrow{\mathbf{f}^*}_{\mathbf{A}}$ represents the sum of all force vectors exerted on this rigid body, $\overrightarrow{\mathbf{m}^*}_{\mathbf{A}}$ depicts the totality of moment vectors and all force-induced moment vectors applied to the rigid body, then ${}^{\mathbf{A}}\mathbf{f}^*$ and ${}^{\mathbf{A}}\mathbf{m}^* \in \mathbb{R}^3$ represent the net force and moment vectors written in frame $\{\mathbf{A}\}$, accordingly.

Definition 2.5. *Let* ${}^{\mathbf{A}}\mathbf{f}^* \in \mathbb{R}^3$ *and* ${}^{\mathbf{A}}\mathbf{m}^* \in \mathbb{R}^3$ *defined in (2.13) and (2.14), respectively be the net forces and moment vectors that are being exerted to an inflexible body, and being determined in and represented in a body frame* $\{\mathbf{A}\}$*. The net force/ moment vector of the rigid body in frame* $\{\mathbf{A}\}$ *is defined as (Zhu 2010, p.30)*

$${}^{\mathbf{A}}\mathbf{F}^* \stackrel{\text{def}}{=} \begin{bmatrix} {}^{\mathbf{A}}\mathbf{f}^* \\ {}^{\mathbf{A}}\mathbf{m}^* \end{bmatrix} \in \mathbb{R}^6. \tag{2.15}$$

2.7.2 Dynamics of Rigid Body

If two frames $\{\mathbf{A}\}$ and $\{\mathbf{B}\}$ are attached to an inflexible object. Then, if frame $\{\mathbf{A}\}$ is utilized for expressing the body dynamics, and frame $\{\mathbf{B}\}$ is acknowledged to be placed at the mass center of the body, the dynamics of the rigid body in free motion, written in the inertial reference frame $\{\mathbf{I}\}$, becomes

$$\begin{bmatrix} {}^{m}\mathbf{A}\boldsymbol{I}_{\mathbf{3}} & \\ & \boldsymbol{I}_0(t) \end{bmatrix} \begin{bmatrix} \dot{\mathbf{v}} \\ \dot{\boldsymbol{\omega}} \end{bmatrix} + \begin{bmatrix} {}^{m}\mathbf{A}g \\ (\boldsymbol{\omega}\times)\boldsymbol{I}_{\mathbf{0}}(\boldsymbol{t})\boldsymbol{\omega} \end{bmatrix} = \begin{bmatrix} \mathbf{f}^* \\ \mathbf{m}^* \end{bmatrix} \tag{2.16}$$

$\mathbf{I_3}$ is a 3×3 identity matrix, ${}^{m}\mathbf{A} \in \mathbb{R}$ represents the mass of the rigid body, $\mathbf{I}_0(t) \in \mathbb{R}^{3\times 3}$ denotes the moment of inertia matrix about the center of mass, $\mathbf{v} \in \mathbb{R}^3$ and $\boldsymbol{\omega} \in \mathbb{R}^3$ depicts the linear velocity vector of the center of mass and the angular velocity vector, accordingly, $\mathbf{g} = [0 \quad 0 \quad 9.81]^T \in \mathbb{R}^3$ is the gravitational vector, and $\mathbf{f}^* \in \mathbb{R}^3$ and $\mathbf{m}^* \in \mathbb{R}^3$ represent the net force and moment vectors exerted to the center of mass, respectively.

Therefore, the rigid body can have its net force/ moment vector expressed in frame $\{\mathbf{A}\}$ and re-written linear and angular velocity vectors given, respectively as

$$^{\mathbf{A}}\mathbf{F}^* = {}^{\mathbf{A}}\mathbf{R}_{\mathbf{B}}\, {}^{\mathbf{B}}\mathbf{F}^* = {}^{\mathbf{A}}\mathbf{U}_{\mathbf{B}} \begin{bmatrix} {}^{\mathbf{B}}\mathbf{R}_{\mathbf{I}} & 0 \\ 0 & {}^{\mathbf{B}}\boldsymbol{R}_{\mathbf{I}} \end{bmatrix} \begin{bmatrix} \mathbf{f}^* \\ \mathbf{m}^* \end{bmatrix} \tag{2.17}$$

$$\begin{bmatrix} \mathbf{v} \\ \boldsymbol{\omega} \end{bmatrix} = \begin{bmatrix} {}^{\mathbf{I}}\mathbf{R}_{\mathbf{B}} & 0 \\ 0 & {}^{\mathbf{I}}\mathbf{R}_{\mathbf{B}} \end{bmatrix} {}^{\mathbf{A}}\mathbf{U}_{\mathbf{B}}^{\mathbf{T}}\, {}^{\mathbf{A}}\mathbf{V} \tag{2.18}$$

$^{\mathbf{A}}\mathbf{U}_{\mathbf{B}} \in \mathbb{R}^{6\times\mathbf{6}}$ is given in (2.12).

Finally, after some mathematical operations (differentiation and multiplications) as given in Zhu (2010), the dynamics of the rigid body can be expressed as

$$^{\mathbf{M}}\mathbf{A} \frac{\mathrm{d}}{\mathrm{dt}}\left({}^{\mathbf{A}}\mathbf{V} \right) + {}^{\mathbf{C}}\mathbf{A}\left({}^{\mathbf{A}}\boldsymbol{\omega} \right) {}^{\mathbf{A}}\mathbf{V} + {}^{\mathbf{M}}\mathbf{A} = {}^{\mathbf{A}}\mathbf{F}^* \tag{2.19}$$

where

$$^{\mathbf{M}}\mathbf{A} = \begin{bmatrix} {}^{m}\mathbf{A}\, {}^{\mathbf{A}}\mathbf{R}_{\mathbf{I}}\mathbf{g} \\ {}^{\mathrm{m}}\mathbf{A}\left(\mathbf{A}_{\mathbf{r}_{\mathbf{AB}}} \times\right) {}^{\mathbf{A}}\mathbf{R}_{\mathbf{I}}\mathbf{g} \end{bmatrix} \tag{2.20}$$

$$\begin{aligned} &{}^{\mathbf{C}}\mathbf{A}\left({}^{\mathbf{A}}\boldsymbol{\omega} \right) \\ &= \begin{bmatrix} {}^{m}\mathbf{A}\mathbf{I}_{\mathbf{3}} & -{}^{m}\mathbf{A}({}^{\mathbf{A}}\boldsymbol{\omega} \times)(\mathbf{A}_{\mathbf{r}_{\mathbf{AB}}} \times) \\ {}^{m}\mathbf{A}(\mathbf{A}_{\mathbf{r}_{\mathbf{AB}}} \times)({}^{\mathbf{A}}\boldsymbol{\omega} \times) & \left({}^{\mathbf{A}}\boldsymbol{\omega} \times \right) {}^{I}\mathbf{A} + {}^{I}\mathbf{A}\left({}^{\mathbf{A}}\boldsymbol{\omega} \times \right) - {}^{m}\mathbf{A}(\mathbf{A}_{\mathbf{r}_{\mathbf{AB}}} \times)({}^{\mathbf{A}}\boldsymbol{\omega} \times)(\mathbf{A}_{\mathbf{r}_{\mathbf{AB}}} \times) \end{bmatrix} \end{aligned} \tag{2.21}$$

$$^{\mathbf{G}}\mathbf{A} = \begin{bmatrix} {}^{\mathrm{m}}\mathbf{A}\, {}^{\mathbf{A}}\mathbf{R}_{\mathbf{I}}\mathbf{g} \\ {}^{m}\mathbf{A}\left(\mathbf{A}_{\mathbf{r}_{\mathbf{AB}}}\right) {}^{\mathbf{A}}\mathbf{R}_{\mathbf{I}}\mathbf{g} \end{bmatrix} \tag{2.22}$$

and $^{\mathbf{I}}\mathbf{A} = {}^{\mathbf{A}}\mathbf{R}_{\mathbf{I}}\mathbf{I}_{\mathbf{0}}(\mathrm{t})\, {}^{\mathbf{I}}\mathbf{R}_{\mathbf{A}}$ is time independent (that is, time-invariant).

2.7.3 Required Variable

An important term in the VDC approach is the *required* variable (required velocity, forces, position, etc.). The required variable, say velocity, differs from the desired variable, which oftentimes is the wanted (reference) trajectory of a particular variable as a function of time. The implication of the required velocity (variable) is that if the actual velocity follows the required velocity, then the position and force control objectives may be achieved. Basically, the conventional format of a required velocity is to combine the desired velocity with at least one other term related to the control error- for instance force error or position errors.

In the case where position control is desired, the required velocity may be designed to take the form

$$\dot{\boldsymbol{\theta}}_r = \dot{\boldsymbol{\theta}}_{\boldsymbol{d}} - \lambda(\boldsymbol{\theta}_{\mathrm{d}} - \boldsymbol{\theta})$$

where $\boldsymbol{\theta}_{\mathrm{d}}$ is the desired angular position and λ is a control parameter, which in this case is the position feedback gain. (Zhu 2010.)

2.7.4 Linear Parametrization of Body Dynamics

A rigid body dynamics can be written in a parametric form given in (2.23). If the required vector, being a design vector which , for the linear/ angular velocity vector ${}^{\mathbf{A}}\mathbf{V} \in \mathbb{R}^6$ is ${}^{\mathbf{A}}\mathbf{V}_{\mathbf{r}} \in \mathbb{R}^6$.

$$\mathbf{Y_B}\boldsymbol{\theta}_{\mathbf{B}} \stackrel{\text{def}}{=} {}^{M}\mathbf{B}\frac{\mathbf{d}}{\mathbf{dt}}\left({}^{\mathbf{B}}\mathbf{V_r}\right) + {}^{C}\mathbf{B}\left({}^{\mathbf{B}}\boldsymbol{\omega}\right){}^{\mathbf{B}}\mathbf{v} + {}^{\mathbf{G}}\mathbf{B} \tag{2.23}$$

${}^{M}\mathbf{B},\ {}^{\mathbf{C}}\mathbf{B}\left({}^{\mathbf{B}}\boldsymbol{\omega}\right)$, and $\boldsymbol{G}_{\mathbf{B}}$ are defined in (2.20) $-$ (2.22). While full description of the regressor matrix $\boldsymbol{Y}_{\mathbf{B}} \in \epsilon\ \mathbb{R}^{6\times\mathbf{13}}$ as well as the parameter vector $\boldsymbol{\theta}_{\mathbf{B}} \boldsymbol{\epsilon} \mathbb{R}^{\mathbf{13}}$ are presented in Appendix A, and available in Appendix A of (Zhu 2010) as well.

2.8 Parameter Projection Function

Only one of the two parameter projection functions for parameter adaption in Zhu (2010) is described and considered in this work. Although parameter adaptation is not included in the experimentations, it is factored into the control equations in order to facilitate its implementation in future works.

Definition 2.6. *A differentiable scalar function defined for $t \geq 0$ such that its time derivative is ruled by (2.24) is called a projection function given as $\mathcal{P}(s(t), \kappa, x(t), y(t), t) \epsilon \mathbb{R}$.*

$$\dot{\mathcal{P}} = \kappa \mathrm{s(t)} \kappa \tag{2.24}$$

where

$$\kappa = \begin{cases} 0 & \text{if } \mathcal{P} \leq \mathrm{x(t) and\ s(t)} \leq 0 \\ 0 & \text{if } \mathcal{P} \geq \mathrm{y(t) and\ s(t)} \geq 0 \\ 1 & \text{Otherwise} \end{cases}$$

and $s(t)\epsilon\mathbb{R}$ *is a scalar variable,* κ *is a non-zero positive constant, and* $x(t) \leq y(t)$ *is true.*

A proof for this parameter function is given in (Zhu 2010, p.32). The main essence of using the $\mathcal{P}$ *function is to avoid parameter estimates from drifting beyond limits, so that within the range [x(t), y(t)]* $\dot{\mathcal{P}}$ *is driven by s(t).*

2.9 Virtual Cutting Point and Oriented Graphs

Two important concepts in VDC approach are discussed in this section. The first is virtual cutting point and the second is oriented graphs.

2.9.1 Virtual Cutting Points

It is categorically stated in Zhu (2010) that VCP is a crucial concept to the VDC approach. It represents a surface, which may be used to *conceptually* decompose a complex robotics system into different subsystems. Their virtuality means they are only conceptual rather than physical. Three dimensional force vectors and moment vectors may be applied from one body to another at a virtual cutting point.

Cutting points may be classified into two groups, namely: *driving* and *driven*. Any cutting point is mutually attached to two adjoining bodies. One body interprets it as a driving cutting point while the other interprets it as a driven cutting point. Formal definition and general properties of VCP are detailed in. (Zhu 2010.)

2.9.2 Oriented Graphs

Simple oriented graphs are used to represent the topology and control interactions of a compound robot.

Definition 2.7. *A graph consists of nodes and edges. A directed graph is a graph in which all the edges have directions. An oriented graph is a directed graph in which each edge* has a unique direction. A simple oriented graph is an oriented graph in which no loop is formed *(Chartrand 1985; Zhu 2010).*

As described in the definition above, graphs are made of nodes and graphs. A simple oriented graph represents each subsystem in a decomposed complex robot as a node and each cutting point is shown as a directed edge indicating the orientation of the forces and moments moving through the cutting point. Some nodes are labelled as *source* (with only edges pointing away) and the others as *sink node* with pointing-to edges alone.

2.10 Virtual Stability

After virtually decomposing a complex system with VCP, a primary concern is the stability of each detached subsystems, which then leads to the concept of *virtual stability* (Zhu 2010). The idea is to assign a non-negative accompanying function to each detached subsystem and proof virtual stability with the concept of virtual power flow (an inner product of velocity vector error and force vector error in rigid bodies) at all virtual cutting points attached to the subsystems.

The concept of spaces and groups earlier described are used to conclude virtual stability based on Lebesgue L_2 and L_∞ space and stability. This concept is used liberally throughout this work. (Zhu 2010.)

2.10.1 Non-Negative Accompanying Functions

According to (Zhu 2010) the definition of non-negative accompanying function is given as

Definition 2.8. *Non-negative accompanying function* $\upsilon(t)\epsilon\ \mathbb{R}$ *is a piecewise differentiable function having the properties as follows:*

(i) $\upsilon(t) \geq 0\ for\ t > 0, and$
(ii) $\dot{\upsilon}(t)$ *subsists almost at every point.*

It is customary in the VDC approach to assign a non-negative accompanying function to each subsystem for conducting virtual stability and convergence study.

2.10.2 Virtual Power Flow

In reference to an arbitrary frame $\{\mathbf{B}\}$ the virtual power flow is defined.

Definition 2.9. *Virtual power flow is the inner product of the linear/ angular velocity vector error and the force/ moment vector error, i.e.,*

$$p_{\boldsymbol{B}} \stackrel{\text{def}}{=} \left({}^{\mathbf{B}}\mathbf{V}_{\mathrm{r}} - {}^{\mathbf{B}}\mathbf{V}\right)^{\mathrm{T}}\left({}^{\mathbf{B}}\mathbf{F}_{\mathrm{r}} - {}^{\mathbf{B}}\mathbf{F}\right) \tag{2.25}$$

where ${}^{\mathbf{B}}\mathbf{V}_{\mathrm{r}}\epsilon\mathbb{R}^6$ and ${}^{\mathbf{B}}\mathbf{F}_{\mathrm{r}}\epsilon\mathbb{R}$ are the design (required) vectors of ${}^{\mathbf{B}}\mathbf{V}\epsilon\mathbb{R}^6$ and ${}^{\mathbf{B}}\mathbf{F}\epsilon\mathbb{R}^6$, accordingly.

This quantity is defined and applied to describe the dynamic relations among decomposed subsytems of a complex robotic system. The Virtual stability concept takes deep roots in the virtual power flow terminology. (Zhu 2010.) It should be noted that when the same constraints apply to the required linear/ angular velocity vectors and the required force/ moment vectors of a rigid body to which two frames $\{\mathbf{B}\}$ and $\{\mathbf{C}\}$ are attached, then it holds that

$$p_{\boldsymbol{B}} = p_{\boldsymbol{C}} \tag{2.26}$$

since the relationships (2.27) and 2.28) becomes applicable in view of (2.10) and (2.11).

$$^{\mathbf{B}}\mathbf{V}_{\mathrm{r}} = \ ^{\mathbf{C}}\mathbf{U}_{\mathbf{B}}^{\mathbf{T}}\ ^{\mathbf{C}}\mathbf{V}_{\mathrm{r}} \tag{2.27}$$

$$^{\mathbf{C}}\mathbf{F}_{\mathbf{r}} = \ ^{\mathbf{C}}\mathbf{U}_{\mathbf{B}}\mathbf{B}_{\mathbf{F}_{\mathbf{r}}} \tag{2.28}$$

Remark 2.1. *It can be verified from (2.26) that the VPF given in (2.25), similar to the power flow inside a rigid body, is the same for frames attached to common inflexible body. Using the conditions (2.10) and (2.11) to validate (2.26) is necessary condition in control designs. (Zhu 2010.)*

2.10.3 Virtual Stability Concept

After decomposing a complex system, the issue of whether the resulting individual sub-systems are stable for control purpose need to be addressed. To do this, a concept called virtual stability is introduced.

Definition 2.10. *If a subsystem is virtually detached from a complex robotic system, then the subsystem may be guaranteed virtually stable with its affiliated vector* $\boldsymbol{m}(t)$ *being a virtual function in* L_∞ *and its affiliated vector* $\boldsymbol{n}(t)$ *being a virtual function in* L_2*, if and only if there exists a non-negative accompanying function*

$$\upsilon(t) \geq \frac{1}{2}\boldsymbol{m}^{\mathrm{T}}(t)\boldsymbol{G}\boldsymbol{m}(t) \tag{2.29}$$

such that

$$\dot{\upsilon}(\mathrm{t}) \leq -\mathbf{n}^{\mathrm{T}}(\mathrm{t})\mathbf{H}\mathbf{n}(\mathrm{t}) - \mathrm{s}(\mathrm{t}) + \textstyle\sum_{\{\mathbf{A}\in\boldsymbol{\Phi}\}} \mathrm{p}_{\mathbf{A}} - \sum_{\{\mathbf{B}\in\boldsymbol{\Psi}\}} \mathrm{p}_{\mathbf{B}} \tag{2.30}$$

holds, subject to

$$\int_0^\infty s(t)d\tau \geq -\gamma_s \qquad (2.31)$$

where $0 \leq \gamma_s \leq \infty$, ***G*** *and* ***H*** *are two block-diagonal positive-definite matrices, set* Φ *and* Ψ*, respectively contain frames being placed at the driven and driving cutting points of the subsystem, respectively, and* $p_{\boldsymbol{A}}$ *and* $p_{\boldsymbol{B}}$ *are virtual power flows defined in Definition 2.9.*

Remark 2.2. *The virtual stability of any given subsystem requires that the VPFs appear in the time derivative of the non-negative accompanying function ascribed to the subsystem. By convention, VPFs assume positive sign at the driven cutting points and negative sign at the driving cutting point, which is unique characteristic of virtual stability. It should be noted that* $s(t) = 0$ *is a special case that fulfill (2.31). After every subsystem of a complex system satisfy virtual stability condition, then all the virtual functions in* L_p $(p \in \{2, \infty\})$ *become functions in* L_p*. (Zhu 2010.)*

Now, after establishing the virtual stability of subsystems in a complex system in line with Definition 2.10, it can be shown that any two adjacent virtually stable subsystems are virtually stable and can be equivalent to a single subsystem. The Lemma and proof for this condition are given in (Zhu 2010, p.37.)

Lemma 2.1. *Every two adjacent subsytems that are virtually stable can be equivalent to a single subsystem that is virtually stable in the sense of Definition 2.10. 'Every virtual function in* L_p *affiliated with any one of the two adjacent subsystems remains a virtual function in* L_p *affiliated with the equivalent subsystem for* $p \in \{2, \infty\}$'. (Zhu 2010).

Likewise, when all the subsystems in a complex system are *virtually stable according to Definition 2.10, then the Theorem 2.1 ensures that the* L_2 *and* L_∞ *stability of the entire robotic system can be guaranteed.*

Theorem 2.1. *Consider a complex manipulator that is virtually disintegrated into subsystems and is denoted by a simple oriented graph in Definition 2.7. If every subsystem is virtually stable according to the Definition 2.10, then all virtual functions in* L_2 *are functions in* L_2 *and all virtual functions in* L_∞ *are functions in* L_∞*.*

The proof of this theorem is presented in (Zhu 2010, p.38-40).

Remark 2.3. *Theorem 2.1 is the most important theorem to the theory of VDC. It sets the basis for the equivalence between the virtual stability of all subsystems and that of the complex system as a whole. Thus, this permits laying emphasis on the assurance of virtual stability of every subsystem, rather than the stability of the entire complex system. The theorem is the groundwork of VDC.*

2.11 Backlash Non-linearity and its Inverse

The helical gear type of rotary actuator applied in the manipulator/ robot under study has gear mechanisms, thus inherent backlash characteristics. Backlash refers to the play between gear teeth or screws in power and motion transmission systems. It is a common non-smooth nonlinearity (just as dead-zone, hysteresis, friction, saturation and time delays) in control systems. Typical of all non-smooth non-linearities, backlash characteristics are often unknown or poorly known. They are discontinuous, making the control of systems where they exist very challenging. They often need adaptive schemes to track their parameters and neutralize their effects by some inverses. They are briefly described below. ((Tao and Kokotovic, 2010).)

2.11.1 Backlash Nonlinearity

Figure 2.2 (a) gives a graphical conception of backlash as a clearance between two mating gear teeth (Drago1998). According to Tao and Kokotovic (1996), although seemingly straightforward at first glance, the phenomenon is far more intricate than it looks. Summarily, a pair of slanted parallel straight lines linked by horizontal lines Figure 2.2 (b) describes backlash. The slanted line on the right side represents the upward motion when both the input and output are simultaneously increasing; whereas, the corresponding line on the left depicts downward movement during which both *v(t)* and *u(t)* are decreasing. As described earlier, backlash is a somewhat dynamic characteristic with memory.

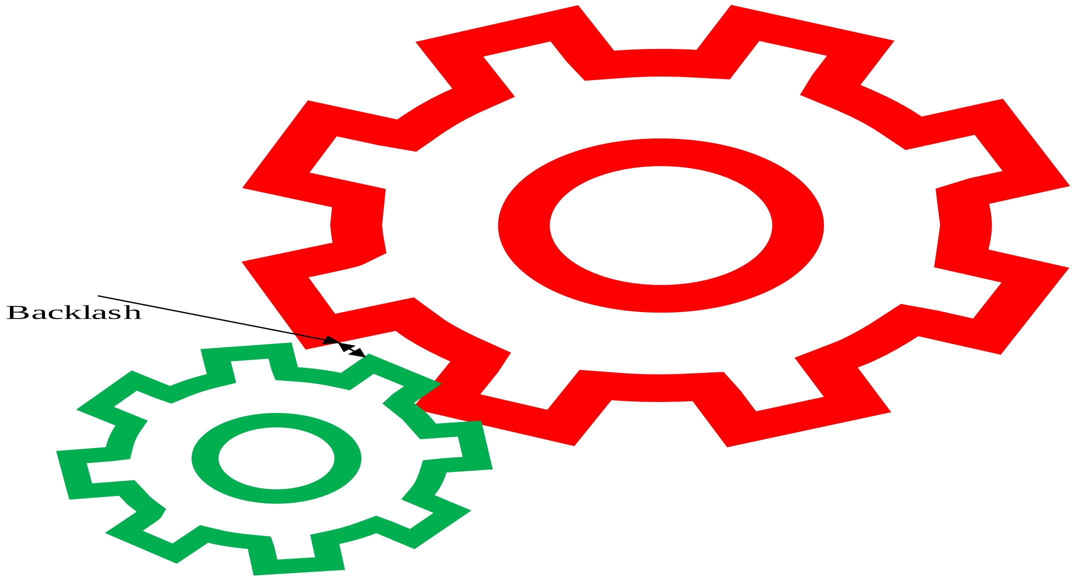

(a)

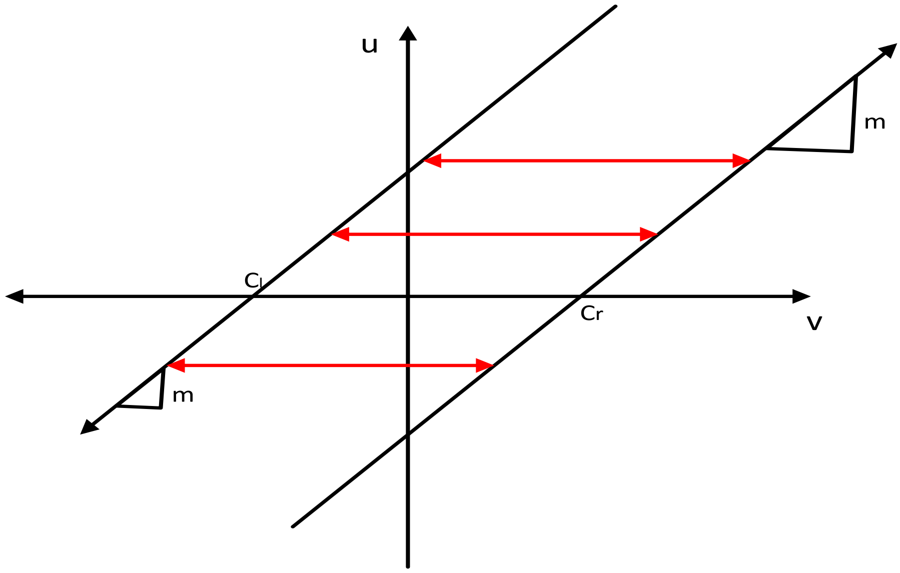

(b)

Figure 2.2. *Graphical interpretation and descriptions of backlash characteristic.*

The right and left *'crossing points'* are, respectively such that $c_r > 0$ and $c_l < 0$, and m_r and m_l are the right and left slopes respectively, which for a symmetric case may just be assumed equal to a single value m.

That is, backlash characteristics is of the form:

$$u(t) = BS\,(v(t)) = BS\,(m, c_r\,, c_l\,;\; v(t)) \tag{2.32}$$

$$u(t) = m(v(t) - c_r), when\ \dot{v}(t) > 0\ and\ \dot{u}(t) > 0 \tag{2.33}$$

where BS represent backlash description such that

$$u(t) = m(v(t) - c_l),\ \text{when}\ \dot{v}(t) < 0\ and\ \dot{u}(t) < 0, \tag{2.34}$$

and for motion within the inner segment. (Tao and Kokotovic 1996).

$$\dot{u}(t) = 0$$

Given that $m > 0$ and $c_r > c_l$ are constant backlash parameters.

In a compact continuous-time (CT) notation, backlash is described by a multi-region piecewise linear function as (Tao and Kokotovic 1996)

$$\dot{u}(t) = \begin{cases} m\dot{v}(t) & \dot{v}(t) > 0\ and\ u(t) = m(v(t) - c_r), or \\ & \dot{v}(t) < 0\ and\ u(t) = m(v(t) - c_l), \\ 0 & Othewise \end{cases} \tag{2.35}$$

In discrete time (DT) notation, the characteristics may be expressed as:

$$u(t) = \begin{cases} m(v(t) - c_r) & v(t) > v_r \\ m(v(t) - c_l) & v(t) \leq v_l \\ 0 & v_l < v(t) < v_r \end{cases} \tag{2.36}$$

$$where\ v_r = \frac{u(t-1)}{m} + c_r\ and\ v_l = \frac{u(t-1)}{m} + c_l \tag{2.37}$$

This DT version is based on intuitive deductions of the projections of the crossings of the two slanting parallel lines with the flat inner segment where $u(t - 1)$ is located. In addition, t in (2.36) and (2.37) represents DT, such that it can only assume integer values t = 0, 1, 2….

2.11.2 Backlash Inverse Model

Since backlash is an unwanted characteristic in control systems, it is often desired to neutralize its effects by designing an inverse characteristic, so that the nonlinear phenomena may be eliminated. Truxal questioned the existence of an exact backlash inverse in 1958, followed by Tao in 1993. Tao and Kokotovic provided a response to the question in 1996, where a graphical depiction and multi-region describing function for backlash inverse was given as presented in Figure 2.3 and equation (2.38), respectively. (Truxal 1958; Tao and Kokotovic 1996.)

$$\dot{v}(t) = BSI(u_d(t)) = \begin{cases} -\frac{1}{m}\dot{u}_d(t), & if\ \dot{u}_d(t) > 0, v(t) = \frac{u_d(t)}{m} + c_r\ or \\ & if\ \ \dot{u}_d(t) < 0, v(t) = \frac{u_d(t)}{m} + c_l \\ 0, & if\ \dot{u}_d(t) = 0 \\ g(t,t) & if\ \dot{u}_d(t) > 0, v(t) = \frac{u_d(t)}{m} + c_l \\ -g(t,t) & if\ \dot{u}_d(t) < 0, v(t) = \frac{u_d(t)}{m} + c_l \end{cases} \tag{2.38}$$

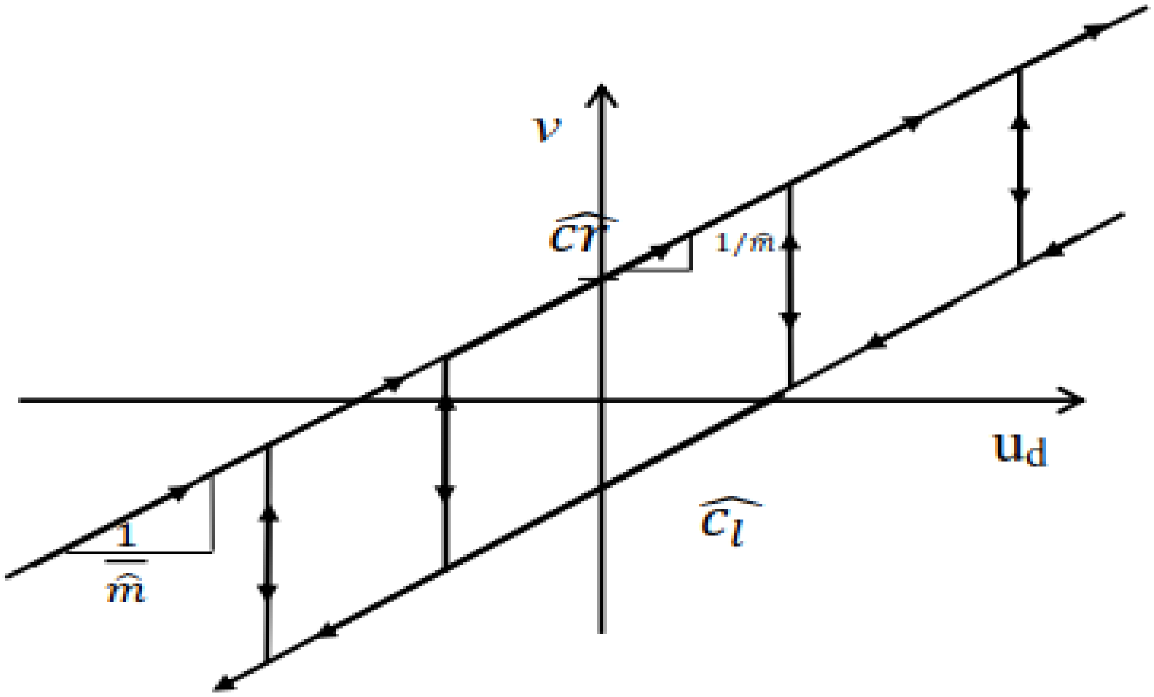

Figure 2.3. *Graphical representation of backlash inverse.*

This definition of BSI in (2.38) gives the assurance that a flat inner portion of the backlash characteristic corresponds to a vertical jump depicted as the time integral of the impulse function (2.39a).

$$g(\tau, t) \;=\; \delta(\tau - \; t)(c_r \; - c_l) \tag{2.39a}$$

δ(t) being the Dirac $\delta -$ function. So that a jump in the upward direction in the backlash inverse is equivalent to

$$v(t^+) = v(t^-) + \int_{t^-}^{t^+} g(\tau, t) d\tau = \frac{u_d(t^-)}{m} + c_r \tag{2.39b}$$

This jump is the essence of backlash inversion; its effect is to remove the time delay caused by inner segment of $BS\ (.)$. In addition, (2.39a) results in the recovery of the data that would rather have been lost in (2.35). This is demonstrated extensively in Tao and Kokotovic (1996) by proving that the BSI characteristic in (2.38) is *an exact right-hand inverse* of (2.35).

2.11.3 Backlash Inverse Parametrization

As done in Tao and Kokotovic (1996), in order to arrive at a cleaner expressions for backlash inverse control error $u(t) \; - \; u_d\ (t)$ and to suit adaptive compensation structure, an indicator function $\chi\ [Y]$ is defined for an event Y, such that

$$\chi\,[Y] = \begin{cases} 1 & if\ Y\ is\ true \\ 0 & Otherwise \end{cases} \tag{2.40}$$

If $\hat{\chi}$ is adopted as the indicator function utilizing estimates

$$\hat{\chi}_r(t) = \chi\left[v(t) = \frac{u_d(t)}{\hat{m}} + \hat{c}_r\right] \tag{2.41}$$

$$\hat{\chi}_l(t) = \chi\left[v(t) = \frac{u_d(t)}{\hat{m}} + \hat{c}_l\right] \tag{2.42}$$

Therefore, it is logical to deduce, based on mutual exclusivity of the two events described, that

$$\hat{\chi}_r(t) + \hat{\chi}_l(t) = 1 \tag{2.43}$$

$$\hat{\chi}_r^2(t) = \hat{\chi}_r(t), \hat{\chi}_l^2(t) = \hat{\chi}_l(t) \text{ and } \hat{\chi}_r(t)\hat{\chi}_l(t) = 0 \tag{2.44}$$

Hence, the expression for $v(t)$ may be written as

$$v(t) = \left(\hat{\chi}_r(t) + \hat{\chi}_l(t)\right) v(t) = \frac{\hat{\chi}_r(t)}{\hat{m}}\,(u_d(t) + \hat{m}\hat{c}_r) + \frac{\hat{\chi}_l(t)}{\hat{m}}\,(u_d(t) + \hat{m}\hat{c}_l) \tag{2.45}$$

Furthermore, indicator functions are also defined for the backlash model

$$\chi_r(t) = \chi[\dot{u}(t) > 0], \chi_l(t) = \chi[\dot{u}_d(t) < 0] < 0, \chi_s(t) = \chi[\dot{u}_d(t) = 0]$$

Also clearly,

$$\chi_r(t) + \chi_l(t) + \chi_s(t) = 1$$

$$\chi_r^2(t) = \chi_r(t), \chi_l^2(t) = \chi_l(t), \chi_s^2(t) = \chi_s(t)$$

$$\chi_r(t)\chi_l(t) = 0,\ \chi_l(t)\chi_s(t) = 0,\ \chi_s(t)\chi_r(t) = 0 \tag{2.46}$$

Thence, the compact expression for backlash output $u(t)$ may be concluded as

$$\begin{aligned} u(t) &= (\chi_r(t) + \chi_l(t) + \chi_s(t))\,u(t) \\ &= \chi_r(t)m(v(t) - c_r) + \chi_l(t)m(v(t) - c_l) + \chi_s(t)u_s \end{aligned} \tag{2.47}$$

u_s is a generic constant equivalent to the value of $u(t)$ at any active inside portion of the backlash characterized by

$$\frac{u_s}{m} + c_l \leq v(t) \leq \frac{u_s}{m} + c_r \tag{2.48}$$

The application of (2.44) to the product of (2.45) and $\hat{\chi}_l(t)$ yields

$$\hat{\chi}_l(t)u_d(t) = \hat{\chi}_l(t)(\widehat{m}v(t) - \widehat{m}\hat{c}_l) \tag{2.49}$$

Likewsie for $\hat{\chi}_r$ yields,

$$\hat{\chi}_r(t)u_d(t) = \hat{\chi}_r(t)(\widehat{m}v(t) - \widehat{m}\hat{c}_r) \tag{2.50}$$

Combining (2.43), (2.49), and (2.50), the expression (2.51) is concluded for the control input $u_d(t)$.

$$u_d(t) = \big(\hat{\chi}_r(t) + \hat{\chi}_l(t)\big)u_d(t) = \hat{\chi}_r(t)(\widehat{m}v(t) - \widehat{m}\hat{c}_r) + \hat{\chi}_l(t)(\widehat{m}v(t) - \ \widehat{m}\hat{c}_l) \tag{2.51}$$

Also from (2.43), (2.48), and (2.51), the following expression between $u(t)$ and $u_d(t)$ exists

$$\big(u(t) - u_d(t)\big) = \hat{\chi}_r(t)(m(v(t) - c_r) - \widehat{m}v(t) + \widehat{m}\hat{c}_r + \hat{\chi}_l(t)(m(v(t) - c_l) - \widehat{m}v(t) + \widehat{m}\hat{c}_l + d_b(t) \tag{2.52}$$

where the term $d_b(t)$ is the unparametrized portion of the control error $\big(u(t) - u_d(t)\big)$, which in most adaptive compensation schemes acts as an unknown disturbance. it has some interseting characteristics, including its disappearance when the parameter estimates are exactly the same as the true paramter values as described in Tao and Kokotovic (1996).

$$d_b(t) = (\chi_r(t) - \hat{\chi}_r(t))(m(v(t) - c_r)) + (\chi_l(t) - \hat{\chi}_l(t))(m(v(t) - c_l)) + \chi_s(t)u_s \tag{2.53}$$

From (2.35) it is deduced that

$$d_b(t) = 0, \ iff \ \chi_r(t) = \hat{\chi}_r(t), \ \chi_l(t) = \hat{\chi}_l(t) \ or \ \hat{\chi}_s(t) = 0$$

This expression is bounded for all times $t \geq 0$.

In an attempt to form a more compact expression for the backlash control error (3.22), letting $\widehat{mc}_r = \widehat{m}\hat{c}_r$, $\widehat{mc}_l = \widehat{m}\hat{c}_l$ and defining parameter vectors θ_b^*, θ_b and backlash regressor $\omega_b(t)$ as

$$\theta_b^* = (mc_r, m, mc_l)^T \tag{2.54}$$

$$\theta_b = (\widehat{mc}_r, \widehat{m}, \widehat{mc}_l)^T \tag{2.55}$$

$$\omega_b(t) = (\hat{\chi}_r(t), -v(t), \hat{\chi}_l(t))^T \tag{2.56}$$

(2.51), (2.55) together with (2.56) reduce the backlash inverse expression (2.38) (which in DT notation and more compact form is given by 2.57) to (2.58)

$$v(t) = BSI\big(u_d(t)\big) = \begin{cases} \frac{1}{m}u_d(t) + c_r, & if\ u_d(t) > u_d(t-1) \\ \frac{1}{m}u_d(t) + c_l, & if\ u_d(t) < u_d(t-1) \\ v(t-1) & if\ u_d(t) = u_d(t-1) \end{cases} \tag{2.57}$$

$$u_d(t) = -\theta_b^T \omega_b(t) \tag{2.58}$$

Therefore, conclusion can be made from (2.52) and (2.54) - (2.56), that the control error in terms of parameter error $\theta_b - \theta_b^*$ and the unparametrized part $d_b(t)$, is summarily (Tao and Kokotovic 1996)

$$u(t) - u_d(t) = (\theta_b - \theta_b^*)^T \omega_b(t) + d_b(t) \tag{2.59}$$

Equations (2.58) and (2.59) are applicable to both CT and DT scenarios and they are used in the construction of adaptive baclash inverse compensator.

2.11.4 Adaptive Backlash Inverse Control

The adaptive backlash inverse control objective may be summarized below and full theory of the control approach are available in reputable references (Tao and Kokotovic (1996); Ahmad and Khorrami 1999).

Consider a system described as

$$y(t) = G(D)[u](t),\ u(t) = BS(v(t)) \tag{2.60}$$

where $y(t)$ represents the measured plant output, $u(t)$ is the unobservable output of the backlash dynamics and $v(t)$ is the available control input. The Laplace or the z-transform operator is represented by 'D', depending on whether the design is done in CT or DT domain.

That is, the adaptive backlash compensation goal for a plant with backlash is to construct a feedback control signal $v(t)$, which ensures boundedness of all closed loop signals so that the plant output asymptotically tracks the desired trajectory.

The adaptive backlash inverse, parametrized by the adaptive estimate $\theta_b = (\widehat{mc}_r, \widehat{m}, \widehat{mc}_l)$, takes the form

$$v(t) = \widehat{BSI}\big(u_d(t)\big) \tag{2.61}$$

$$m_1 \leq m \leq m_2, 0 \leq c_r \leq c_{r0}, -c_{l0} \leq c_l \leq 0,$$

subject to the assumptions and constraint that m_1, m_2, c_{r0} and c_{l0} are some known constants.

Earlier, it was demonstrated that the adaptive backlash inverse given in (2.61) leads to the control error (2.62) expressed as a sum of a parameterized term (θ_b, ${\theta^*}_b$ and $\omega_b(t)$) and an unparametrized part, $d_N(t)$ which disappears for any time after the initial time t_0 when the parameter estimates match the actual parameter, provided the initialization is appropriately set to (2.63)

$$u(t) - u_d(t) = (\theta_b(t) - {\theta^*}_b)\omega_b(t) + d_N(t) \tag{2.62}$$

$$u_d(t_0) = BS(BSI(u_d(t_0))) \tag{2.63}$$

An adaptive update law is required to generate the control signal $v(t)$, since the backlash nonlinearity BS(.) is unknown. According to Tao and Kokotovic (1996), the tracking error may simply be expressed as the difference between the plant output and the desired output and parametrized as shown in (2.64)

$$e(t) = y(t) - y_m(t) = W(D)[\theta_N^T \omega_N](t) + d(t) \tag{2.64}$$

where $W(D) = k_p\left(1 - \theta_1^{*T} a_\lambda(D)\right) D^{-n^*}$ represent some filter, k_p is an adaptive gain and n^* is the relative order of the plant ensuring that $d(t)$ is bounded, such that

$$d(t) = W(D)[d_N](t).$$

Based on the error expression (2.6), it implies that the adaptive update law should be of the form

$$\theta_N(t+1) = \theta_N^T(t) - \frac{\Gamma_N \phi_N(t) \kappa_N(t)}{1 + \phi_N^T(t)\phi_N(t) + \delta_N^2(t)} + f(t) \tag{2.65}$$

with

$$\kappa_N(t) = e(t) + \delta_N(t) \tag{2.66}$$

$$\delta_N(t) = \theta_N^T(t)\phi_N(t) - W(D)[\theta_N^T \omega_N](t) \tag{2.67}$$

the function $f(t)$is a projection adjustment term designed by adopting the parameter projection which ensures that the elements of the estimated parameter vector $\theta_N(t)$ are confined within a predefined region, and the step size Γ_N is selected in line with the choice of the parameter projection function $f(t)$. (Tao and Kokotovic 1996.)

Subject to the given constraints and conditions guiding (2.61), the actual parameters contained in $\theta_b^*(t)$ are kept within a convergence region given as

$$\theta_b^* = (\theta_{b1}^*, \theta_{b2}^*, \theta_{b3}^*)^T, \theta_{bi}^* = \left[\theta_{bi}^a, \theta_{bi}^b\right],\ i = 1,2,3. \tag{2.68}$$

$$\theta_{b1}^a = 0, \theta_{b1}^a = m_1, \theta_{b3}^a = -m_2 c_{l0} \tag{2.69}$$

$$\theta_{b1}^b = m_2 c_{r0}, \theta_{b2}^b = m_2, \theta_{b3}^a = 0 \tag{2.70}$$

The adaptive step size matrix is given as

$$\Gamma_N = diag\{\Omega_1, \Omega_2, \Omega_3\}, 0 < \Omega_i < 2, i = 1,2,3$$

Making,

$$\bar{\theta}_{bi}(t) = \theta_{bi}(t) + g_{bi}(t) \tag{2.71}$$

$$g_N(t) = \frac{\Gamma_N \phi_N(t) \kappa_N(t)}{1 + \phi_N^T(t)\phi_N(t) + \delta_N^2(t)} \tag{2.72}$$

Thereafter, representing the i^{th} terms of $\theta_N(t), f_N(t)$, and $g_N(t)$ as $\theta_{Ni}(t)$ $f_{Ni}(t)$ and $g_N(t)$, and making initialization in line with (2.68), the following expression for $f_b(t)$ is arrived at

$$f_{bi}(t) = \begin{cases} 0 & if\ \bar{\theta}_{bi}(t) \epsilon\ [\theta_{bi}^a, \theta_{bi}^b] \\ \theta_{bi}^a - \bar{\theta}_{bi}(t) & if\ u_d(t) < u_d(t-1) \\ \theta_{bi}^a - \bar{\theta}_{bi}(t) & if\ u_d(t) = u_d(t-1) \end{cases} \tag{2.73}$$

This method for designing parameters gives the assurance that the estimated parameters are within the predefined appropriately initialized region, and remain there unceasing.

These backlash and backlash inverse expressions are combined with the VDC equations to guarantee the virtual stability of the entire manipulator system under study. In fact, the adaptive backlash inverse controller is stable on its own, provided that the initial parameter estimates are within the appropriate range. Thus, if a stable VDC controller is combined with the adaptive backlash inverse equations/ model (which in a sense may be viewed as a subsystem), the assurance of stability of the entire controller can be guaranteed.

Remark 2.2. *All these concepts have provided sufficient background for the development of VDC to effectively control a hydraulic manipulator with backlash (i.e., actuated by a helical type hydraulic rotary actuator). In subsequent chapters, the concepts are used to formulate a VDC scheme for the manipulator under study with the view of achieving desired system dynamics.*

3. VIRTUAL DECOMPOSITION CONTROL OF THE TARGET SYSTEM

This chapter is dedicated to modelling of the hydraulic manipulator under review. Thereafter, it is virtually decomposed to develop control equations that guarantee its virtual stability in view of Definition 2.10.

The chapter is organized as follows. Firstly, the concept of virtual decomposition is introduced, followed by presentation of the kinematics and dynamics of the studied manipulator. Thereafter, the control equations of the manipulator are given. The virtual stability of the manipulator is proven, and then the dynamics and control of the hydraulic actuator are given. Finally, the issue of virtual stability of the manipulator in view of the adaptive backlash inverse control is discussed.

3.1 Virtual Decomposition

The hydraulic manipulator under study is shown in Figure 1.2. The output shaft is used to rotate an inertia load composed of an arm and an adjustable mass at its free end as described in Section 1.3. The rotary motion of the shaft is obtained through conversion of the translatory motion of the actuator piston into a rotary motion by means of helical spline connections (between shaft and housing attached ring and between piston and shaft). The hydraulic rotary actuator operates in a somewhat similar way as the hydraulic cylinder, in the sense that the admittance of fluid into either port of the actuator creates pressure differential across the two chambers of the actuator causing the piston to translate. However, in addition to the translatory motion, the piston acquires rotary motion from its meshing with the ring gear mounted on the inside of the actuator housing.

Therefore, the decomposition of the hydraulic rotary actuator can be done in a similar manner to the decomposition of the hydraulic cylinder given in (Zhu 2010, 168-170), with the incorporation of the rotary motion.

Hence, the assembly has two rigid bodies (the piston and the shaft) and two objects (the arm and the vertical frame/ support together with the ring).

As depicted in Figure 3.1, three body-fixed frames are attached to this assembly. Frame $\{\boldsymbol{T}\}$ is mutually attached to the shaft and the attached arm, and it is attached at the cutting point called the driving cutting point of the hydraulic actuator subsystem. Frame $\{\boldsymbol{B_2}\}$ is fixed to the piston, while frame $\{\boldsymbol{B_1}\}$ is fixed to the base of the actuator (which is modelled to include the ring gear, thereby simplifying the whole analysis). All the frames have their x-y planes as indicated; whereby the x-axis of the frames align with the respective link axis, while the z- axis is perpendicular to these planes, thereby pointing out of the page in each case. In addition, frame $\{\mathbf{O}\}$ is attached to the center of mass of the first object (i.e., the arm together with the load) to describe its motion. The simple oriented graph of the entire manipulator is shown in Figure 3.2.

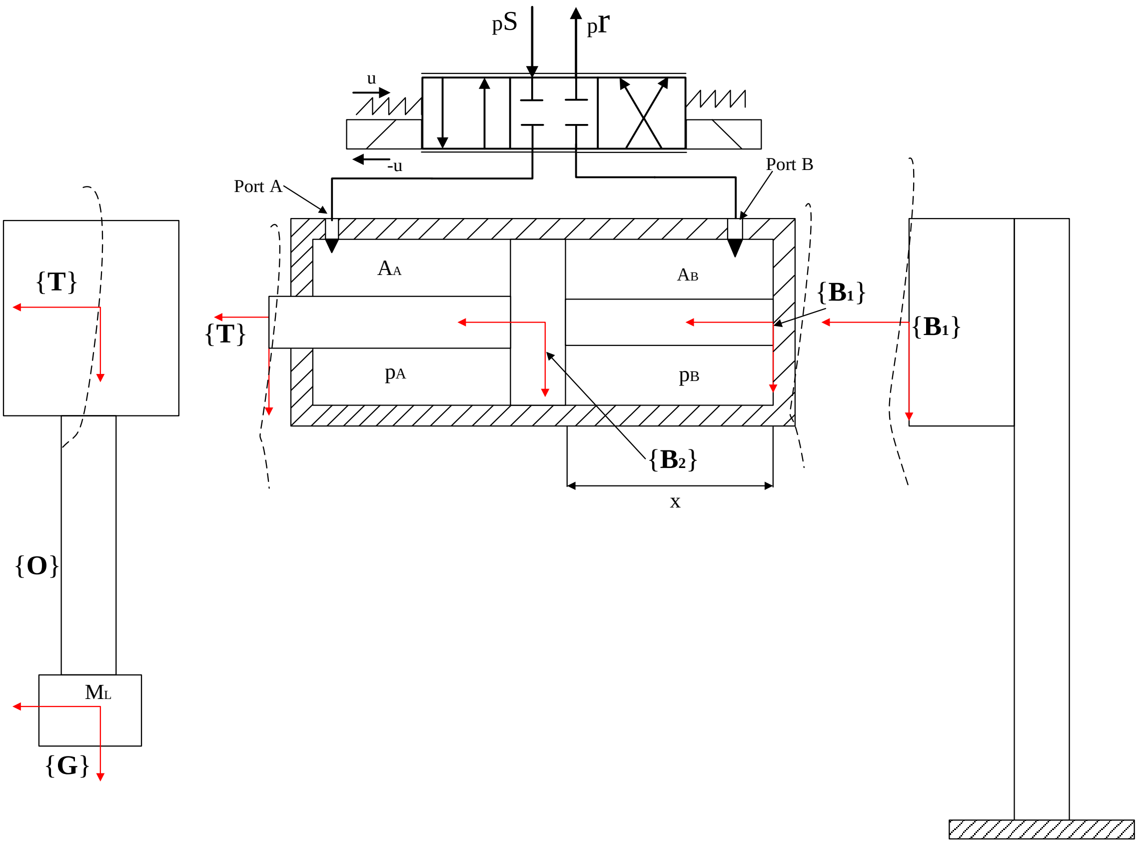

Figure 3.1. Virtual decomposition of the hydraulic manipulator

In view of Figure 3.1, it follows that

- The first object has one driven cutting point associated with frame {**T**}.
- The hydraulic actuator subsystem has two cutting points; a driving cutting point associated with frame {**T**} and one driven cutting point associated with frame{$\mathbf{B_1}$}.
- The vertical frame has one driving cutting point associated with frame {$\mathbf{B_1}$}.

3.2 Kinematics and Dynamics

The kinematics and dynamics of the hydraulic manipulator are presented in this section for later use in the control design.

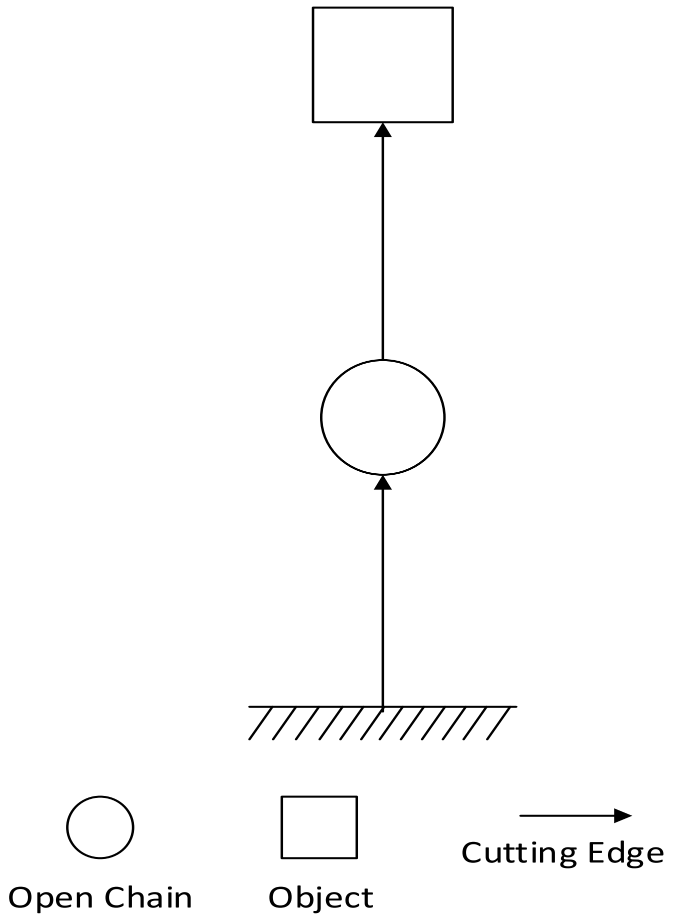

Figure 3.2. *Simple oriented graph of the manipulator.*

3.2.1 Kinematics

In view of the duality between force and velocity (2.63) and Figure 3.1, the relationships among the linear / angular velocity vectors of the three body attached frames are

$$ {}^{T}\mathbf{V} = \mathrm{u}_2\,{}^{\mathbf{B_2}}\mathbf{U}_{\mathbf{T}}^{\mathbf{T}}\left({}^{B_2}\mathbf{V} - \mathbf{x}_\mathrm{f}\dot{x}\right) \tag{3.1} $$

$$ {}^{\mathbf{B_2}}\mathbf{V} = \mathbf{x}_f\dot{x} + u_1\boldsymbol{x}_\tau\omega + u_1\,{}^{\mathbf{B_1}}\mathbf{U}_{\mathbf{B_2}}^{\mathbf{T}}\,{}^{\mathbf{B_1}}\mathbf{V} \tag{3.2} $$

$$ {}^{\mathbf{B_1}}\mathbf{V} = 0 \tag{3.3} $$

where u_1 is the gear ratio between the piston and the ring (housing), and u_2 is the gear ratio between the piston and the shaft,

$$ \mathbf{x}_\mathrm{f} = [1,0,0,0,0,0]^\mathrm{T} \in \mathbb{R}^6 \tag{3.4} $$

$$ \boldsymbol{x}_\tau = [0,0,0,1,0,0]^\mathbf{T} \in \mathbb{R}^6 \tag{3.5} $$

3.2.2 Dynamics

In view of (2.19), the dynamics of the two rigid bodies (piston and shaft) may be expressed as

$$^{\mathbf{M}}\mathbf{B_1}\frac{\mathrm{d}}{\mathrm{dt}}\left({}^{\mathbf{B_1}}\mathbf{V}\right) + {}^{\mathbf{C}}\mathbf{B_1}\left({}^{\mathbf{B_1}}\boldsymbol{\omega}\right){}^{\mathbf{B_1}}\mathbf{V} + {}^{\mathbf{G_1}}\mathbf{B_1} = {}^{\mathbf{B_1}}\mathbf{F}^* \tag{3.6}$$

$$^{\mathbf{M}}\mathbf{B_2}\frac{\mathrm{d}}{\mathrm{dt}}\left({}^{\mathbf{B_2}}\mathbf{V}\right) + {}^{\mathbf{C}}\mathbf{B_2}\left({}^{\mathbf{B_2}}\boldsymbol{\omega}\right){}^{\mathbf{B_2}}\boldsymbol{V} + {}^{\mathbf{G_2}}\mathbf{B_2} = {}^{\mathbf{B_2}}\mathbf{F}^* \tag{3.7}$$

with substitution of frames $\{\mathbf{B_1}\}$ and $\{\mathbf{B_2}\}$ for frame $\{\mathbf{A}\}$, respectively.

In addition, the resultant force of the frame $\{\mathbf{T}\}$ may be computed from the mass/ inertia and the desired angular velocity of the end effector and the attached load. That is, $\mathbf{T}_{\mathrm{F}}$ can be computed from the mass of the arm and the load, and the rotational speed (i.e.,$\mathbf{T}_{\mathrm{F}} = \boldsymbol{x_\tau} J\dot{\omega}$**,** where J is the inertia of the load and the arm).

Then, the force resultant equations of the two rigid bodies may be expressed as

$$^{\mathbf{B_2}}\mathbf{F}^* = {}^{\mathbf{B_2}}\mathbf{F} - \frac{1}{u_2}\,{}^{\mathbf{B_2}}\mathbf{U_T}\;{}^{\mathbf{T}}\mathbf{F} \tag{3.8}$$

$$^{\mathbf{B_1}}\mathbf{F}^* = {}^{\mathbf{B_1}}\mathbf{F} - \frac{1}{u_1}\,{}^{\mathbf{B_1}}\mathbf{U_{B_2}}\;{}^{\mathbf{B_2}}\mathbf{F} \tag{3.9}$$

Then the actuation force and torque of the cylinder is expressed as

$$f_c = \mathbf{x}_{\mathrm{f}}^{\mathrm{T}}\,{}^{\mathbf{B_2}}\mathbf{F} \in \mathbb{R}$$

$$\tag{3.10}$$

$$\tau_c = \mathbf{x}_{\boldsymbol{\tau}}^{\mathrm{T}}\,{}^{\mathbf{B_2}}\mathbf{F} \in \mathbb{R}$$

Remark 3.1. *The actuation force (torque) of the actuator to produce the desired torque required to drive the shaft through required trajectory is given by (3.10).*

3.3 Control Equations

Next, the focus is shifted to the development of control equations for the hydraulic manipulator assembly.

3.3.1 Required Velocities

In order to validate the expression (2.27), the linear/ angular velocity vectors given in (3.1) and (3.2) also apply to the required linear/ angular velocity vectors. Then, it may be written that.

$$ {}^{\mathbf{T}}\mathbf{V_r} = \mathrm{u}_2\, {}^{\mathbf{B_2}}\mathbf{U_T^T}\, ({}^{\mathbf{B_2}}\mathbf{V_r} - \mathbf{x}_\mathrm{f}\dot{x}_r) \tag{3.11} $$

$$ {}^{\mathbf{B_2}}\mathbf{V_r} = \mathbf{x}_f \dot{x}_r + u_1 \boldsymbol{x}_\tau \omega_r + u_1\, {}^{\mathbf{B_1}}\mathbf{U_{B_2}^T}\, {}^{\mathbf{B_1}}\mathbf{V_r} \tag{3.12} $$

$$ {}^{\mathbf{B_1}}\mathbf{V_r} = [0, 0, 0, 0, 0, 0]^T \tag{3.13} $$

holds.

Remark 3.2. *There exists only one (degree of freedom) independent design variable, which can either be chosen as the shaft required rotation speed, $\dot{\omega}_r$, or the piston required linear velocity, $\dot{x}_r$,along the actuator axis.*

3.3.2 Required Net Force/ Moment Vectors with Parameter Adaptation

The required net force/ moment vectors of the two rigid bodies can be parametrized as (Zhu 2010, p.174, p.75).

$$ {}^{\mathbf{B_1}}\mathbf{F_r^*} = \mathbf{Y_{B_1}}\widehat{\boldsymbol{\theta}}_{\mathbf{B_1}} + \mathbf{K_{B_1}}\left({}^{\mathbf{B_1}}\mathbf{V_r} - {}^{\mathbf{B_1}}\mathbf{V}\right) \tag{3.14} $$

$$ \mathbf{B_1}_{\mathbf{F_r^*}} = \mathbf{Y_{B_2}}\widehat{\boldsymbol{\theta}}_{\mathbf{B_2}} + \mathbf{K_{B_2}}\left({}^{\mathbf{B_2}}\mathbf{V_r} - {}^{\mathbf{B_2}}\mathbf{V}\right) \tag{3.15} $$

where

$\mathbf{K_{B_1}} \in \mathbb{R}^{6\times6}$ Is a positive-definite gain matrix

$\mathbf{K_{B_2}} \in \mathbb{R}^{6\times6}$ Is a positive-definite gain matrix

$\widehat{\boldsymbol{\theta}}_{\mathbf{B_1}} \in \mathbb{R}^{13}$ Is the parameter estimate of $\boldsymbol{\theta}_{\boldsymbol{B_1}} \in \mathbb{R}^{13}$

$\widehat{\boldsymbol{\theta}}_{\mathbf{B_2}} \in \mathbb{R}^{13}$ Is the parameter estimate of $\boldsymbol{\theta}_{\boldsymbol{B_2}} \in \mathbb{R}^{13}$

$\mathbf{Y_{B_1}}\widehat{\boldsymbol{\theta}}_{\mathbf{B_1}} \in \mathbb{R}^6$ Is Model-based feedforward term defined by (2.23) and expressed in Appendix A with frame $\{\mathbf{B_1}\}$ substituted for frame $\{\mathbf{A}\}$, accordingly

$\mathbf{Y_{B_1}}\widehat{\boldsymbol{\theta}}_{\mathbf{B_1}} \in \mathbb{R}^6$ Is Model-based feedforward term defined by (2.23) and expressed in Appendix A with frame $\{\mathbf{B}\}$ substituted for frame $\{\mathbf{A}\}$, accordingly.

In view of (14) and (15), define

$$ \mathbf{s_{B_1}} = \mathbf{Y_{B_1}^T}\left({}^{\mathbf{B_1}}\mathbf{V_r} - {}^{\mathbf{B_1}}\mathbf{V}\right) \tag{3.16} $$

$$ \mathbf{s_{B_2}} = \boldsymbol{Y}_{\boldsymbol{B}_2}^{\boldsymbol{T}}\left({}^{\mathbf{B_2}}\mathbf{V_r} - {}^{\mathbf{B_2}}\mathbf{V}\right) \tag{3.17} $$

Each of the 13 parameters of the rigid bodies can be updated using the $\mathcal{P}$ function defined in (2.24) as:

$$\widehat{\boldsymbol{\theta}}_{\boldsymbol{B}\mathbf{1}_\gamma} = \mathcal{P}(s_{\boldsymbol{B}_{1_\gamma}}, \rho_{B\mathbf{1}_\gamma}, \underline{\theta}_{B_{1_\gamma}}, \overline{\theta}_{B_{1_\gamma}}, t) \tag{3.18}$$

$$\widehat{\boldsymbol{\theta}}_{\boldsymbol{B}\mathbf{1}_\gamma} = \mathcal{P}(s_{\boldsymbol{B}_{2_\gamma}}, \rho_{B\mathbf{2}_\gamma}, \underline{\theta}_{B_{2_\gamma}}, \overline{\theta}_{B_{2_\gamma}}, t) \tag{3.19}$$

for all $\gamma \in \{1{,}13\}$ where

$\widehat{\boldsymbol{\theta}}_{\boldsymbol{B}\mathbf{1}_\gamma}$	Is the γ^{th} element of $\widehat{\boldsymbol{\theta}}_{\boldsymbol{B}\mathbf{1}}$
$\widehat{\boldsymbol{\theta}}_{\boldsymbol{B}\mathbf{1}_\gamma}$	Is the γ^{th} element of $\widehat{\boldsymbol{\theta}}_{\boldsymbol{B}\mathbf{2}}$
$\rho_{B\mathbf{1}_\gamma}$	Is parameter update gain
$\rho_{B\mathbf{2}_\gamma}$	Is parameter update gain
$\underline{\theta}_{B_{1_\gamma}}$	Is the lower limit of $\theta_{B_{1_\gamma}}$
$\underline{\theta}_{B_{2_\gamma}}$	Is the lower limit of $\theta_{B_{2_\gamma}}$
$\overline{\theta}_{B_{1_\gamma}}$	Is the upper limit of $\theta_{B_{1_\gamma}}$
$\overline{\theta}_{B_{2_\gamma}}$	Is the upper limit of $\theta_{B_{2_\gamma}}$

3.3.3 Required Force/ Moment Vector Transformations

In view of Figure 3.1, given a required force/ moment vector in frame $\{\boldsymbol{T}\}$, (that is, in the driving cutting point of the hydraulic shaft, and of course, of the hydraulic actuator) denoted as $\boldsymbol{T}_{\boldsymbol{F}_r} \in \mathbb{R}^6$.

$$^{\mathbf{T}}\mathbf{F_r} \;=\; \boldsymbol{x}_\tau J \dot{\omega}_r \in \mathbb{R}^6 \tag{3.20}$$

Then, the required force/ moment vector in frame $\{\boldsymbol{B_1}\}$ and $\{\boldsymbol{B_2}\}$ may be computed as

$$^{\mathbf{B_2}}\mathbf{F}_\mathbf{r}^* \;= \mathbf{B}_{\mathbf{2}_{\mathbf{F_r}}} - \frac{1}{u_2}\,{}^{\mathbf{B_2}}\mathbf{U_T}\;\;{}^{\mathbf{T}}\mathbf{F_r} \tag{3.21}$$

$$^{\mathbf{B_1}}\mathbf{F}_\mathbf{r}^* \;= {}^{\mathbf{B_1}}\mathbf{F_r} - \frac{1}{u_1}\,{}^{\mathbf{B_1}}\mathbf{U}_{\mathbf{B_2}}\;\;{}^{\mathbf{B_2}}\mathbf{F_r} \tag{3.22}$$

From equation (3.10), the required actuation force along the actuator axis designed as:

$$f_{cr} \;= \mathbf{x}_\mathrm{f}^{\mathrm{T}}\,{}^{\mathbf{B_2}}\mathbf{F_r} \in \mathbb{R} \tag{3.23}$$

Remark 3.3. Once the required force/ moment (in the x-direction) has been obtained from (3.21) and (3.22) then the required actuation force of the piston may be computed from (3.23).

Summarily, the procedure for controlling the hydraulic actuator assembly can be given as

Step 1: For a given $\dot{x}_r$ and ω_r compute all required velocities in terms of (3.11) − (3.13).

Step 2: Compute ${}^{\mathbf{B_1}}\mathbf{F}_\mathbf{r}^*$ and ${}^{\mathbf{B_2}}\mathbf{F}_\mathbf{r}^*$ using (3.14) − (3.15), and update unknown parameters by using (3.16) − (19).

Step 3: For a given ${}^{\mathbf{T}}\mathbf{F}_\mathbf{r}$ compute ${}^{\mathbf{B_1}}\mathbf{F}_\mathbf{r}$ using (3.20) − (3.22).

Step 4: Compute f_{cr} from (3.23).

3.4 Virtual Stability

The virtual stability of the entire manipulator is given in respect of the Definition 2.10 of *VPF.*

Theorem 3.1. The first object (i.e., the lever arm together with the attached load) of the hydraulic manipulator under study described by (3.1) and (3.20), combined with its control equations (3.11) and (3.20) is virtually stable in respect of Definition 2.10.

Proof: based on the knowledge of the required force of the object 1 and the force of the frame $\{\mathbf{O}\}$, it follows that

$$\left({}^{G}\mathbf{F}_\mathbf{r} - {}^{\mathbf{G}}\mathbf{F} \right) = 0 \tag{3.24}$$

holds. since the arm undergoes a contactless motion- wherefore the net force of frame $\{\mathbf{O}\}$ is nought. Setting the non-negative accompanying function to *zero*, and premultiplying (3.24) by $\left({}^{G}\boldsymbol{V}_{\boldsymbol{r}} - {}^{G}\boldsymbol{V} \right)^T$ and using the Definition 2.9 leads to

$$0 = \left({}^{\mathbf{G}}\mathbf{V}_\mathbf{r} - {}^{G}\mathbf{V} \right)^T \left({}^{\mathbf{G}}\mathbf{F}_\mathbf{r} - {}^{\mathbf{G}}\mathbf{F} \right) \tag{3.24a}$$

Also, considering the dynamics of frame $\{\mathbf{T}\}$ on the first object, the velocity error of the frame is represented as $\left({}^{\mathbf{T}}\mathbf{V}_\mathbf{r} - {}^{\mathbf{T}}\mathbf{V} \right)$. Thus, calling on Definition 2.9 and (2.25), the inner product of this quantity and the force error of the frame yields the VPF at the frame $\{\mathbf{T}\}$ of the first object.

$$\left({}^{\mathbf{T}}\mathbf{V}_\mathbf{r} - {}^{\mathbf{T}}\mathbf{V} \right)^T \left({}^{\mathbf{T}}\mathbf{F}_\mathbf{r} - {}^{\mathbf{T}}\mathbf{F} \right) = p_\mathbf{T} \tag{3.24b}$$

which proves the Theorem 3.1 in respect of Definition 2.9.

Lemma 3.1. Consider the hydraulic actuator subsystem (composed of the piston and the shaft), described by (3.2) - (3.3), (6.6) and (3.7) together with its respective control equations (3.11) − (3.15), (3.21) −(3.23), together with the parameter adaptation (3.16) − (3.19),

Permit

$$v_1 = v_{B_1} + v_{B_2} \tag{3.26}$$

to be the non-negative accompanying function assigned to the subsystem (that is, to the piston and shaft)

where

$$v_{B_1} = \frac{1}{2}\left({}^{\mathbf{B_1}}\mathbf{V_r} - {}^{\mathbf{B_1}}\mathbf{V}\right)^T \mathbf{M}_{B_1}\left({}^{\mathbf{B_1}}\mathbf{V_r} - {}^{\mathbf{B_1}}\mathbf{V}\right) + \sum_{\gamma=1}^{13}\left(\theta_{B_{1_\gamma}} - \hat{\theta}_{B_{1_\gamma}}\right)^2 / \rho_{B_{1\gamma}} \tag{3.27}$$

$$v_{B_2} = \frac{1}{2}\left({}^{\mathbf{B_2}}\mathbf{V_r} - {}^{\mathbf{B_2}}\mathbf{V}\right)^T \boldsymbol{M}_{B_2}\left({}^{\mathbf{B_2}}\mathbf{V_r} - {}^{\mathbf{B_2}}\mathbf{V}\right) + \sum_{\gamma=1}^{13}\left(\theta_{B_{1_\gamma}} - \hat{\theta}_{B_{1_\gamma}}\right)^2 / \rho_{B_{2\gamma}} \tag{3.28}$$

are the duo non-negative accompanying functions allotted to the subsystem. Thus, the time rate of (3.26) may be written as:

$$\dot{v}_1 = \dot{v}_{\boldsymbol{B_1}} + \dot{v}_{\boldsymbol{B_2}} \leq -\left({}^{\mathbf{B_1}}\mathbf{V_r} - {}^{\mathbf{B_1}}\mathbf{V}\right)^T \mathbf{K_{B_1}}\left({}^{\mathbf{B_1}}\mathbf{V_r} - {}^{\mathbf{B_1}}\mathbf{V}\right) - \left({}^{B_2}\boldsymbol{V_r} - {}^{\mathbf{B_2}}\mathbf{V}\right)^T \mathbf{K_{B_2}}\left({}^{\mathbf{B_2}}\mathbf{V_r} - {}^{\mathbf{B_2}}\mathbf{V}\right) + p_{\boldsymbol{B_1}} - p_{\boldsymbol{T}} + \left(1 - \frac{1}{u_1}\right)(\dot{x}_r - \dot{x})(f_{cr} - f_c) + (\dot{\omega}_r - \dot{\omega})(\tau_{cr} - \tau_c) \tag{3.29}$$

with $p_{\boldsymbol{B_1}}$ and $p_{\boldsymbol{T_1}}$ representing the two virtual power flows at the cutting points of the subsystem.

Proof: It ensues from (6), (7), (14) and (15), (16) and (17), (18) and (19) and Lemma 4.1 of (Zhu 2010) that:

$$\dot{v}_{\boldsymbol{B_1}} \leq -\left({}^{\mathbf{B_1}}\mathbf{V_r} - {}^{\mathbf{B_1}}\mathbf{V}\right)^{\mathrm{T}} \mathbf{K_{B_1}}\left({}^{\mathbf{B_1}}\mathbf{V_r} - {}^{\mathbf{B_1}}\mathbf{V}\right) + \left({}^{\mathbf{B_1}}\mathbf{V_r} - {}^{\mathbf{B_1}}\mathbf{V}\right)^T \left({}^{\mathbf{B_1}}\mathbf{F_r^*} - {}^{\mathbf{B_1}}\mathbf{F}\right) \tag{3.30}$$

$$\dot{v}_{\boldsymbol{B_2}} \leq -\left({}^{\mathbf{B_1}}\mathbf{V_r} - {}^{\mathbf{B_1}}\mathbf{V}\right)^T \boldsymbol{K_{B_2}}\left({}^{\mathbf{B_2}}\mathbf{V_r} - {}^{\mathbf{B_2}}\mathbf{V}\right) + \left({}^{\mathbf{B_2}}\mathbf{V_r} - {}^{\mathbf{B_2}}\mathbf{V}\right)^{\mathrm{T}} \left({}^{\mathbf{B_2}}\mathbf{F_r^*} - {}^{\mathbf{B_2}}\mathbf{F}\right) \tag{3.31}$$

In view of the definition of virtual power flow, (3.1)−(3.3), (3.8) – (3.9), (3.11) − (3.13), (3.21) – (3.23) it results in:

$$\left({}^{\mathbf{B_1}}\mathbf{V_r} - {}^{\mathbf{B_1}}\mathbf{V}\right)^T \left[\left({}^{\mathbf{B_1}}\mathbf{F_r} - {}^{\mathbf{B_1}}\mathbf{F}\right) - \frac{1}{u_1}\, {}^{\mathbf{B_1}}\mathbf{U_{B_2}} \left({}^{\mathbf{B_2}}\mathbf{F_r} - {}^{\mathbf{B_2}}\mathbf{F}\right)\right]$$

$$= p_{B_1} - \left[u_1 {}^{\mathbf{B_2}}\mathbf{U}_{\mathbf{B_1}}^{\mathbf{T}} \left({}^{\mathbf{B_2}}\mathbf{V_r} - {}^{\mathbf{B_2}}\mathbf{V}\right) - u_1 {}^{\mathbf{B_2}}\mathbf{U}_{\mathbf{B_1}}^{\mathbf{T}} \mathbf{x}_f(\dot{x}_r - \dot{x}) - u_1 {}^{\mathbf{B_2}}\mathbf{U}_{\mathbf{B_1}}^{\mathbf{T}} \boldsymbol{x}_\tau(\omega_r - \omega)\right]^T \times \frac{1}{u_1} {}^{\mathbf{B_1}}\mathbf{U}_{\mathbf{B_2}}^{\mathbf{T}} \left({}^{\mathbf{B_2}}\mathbf{F_r} - {}^{\mathbf{B_2}}\mathbf{F}\right)$$

$$= p_{\mathbf{B_1}} - \left[u_1\left({}^{\mathbf{B_2}}\mathbf{V_r} - {}^{\mathbf{B_2}}\mathbf{V}\right)^T \left({}^{\mathbf{B_2}}\mathbf{U}_{\mathbf{B_1}}^{\mathbf{T}}\right)^T - u_1(\dot{x}_r - \dot{x})\mathbf{x}_f^{\mathbf{T}}\left({}^{\mathbf{B_2}}\mathbf{F_r} - {}^{\mathbf{B_2}}\mathbf{F}\right) - u_1(\omega_r - \omega)\boldsymbol{x}_\tau^{\mathbf{T}} {}^{\mathbf{B_2}}\mathbf{U}_{\mathbf{B_1}}\right] \times \frac{1}{u_1} {}^{\mathbf{B_1}}\mathbf{U}_{\mathbf{B_2}} \left({}^{\mathbf{B_2}}\mathbf{F_r} - {}^{\mathbf{B_2}}\mathbf{F}\right)$$

$$= p_{\mathbf{B_1}} - \left({}^{\mathbf{B_2}}\mathbf{V_r} - {}^{\mathbf{B_2}}\mathbf{V}\right)^{\mathbf{T}}\left({}^{\mathbf{B_2}}\mathbf{F_r} - {}^{\mathbf{B_2}}\mathbf{F}\right) + (\dot{\boldsymbol{x}}_r - \dot{\boldsymbol{x}})\boldsymbol{x}_f^T\left({}^{\mathbf{B_2}}\mathbf{F_r} - {}^{\mathbf{B_2}}\mathbf{F}\right) + (\boldsymbol{\omega}_r - \boldsymbol{\omega})\boldsymbol{x}_\tau^T\left({}^{\mathbf{B_2}}\mathbf{F_r} - {}^{\mathbf{B_2}}\mathbf{F}\right)$$

$$= p_{\mathbf{B_1}} - p_{\mathbf{B_2}} + (\dot{\mathrm{x}}_r - \dot{x})x_f^T\left({}^{\mathbf{B_2}}\mathbf{F_r} - {}^{\mathbf{B_2}}\mathbf{F}\right) + (\omega_r - \omega)\boldsymbol{x}_\tau^T\left(\mathbf{B}_{2_{\mathbf{F_r}}} - \mathbf{B}_{2_{\mathbf{F}}}\right)$$

$$= p_{\mathbf{B_1}} - p_{\mathbf{B_2}} + (\dot{x}_r - \dot{x})(f_{cr} - f_c) + (\omega_r - \omega)(\tau_{cr} - \tau_c) \tag{3.32}$$

$$\left({}^{\mathbf{B_2}}\mathbf{V_r} - {}^{\mathbf{B_2}}\mathbf{V}\right)^{\mathrm{T}}\left({}^{\mathbf{B_2}}\mathbf{F_r^*} - {}^{\mathbf{B_2}}\mathbf{F_r}\right) = \left({}^{\mathbf{B_2}}\mathbf{V_r} - {}^{\mathbf{B_2}}\mathbf{V}\right)^{\mathrm{T}}\left[\left({}^{\mathbf{B_2}}\mathbf{F_r^*} - {}^{\mathbf{B_2}}\mathbf{F}\right) - \frac{1}{\mathrm{u}_2} {}^{\mathbf{B_2}}\mathbf{U_T}\left({}^{\mathbf{T}}\mathbf{F_r} - {}^{\mathbf{T}}\mathbf{F}\right)\right]$$

$$= \left({}^{\mathbf{B_2}}\mathbf{V_r} - {}^{\mathbf{B_2}}\mathbf{V}\right)^T\left({}^{\mathbf{B_2}}\mathbf{F_r} - {}^{\mathbf{B_2}}\mathbf{F}\right) - \left[\frac{1}{u_2} {}^{\mathbf{T}}\mathbf{U}_{\mathbf{B_2}}^{\mathbf{T}}\left({}^{\mathbf{T}}\mathbf{V_r} - {}^{\mathbf{T}}\mathbf{V}\right) + \boldsymbol{x}_f(\dot{\boldsymbol{x}}_r - \dot{\boldsymbol{x}})\right]^{\mathrm{T}} \times \frac{1}{u_1} {}^{\mathbf{B_2}}\mathbf{U_T}\left({}^{\mathbf{T}}\mathbf{F_r} - {}^{\mathbf{T}}\mathbf{F}\right)$$

$$= p_{\mathbf{B_2}} - p_{\mathbf{T}} - \frac{1}{u_2}(\dot{x}_r - \dot{x})\boldsymbol{x}_f^T\left({}^{\mathbf{B_2}}\mathbf{F_r} - {}^{\mathbf{B_2}}\mathbf{F}\right) = p_{\mathbf{B_2}} - p_{\mathbf{T}} - \frac{1}{u_2}(\dot{x}_r - \dot{x})(f_{cr} - f_c) \tag{3.33}$$

Inserting (3.32) and (3.33) into (3.30) and (3.31) results in (3.29)

Theorem 3.2. The second object (that is the supporting vertical frame) is virtually stable in the sense of Definition 2.10.

Proof: It follows from the attached frame that

$$\left({}^{\mathbf{B_1}}\mathbf{V_r} - {}^{\mathbf{B_1}}\mathbf{V}\right)^{\mathrm{T}} = 0 \tag{3.34}$$

in view of the fact that the frame is stationary.

Hence, postmultiplying (3.34) by $\left({}^{\mathbf{B_1}}\mathbf{F_r^*} - {}^{\mathbf{B_1}}\mathbf{F}\right)$, and letting the non-negative accompanying function be *zero*, together with the use of the definition of virtual power flow, yield the following

$$0 = \left({}^{\mathbf{B_1}}\mathbf{V_r} - {}^{\mathbf{B_1}}\mathbf{V}\right)^{\mathrm{T}}\left({}^{\boldsymbol{B_2}}\mathbf{F}_{\boldsymbol{r}}^{*} - {}^{\mathbf{B_2}}\mathbf{F}\right) \tag{3.35}$$

proving Theorem 3.2 in view of Definition 2.10.

Remark 3.4. *The virtual stability of the two objects resulting from the virtual decomposition has been ensured by theorems (3.1) and (3.2); however, the virtual stability of the actuator subsystem (i.e., piston and shaft) has been prevented at this point, in view of virtual stability of the Lemma 3.1, due to the appearance of the term* $(\frac{u_1-1}{u_1})(\dot{x}_r - \dot{x})(f_{cr} - f_c) + (\omega_r - \omega)(\tau_{cr} - \tau_c)$. This term is resolved in the subsequent section.

3.5 Hydraulic Actuator Dynamics and Control

The main objective of this section is to develop the pertinent dynamics and control constructions linked with the hydraulic actuator, focused on resolving the term $(\frac{u_1-1}{u_1})(\dot{x}_r - \dot{x})(f_{cr} - f_c) + (\omega_r - \omega)(\tau_{cr} - \tau_c)$ in (3.29).

3.5.1 Friction Model

The dominant friction force of the hydraulic actuator is the piston friction, that is, the friction force between the piston seal and the cylinder wall. This accounts for a significant reduction in the pressure induced force and the actual torque of the hydraulic actuator (Zhu 2010). The following hold for linear and rotary actuators, respectively.

$$f_{\mathrm{f}} = \boldsymbol{Y_f}\boldsymbol{\theta_f} \tag{3.38}$$

$$\tau_f = \boldsymbol{Y_\tau}\boldsymbol{\theta_\tau} \tag{3.39}$$

with $\boldsymbol{Y_f}$ and $\boldsymbol{Y_\tau}$ being differentiable regressor matrices. (Zhu 2010; Zhu and Piedboeuf 2005).

3.5.2 Hydraulic Fluid Dynamics

Generally, in hydraulic system studies the dynamics of the servo valve is treated as being proportional to the control voltage signal in the frequency range of interest (Sohl and Bobrow 1999; Zhu 2005; Yao et al. 2000).

From the knowledge of static flow equation (Merritt 1976; Zhu 2010, p.41), the flow rate through an orifice, denoted as Q is directly related to the product of valve control signal (voltage) and the half power of the pressure differential over the orifice, which mathematically implies:

$$Q = c\sqrt{\Delta p}u \tag{3.40}$$

with $c > 0$ being a positive non-zero constant, $p > 0$ represents the pressure drop across the valve (orifice) ports, and u represents the control voltage of valve.

The dynamic equation for the fluid compressibility in an actuator compartment may be expressed in terms of bulk modulus (Sirouspour and Salcudean 2001; Sohl and Bobrow 1999)

$$\dot{p} = \frac{B}{V_c}(Q - V_c) \tag{3.41}$$

where Q represents the flow rate into the compartment, V_c is the compartment volume and p is the compartment pressure.

Express a selective function (Zhu 2010):

$$\varepsilon(y) \stackrel{\text{def}}{=} \begin{cases} 1 & if\ y > 0 \\ 0 & if\ y \leq 0 \end{cases} \tag{3.42}$$

Moreover, a sign function

$$sign(y) \stackrel{\text{def}}{=} \begin{cases} 1 & if\ y > 0 \\ 0 & if\ y = 0 \\ -1 & if\ y < 0 \end{cases} \tag{3.43}$$

In addition, a function related to pressure differential

$$\mathcal{V}(y) \stackrel{\text{def}}{=} \sqrt{|y|}sign(y) \tag{3.44}$$

Remark 3.5. *The expression in (3.44), that is,$\mathcal{V}(y)$ is a monotonically increasing function.*

For a typical hydraulic actuator (the rotary actuator in this case), if Q_A is the flow rate entering the left compartment and Q_B is the flow rate entering the right chamber, and if p_A and p_B are the pressures inside the respective chambers. Then, it follows from the flow rate in (3.40) that

$$Q_A = c_{p_1}\mathcal{V}(p_s - p_A)u\varepsilon(u) + c_{n_1}\mathcal{V}(p_A - p_r)u\varepsilon(-u) \tag{3.45}$$

$$Q_B = -c_{n_2}\mathcal{V}(p_B - p_r)u\varepsilon(u) - c_{n_1}\mathcal{V}(p_s - p_B)u\varepsilon(-u) \tag{3.46}$$

hold, where $c_{p_1} > 0$, $c_{n_1} > 0$, $c_{p_2} > 0$, $c_{n_2} > 0$ are four constant parameters which are equal for an ideal valve. $p_s > 0$ and $p_r > 0$ denote the supply and return line pressures where $p_s \gg p_r$.

In view of (3.41), the pressure relation of the two compartment can be expressed as:

$$\dot{p}_A = \frac{B}{A_A(l - x_0)}(Q_A + A_A\dot{x}) \tag{3.47}$$

$$\dot{p}_B = \frac{B}{A_B x}(Q_B + A_B\dot{x}) \tag{3.48}$$

$A_A > 0$ and $A_B > 0$ are the piston areas at both chambers with $A_A < A_B$, x is the piston displacement, and l_0 is the effective length of the actuator.

The net pressure force of the two compartments can be obtained from the pressures as:

$$f_p = A_B p_B - A_A p_A \tag{3.49}$$

so that the net torque output of the actuator (treated as a screw) may be expressed as $\tau_p = \frac{u_1 u_2 D f_p}{5000}$ where D is the nominal diameter of the shaft.

Premultiplying A_A and A_B to (3.47) and (3.48), respectively, and combined with (3.45) and (3.46) results in

$$\dot{f}_p = B\left[u_f - \left(\frac{A_A}{l_0 - x} + \frac{A_B}{x}\right)\dot{x}\right] \tag{3.50}$$

where

$$u_f = \left[\frac{Q_A}{x} - \frac{Q_A}{l_0 - x}\right] = -\left(\frac{c_{p1}\mathcal{V}(p_s - p_a)}{l_{0-x}} + \frac{c_{n2}\mathcal{V}(p_b - p_r)}{x}\right)u\varepsilon(u)$$
$$-\left(\frac{c_{n1}\mathcal{V}(p_a - p_r)}{l_{0-x}} + \frac{c_{p2}\mathcal{V}(p_s - p_b)}{x}\right)u\varepsilon(-u) \stackrel{\text{def}}{=} -\mathbf{Y}_v(u)\boldsymbol{\theta}_v \tag{3.51}$$

and

$$\dot{\tau}_p = \frac{D\dot{f}_p}{5000} = \frac{u_1 u_2 D}{5000}\boldsymbol{Y}_v(u)\boldsymbol{\theta}_v \tag{3.52}$$

with

$$\boldsymbol{Y}_v(u) = \begin{bmatrix} \frac{\mathcal{V}(p_s - p_a)}{l_{0-x}}u\varepsilon(u) \\ \frac{\mathcal{V}(p_a - p_r)}{l_{0-x}}u\varepsilon(-u) \\ \frac{\mathcal{V}(p_a - p_r)}{x}u\varepsilon(-u) \\ \frac{\mathcal{V}(p_b - p_r)}{x}u\varepsilon(u) \end{bmatrix}^T \epsilon\mathbb{R}^{1\times 4} \tag{3.53}$$

$$\boldsymbol{\theta}_v = \left[c_{p1}\ c_{n1}\ c_{p2}\ c_{n2}\right]^T \epsilon\mathbb{R}^4 \tag{3.54}$$

It is assumed that the piston never reaches its two ends to prevent singularity, so that

$$0 < x < l_0 \tag{3.55}$$

Therefore, based on this assumption, there is univalence between u and u_f provided that:

$$\frac{c_{p1}\mathcal{V}(p_s-p_a)}{l_{0-x}} + \frac{c_{n2}\mathcal{V}(p_b-p_r)}{x} > 0 \tag{3.56}$$

$$\frac{c_{n1}\mathcal{V}(p_a-p_r)}{l_{0-x}} + \frac{c_{p2}\mathcal{V}(p_s-p_b)}{x} > 0 \tag{3.57}$$

is true. This implies that for a given u_f, there is the possibility of finding a particular (unique) control u as:

$$u = -\frac{1}{\frac{c_{p1}\mathcal{V}(p_s-p_a)}{l_{0-x}}+\frac{c_{n2}\mathcal{V}(p_b-p_r)}{x}} u_f\varepsilon(-u_f) - \frac{1}{\frac{c_{n1}\mathcal{V}(p_a-p_r)}{l_{0-x}}+\frac{c_{p2}\mathcal{V}(p_s-p_b)}{x}} u_f\varepsilon(u_f) \tag{3.58}$$

when (3.56) and (3.57) are met.

3.5.3 Actuator Control Equations

Base on the definition of friction models described in (3.36) - (3.39) and the fluid dynamics given in (3.50) and (3.52), the control equations are designed as (Zhu 2010)

$$f_{pr} = f_{cr} + \mathbf{Y}_f\widehat{\boldsymbol{\theta}}_f \tag{3.59}$$

$$\tau_{pr} = \tau_{cr} + \mathbf{Y}_\tau\widehat{\boldsymbol{\theta}}_\tau$$

$$u_{fd} = \frac{1}{B}\dot{f}_{pr} + \left(\frac{\hat{A}_A}{l_0-x} - \frac{\hat{A}_B}{x}\right)\dot{x} + k_{fp}\left(f_{pr}-f_p\right) + k_x(\dot{x}_r-\dot{x}) = \mathbf{Y}_c\widehat{\boldsymbol{\theta}}_c + k_{fp}\left(f_{pr}-f_p\right) + k_x(\dot{x}_r-\dot{x}) \tag{3.60}$$

$$u = -\frac{1}{\frac{\hat{c}_{p1}\mathcal{V}(p_s-p_a)}{l_0-x}+\frac{\hat{c}_{n2}\mathcal{V}(p_b-p_r)}{x}} u_f\varepsilon(-u_{fd}) - \frac{1}{\frac{\hat{c}_{n1}\mathcal{V}(p_a-p_r)}{l_{0-x}}+\frac{\hat{c}_{p2}\mathcal{V}(p_s-p_b)}{x}} u_f\varepsilon(u_{fd}) \tag{3.61}$$

where

$$\mathbf{Y}_c = \begin{bmatrix} \dot{f}_p & \frac{\dot{x}}{l_0-x} & \frac{\dot{x}}{x} \end{bmatrix} \epsilon \mathbb{R}^{1\times 3} \tag{3.62}$$

$$\boldsymbol{\theta}_c = \begin{bmatrix} \frac{1}{B} & A_A & A_B \end{bmatrix}^T \epsilon \mathbb{R}^3 \tag{3.63}$$

f_{pr} is computed from (3.23), $\widehat{\boldsymbol{\theta}}_f$ and $\widehat{\boldsymbol{\theta}}_c$ depict the estimates of $\boldsymbol{\theta}_f$ and $\boldsymbol{\theta}_c$, respectively, $k_{fp} > 0$ and $k_x > 0$ are two feedback gains, and $\dot{x}_r > 0$ is calculated from the relation:

$$\dot{x}_r = \frac{u_2 l_0 \omega_r}{2\pi} \tag{3.64}$$

According to (3.56) and (3.57), the following conditions

$$\frac{\hat{c}_{p1}\mathcal{V}(p_s - p_a)}{l_0 - x} + \frac{\hat{c}_{n2}\mathcal{V}(p_b - p_r)}{x} > 0 \tag{3.65}$$

$$\frac{\hat{c}_{n1}\mathcal{V}(p_a - p_r)}{l_0 - x} + \frac{\hat{c}_{p2}\mathcal{V}(p_s - p_b)}{x} > 0 \tag{3.66}$$

must be met in order for (3.61) to be implementable. So that (3.61) may be inversely expressed from the view of (3.51) in the form

$$u_{fd} = -\mathbf{Y}_v(u)\widehat{\boldsymbol{\theta}}_v \tag{3.67}$$

The three parameter vectors estimates, i.e., $\widehat{\boldsymbol{\theta}}_f$, $\widehat{\boldsymbol{\theta}}_c$, and $\widehat{\boldsymbol{\theta}}_v$ require updating.

To do that, let

$$\boldsymbol{s}_f = (\dot{x}_r - \dot{x})\boldsymbol{Y}_f^{\mathrm{T}};\ \boldsymbol{s}_\tau = (\omega_r - \omega)\mathbf{Y}_{\boldsymbol{\tau}}^{\mathrm{T}} \tag{3.68}$$

$$\boldsymbol{s}_c = \left(f_{pr} - f_p\right)\mathbf{Y}_c^{\mathrm{T}} \tag{3.69}$$

$$\boldsymbol{s}_v = \left(f_{pr} - f_p\right)\mathbf{Y}_v^{\mathrm{T}} \tag{3.70}$$

The γ^{th} elements of $\widehat{\boldsymbol{\theta}}_f$, $\widehat{\boldsymbol{\theta}}_c$, and $\widehat{\boldsymbol{\theta}}_v$ are updated with the $\mathcal{P}$ function given as

$$\hat{\theta}_{f\gamma} = \mathcal{P}\left(s_{f\gamma}, \rho_{f\gamma}, \underline{\theta}_{f\gamma}, \overline{\theta}_{f\gamma}, t\right) \forall\, \gamma$$

$$\hat{\theta}_{\tau\gamma} = \mathcal{P}\left(s_{\tau\gamma}, \rho_{\tau\gamma}, \underline{\theta}_{\tau\gamma}, \overline{\theta}_{\tau\gamma}, t\right) \forall\, \gamma \tag{3.71}$$

$$\hat{\theta}_{c\gamma} = \mathcal{P}\left(s_{c\gamma}, \rho_{c\gamma}, \underline{\theta}_{c\gamma}, \overline{\theta}_{c\gamma}, t\right) \forall\, \gamma = 1,2,3 \tag{3.72}$$

$$\hat{\theta}_{v\gamma} = \mathcal{P}\left(s_{v\gamma}, \rho_{v\gamma}, \underline{\theta}_{v\gamma}, \overline{\theta}_{v\gamma}, t\right) \forall\, \gamma = 1,2,3,4 \tag{3.73}$$

where

$\hat{\theta}_{f\gamma}$	Is the γ^{th} element of $\widehat{\boldsymbol{\theta}}_f$.
$\hat{\theta}_{\tau\gamma}$	Is the γ^{th} element of $\widehat{\boldsymbol{\theta}}_\tau$.
$\hat{\theta}_{c\gamma}$	Is the γ^{th} element of $\widehat{\boldsymbol{\theta}}_c$.

$\hat{\theta}_{\upsilon\gamma}$	Is the γ^{th} element of $\hat{\boldsymbol{\theta}}_{\upsilon}$.
$s_{f\gamma}$	Is the γ^{th} element of $\mathbf{s}_f$
($s_{\tau\gamma}$	Is the γ^{th} element of $\mathbf{s}_{\boldsymbol{\tau}}$
$s_{c\gamma}$	Is the γ^{th} element of $\mathbf{s}_c$
$s_{\upsilon\gamma}$	Is the γ^{th} element of $\mathbf{s}_{\upsilon}$
$\rho_{f\gamma}$	Is parameter update gain
($\rho_{\tau\gamma}$	Is parameter update gain
$\rho_{c\gamma}$	Is parameter update gain
$\rho_{\upsilon\gamma}$	Is parameter update gain
$\underline{\theta}_{f\gamma}$	Is lower bound of $\theta_{f\gamma}$
$\underline{\theta}_{\tau\gamma}$	Is lower bound of $\theta_{\tau\gamma}$
$\underline{\theta}_{c\gamma}$	Is lower bound of $\theta_{c\gamma}$
$\underline{\theta}_{\upsilon\gamma}$	Is lower bound of $\underline{\theta}$
$\overline{\theta}_{f\gamma}$	Is upper bound of $\theta_{f\gamma}$
$\overline{\theta}_{\tau\gamma}$	Is upper bound of $\theta_{\tau\gamma}$
$\underline{\theta}_{c\gamma}$	Is lower bound of $\theta_{c\gamma}$
$\underline{\theta}_{\upsilon\gamma}$	Is lower bound of $\theta_{\upsilon\gamma}$
$\theta_{f\gamma}$	Is γ^{th} element of $\boldsymbol{\theta}_{\boldsymbol{f}}$ defined in (3.38)
$\theta_{\tau\gamma}$	Is γ^{th} element of $\boldsymbol{\theta}_{\boldsymbol{\tau}}$ defined in (3.39)
$\theta_{c\gamma}$	Is γ^{th} element of $\boldsymbol{\theta}_{\boldsymbol{f}}$ defined in (3.63)
$\theta_{\upsilon\gamma}$	Is γ^{th} element of $\boldsymbol{\theta}_{\boldsymbol{\upsilon}}$ defined in (3.54)

3.5.4 Non-Negative Accompanying Function for Fluid Dynamics

A non-negative accompanying function and its derivative are given by the following Lemma, with respect to the foregoing fluid dynamics and the respective control equations.

Lemma 3.2. *Consider the hydraulic actuator dynamics described by (3.36) – (3.39), (3.51) and (3.52) together with the control equations (3.59), (3.60), and (3.62) - (3.72). The time derivative of*

$$v_c = \tfrac{1}{2B}\left(f_{pr} - f_p\right)^2 + \tfrac{1}{2B}\left(\tau_{pr} - \tau_p\right)^2 + \tfrac{k_x}{2}\textstyle\sum_\gamma\left(\theta_{f\gamma} - \hat{\theta}_{f\gamma}\right)^2/\rho_{f\gamma} + \tfrac{k_\omega}{2}\textstyle\sum_\gamma\left(\theta_{\tau\gamma} - \hat{\theta}_{\tau\gamma}\right)^2/\rho_{f\gamma} + \tfrac{1}{2}\textstyle\sum_{\gamma=1}^{3}\left(\theta_{c\gamma} - \hat{\theta}_{c\gamma}\right)^2/\rho_{c\gamma} + \tfrac{1}{2}\textstyle\sum_{\gamma=1}^{4}\left(\theta_{v\gamma} - \hat{\theta}_{v\gamma}\right)^2/\rho_{c\gamma} \tag{3.74}$$

is

$$\dot{v}_c = -k_{fp}\left(f_{pr} - f_p\right)^2 - k_{\tau p}\left(\tau_{pr} - \tau_p\right)^2 - k_x(f_{cr} - f_c)(\dot{x}_r - \dot{x}) - k_\omega(\tau_{cr} - \tau_c)(\omega_r - \omega) \tag{3.75}$$

Proof: It ensues from (51), (60) (62) and (63) that

$$u_{fd} - u_f = \tfrac{1}{B}\left(\dot{f}_{pr} - \dot{f}_p\right) - \mathbf{Y}_c\left(\boldsymbol{\theta}_c - \hat{\boldsymbol{\theta}}_c\right) + k_{fp}\left(f_{pr} - f_p\right) + k_x(\dot{x}_r - \dot{x}) \tag{3.76}$$

holds. Differentiating (3.74) with respect to time and calling (3.36) and (3.37), (3.38) and (3.39), (3.51), (3.59), (3.64) - (3.72), and Lemma 2.9 of (Zhu 2010, p.32) yield

$$\begin{aligned}
\dot{v}_c = {} & \left(f_{pr} - f_p\right)\frac{1}{B}\left(\dot{f}_{pr} - \dot{f}_p\right) - \left(\tau_{pr} - \tau_p\right)\frac{1}{B}\left(\dot{\tau}_{pr} - \dot{\tau}_p\right) - \sum k_x\left(\theta_{f\gamma} - \hat{\theta}_{f\gamma}\right)\frac{\dot{\hat{\theta}}_{f\gamma}}{\rho_{f\gamma}} \\
& - \sum k_\omega\left(\theta_{\tau\gamma} - \hat{\theta}_{\tau\gamma}\right)\frac{\dot{\hat{\theta}}_{\tau\gamma}}{\rho_{\tau\gamma}} - \sum_{\gamma=1}^{3}(\theta_{c\gamma} - \hat{\theta}_{c\gamma})\frac{\dot{\hat{\theta}}_{c\gamma}}{\rho_{c\gamma}} - \sum_{\gamma=1}^{4}(\theta_{v\gamma} - \hat{\theta}_{v\gamma})\frac{\dot{\hat{\theta}}_{v\gamma}}{\rho_{v\gamma}} \\
= {} & \left(f_{pr} - f_p\right)\left(u_{fd} - u_f\right) + \left(f_{pr} - f_p\right)\mathbf{Y}_c\left(\boldsymbol{\theta}_c - \hat{\boldsymbol{\theta}}_c\right) - k_{fp}\left(f_{pr} - f_p\right)^2 \\
& - k_x\left(f_{pr} - f_p\right)(\dot{x}_r - \dot{x}) - \left(\tau_{pr} - \tau_p\right)\frac{1}{B}\left(\dot{\tau}_{pr} - \dot{\tau}_p\right) \\
& - \sum_\gamma k_x\left(\theta_{f\gamma} - \hat{\theta}_{f\gamma}\right)\dot{\hat{\theta}}_{f\gamma}/\rho_{f\gamma} - \sum_\gamma k_\omega\left(\theta_{\tau\gamma} - \hat{\theta}_{\tau\gamma}\right)\dot{\hat{\theta}}_{\tau\gamma}/\rho_{\tau\gamma} \\
& - \sum_{\gamma=1}^{3}(\theta_{c\gamma} - \hat{\theta}_{c\gamma})\dot{\hat{\theta}}_{c\gamma}/\rho_{c\gamma} - \sum_{\gamma=1}^{4}\left(\theta_{v\gamma} - \hat{\theta}_{v\gamma}\right)\dot{\hat{\theta}}_{v\gamma}\Big/\rho_{v\gamma}
\end{aligned}$$

$$= -k_{fp}\left(f_{pr}-f_p\right)^2 - k_x(f_{cr}-f_c)(\dot{x}_r-\dot{x}) + k_x(\dot{x}_r-\dot{x})\mathbf{Y}_{\mathrm{f}}\left(\boldsymbol{\theta}_{\mathrm{f}}-\widehat{\boldsymbol{\theta}}_{\mathrm{f}}\right)$$
$$-\sum_{\gamma} k_x\left(\theta_{\mathrm{f}\gamma}-\hat{\theta}_{f\gamma}\right)\dot{\hat{\theta}}_{f\gamma}/\rho_{f\gamma} + \left(\mathrm{f}_{\mathrm{pr}}-\mathrm{f}_{\mathrm{p}}\right)\mathbf{Y}_{\mathrm{c}}\left(\boldsymbol{\theta}_{\boldsymbol{c}}-\widehat{\boldsymbol{\theta}}_{\mathrm{c}}\right)$$
$$-\sum_{\gamma=1}^{3}\left(\theta_{c\gamma}-\hat{\theta}_{c\gamma}\right)\frac{\dot{\hat{\theta}}_{c\gamma}}{\rho_{c\gamma}} + \left(\mathrm{f}_{\mathrm{pr}}-\mathrm{f}_{\mathrm{p}}\right)\mathbf{Y}_{\mathrm{v}}\left(\boldsymbol{\theta}_{\boldsymbol{v}}-\widehat{\boldsymbol{\theta}}_{\boldsymbol{v}}\right) - \sum_{\gamma=1}^{4}\left(\theta_{v\gamma}-\hat{\theta}_{v\gamma}\right)\frac{\dot{\hat{\theta}}_{v\gamma}}{\rho_{v\gamma}}$$
$$-\left(\tau_{\mathrm{pr}}-\tau_{\mathrm{p}}\right)\frac{1}{\mathrm{B}}\left(\dot{\tau}_{\mathrm{pr}}-\dot{\tau}_{\mathrm{p}}\right) - \sum_{\gamma} k_x\left(\theta_{\tau\gamma}-\hat{\theta}_{\tau\gamma}\right)\dot{\hat{\theta}}_{v\gamma}/\rho_{v\gamma}$$

$$\leq -k_{fp}\left(f_{pr}-f_p\right)^2 - k_x(f_{cr}-f_c)(\dot{x}_r-\dot{x}) - k_{\tau p}\left(\tau_{pr}-\tau_p\right)^2 - k_\omega(\tau_{cr}-\tau_c)(\omega_r-\omega) \tag{3.77}$$

3.6 Virtual Stability of the Hydraulic Manipulator

The virtual stability of the hydraulic actuator- composed of a shaft and piston driven by hydraulic fluid is given by the theorem 3.2.

Theorem 3.2. The hydraulic rotary actuator described by (3.1) - (3.3), (3.6), (3.7), (3.8), (3.9), (3.11) - (3.15), (3.21) - (3.23), (3.59), (3.60) and (3.62) - (3.66) and with the parameter adaptation (3.16) - (3.19), and (3.68) - (3.72), is virtually stable with its affiliated vectors and variables $\left({}^{\mathbf{B_1}}\mathbf{V}_{\boldsymbol{r}} - {}^{\mathbf{B_1}}\mathbf{V}\right)$, $\left({}^{\mathbf{B_2}}\mathbf{V}_{\boldsymbol{r}} - {}^{\mathbf{B_2}}\mathbf{V}\right)$, and $\left(f_{pr}-f_p\right)$ and $\left(\tau_{pr}-\tau_p\right)$ being virtually functions in both L_2 and L_∞, in the sense of Definition 2.10.

The proof for this theorem is possible from Lemmas (3.1) and (3.2), and equations (3.26) and (3.28).

When every subsystem of the rest of the manipulator qualifies to be virtually stable in the sense of Definition 2.10, it follows from Theorem 2.1 that

$$\left(f_{pr}-f_p\right) \epsilon\ L_2 \cap L_\infty \tag{3.78}$$

$$\left(\tau_{pr}-\tau_p\right) \epsilon\ L_2 \cap L_\infty \tag{3.79}$$

$$\left({}^{\mathbf{T}}\mathbf{V}_{\boldsymbol{r}} - {}^{\mathbf{T}}\mathbf{V}\right) \epsilon\ L_2 \cap L_\infty \tag{3.80}$$

$$\left({}^{\mathbf{B_2}}\mathbf{V}_{\boldsymbol{r}} - {}^{\mathbf{B_2}}\mathbf{V}\right) \epsilon\ L_2 \cap L_\infty \tag{3.81}$$

$$\left({}^{\mathbf{B_1}}\mathbf{V}_{\boldsymbol{r}} - {}^{\mathbf{B_1}}\mathbf{V}\right) \epsilon\ L_2 \cap L_\infty \tag{3.82}$$

$$(\dot{x}_r-\dot{x}) \epsilon\ L_2 \cap L_\infty \tag{3.83}$$

$$(x_d-x) \epsilon\ L_2 \cap L_\infty \tag{3.84}$$

3.7 Virtual Stability in View of Adaptive Backlash Inverse Control

When backlashes of the helical (splines) gears on the shaft and the piston are taken into account in the controller design, the issue of stability of the controller changes. The question of whether the manipulator remains stable when the force and or torque of the actuator is adaptively controlled by an adaptive inverse scheme described in section 2.8.2 need to be addressed. The following theorem ensures the stability of the hydraulic manipulator when simultaneously controlled with the VDC and adaptive backlash inverse controller- that is, backlash inverse compensated VDC controller.

Theorem 3.3. The hydraulic actuator described by (3.1) - (3.3), (3.6), (3.7), (3.8), (3.9), (3.11) - (3.15), (3.21) - (3.23), (3.59), (3.60) and (3.62) - (3.66) and with the parameter adaptation (3.16) - (3.19), and (3.68) - (3.72), such that the force/ torque and/ or velocity/ angular speed of the actuator is adaptively controlled with (2.39) - (2.42), is virtually stable with its affiliated vectors and variables $\left({}^{\mathbf{B_1}}\mathbf{V}_r - {}^{\mathbf{B_1}}\mathbf{V}\right)$, $\left({}^{\mathbf{B_2}}\mathbf{V}_r - {}^{\mathbf{B_2}}\mathbf{V}\right)$, $\left(f_{pr} - f_p\right)$, and $\left(\tau_{pr} - \tau_p\right)$, $(\dot{x}_r - \dot{x}) \epsilon\, L_2 \cap L_\infty$, and $(x_d - x) \epsilon\, L_2 \cap L_\infty$ being virtual functions in both L_2 and L_∞, in the sense of Definition 2.10.

Proof: Without loss of generality, assume that the backlash in the hydraulic rotary manipulator is parametrized as described in Chapter 2 and its inverse is likewise adaptively parametrized according to (2.57) and (2.58). Furthermore, if the adaptation law (2.65), under the parameter projection function (2.73) are used to adaptively tune the parameters of the backlash inverse real-time (online), then it follows according to Tao and Kokotovic (1996) that if the initial parameter estimations are within the bounds necessary for the convergence of the parameters (that is, (2.68) - (2.70)), such that the unparametrized term $d_b(t)$ vanishes at time $t > t_0 > 0$, then the stability of the hydraulic rotary actuator remains unchanged

Hence, the entire hydraulic manipulator is guaranteed stable under the resulting backlash inverse compensated VDC controller.

Remark 3.6. *Thus, the issue of virtual stability of the hydraulic rotary actuator controlled by a combination of VDC and adaptive backlash inverse is addressed, and the main task is to ensure that the parameter estimates are set within the required convergence region.*

4. EXPERIMENTAL IMPLEMENTATION

This chapter presents the experimental implementation procedure, as well as the result obtained from the real-time experiments performed with the designed controllers. Section 4.1 presents the experimental set-up, followed by a presentation of the control law for the PID control in section 4.2. Section 4.3 Analyses the results obtained by VDC approach. Finally, a comparison is made between the results obtained by PID and the two VDC controller implementations.

4.1 Experimental Set-up

The experimental implementations of the designed controller were conducted at the heavy machinery laboratory of Automation and Hydraulics of Tampere University of Technology.

Firstly, the VDC control equations, (presented in earlier chapters) were applied to the studied manipulator, using model developed in Matlab/ Simulink environment. After a satisfactory behaviour of the off-line simulation model, further steps were taken to implement the designed controller in real-time environment.

Therefore, the tested VDC model was then compiled to real-time and the code was loaded into dSpace CP1103 PPC controller board available in the laboratory. The controller board has embedded real-time processor and several I/O with high speed and accuracy. The controlled system was controlled and monitored with dSpace ControlDesk 3.7.1, which was also used to capture and record measured system data during simulations. The required derivatives of different signals were obtained using the estimation algorithm presented in (Harrison and Stoten 1995). This algorithm overcomes the noise issue associated with the often-applied backward difference approach. The algorithm is simply expressed as:

$$\dot{x}(kT) = \frac{5x(kT)+3x(kT-T)+x(kT-2T)-x(kT-3T)-3x(kT-4T)-5x(5T)}{35T} \quad (4.1)$$

where x is the signal for which derivative is desired, $\dot{x}$ is the differentiated signal of x, and T is the sample time (or hold time) of the system. A sample time of 1 ms was applied throughout the experimentation phase of this work.

The parameter vectors $\boldsymbol{\theta}_{\boldsymbol{B_1}} \in \mathbb{R}^{13}$ and $\boldsymbol{\theta}_{\boldsymbol{B_2}} \in \mathbb{R}^{13}$, which contain uncertain parameters of the rigid links were determined by direct measurements and computations accordingly. The computed rigid body parameters as well as the valve flow coefficients parameter vector, $\boldsymbol{\theta}_v \epsilon \mathbb{R}^4$ and cylinder control parameter vector, $\boldsymbol{\theta}_c \epsilon \mathbb{R}^3$ are presented in Appendix B.

The angular rotation of the actuator shaft was measured with the *posital fraba* incremental encoder with accuracy of $\pm 0.0878°$ ($\leq 12\ bit$). The encoder can measure angular position up to 6000 rev /min of speed.

Pressure signals in the system, including the supply pressure and pressures in either chambers of the actuator, were measured with Trafag NAH (type 8253.74.2317) hydraulic pressure transmitters having measurement capability of between 0 bar and 250 bar. The pressure resolution of the transmitter is 0.25 bar. The tank pressure was not measured, but assumed constant at value 0 bar- a valid assumption. The pressure signals were filtered using the Geometric Moving Average (GMA) filter algorithm. The algorithm is given as equation (4.2).

$$y(T) = (1 - \sigma_{GMA})y(T-1) + \sigma_{GMA}u(T) \tag{4.2}$$

where u is the signal to be filtered and σ_{GMA} is a filter constant, which was taken to be 0.6 throughout this experimentation.

The Bosch Rexroth servo valve 4WRPEH40C40P-2X/G24A1M with nominal flow of 40 l/min @ 75 bar ($\Delta p = 35$ bar /metering notch) and a bandwidth of 100 Hz @$\pm 5\%$ signals was used in controlling the actuator. Thus, the response of the valve is fast enough to justify the assumption of neglecting its dynamics as applied in the development of VDC control equations.

4.2 PID-Controller Design

As earlier set out as an objective, the experimental results obtained from the designed VDC controller are compared with those of the classical PID control approach. The control equation of PID controller in the actuator space may be written as

$$0 = k_P e(t) + k_I \int_0^t e(t)dt + k_D \dot{e}(t) \tag{4.3}$$

where

$$\theta_{des}(t) - \theta_{mes}(t) = e(t) \tag{4.4}$$

$$\dot{\theta}_{des}(t) - \dot{\theta}_{mes}(t) = \dot{e}(t) \tag{4.5}$$

with the proportional gain k_P, the integral gain k_I, and the derivative gain k_D all being non-negative numbers greater than or equal to zero. The angular position tracking error term denoted as $e(t)$ represents the difference between the desired and the actual (measured) position. The derivative of $e(t)$, given as $\dot{e}(t)$ represents the velocity error in the control and it is penalized by the derivative gain.

In line with Ziegler-Nichols approach (Ziegler and Nichols 1942), the PID controller gains were tuned to achieve the best possible position control result. That is, the critical gain k_c was obtained by adjusting the proportional gain k_P to the point where the position output started to oscillate with a frequency of $\frac{1}{T_c}$. Thereafter, the PID controller gains were computed as half of the critical gain for the k_p and as a function of the oscillation frequency (period) for the other two gains as follows

$$k_P = \frac{k_c}{2} \tag{4.6}$$

$$k_I = 2\frac{k_p}{T_c} \tag{4.7}$$

$$k_D = \frac{k_P T_c}{8} \tag{4.8}$$

4.3 Task Space Position Control

The main control objective in this study was to effect the position control in the end effector space. Therefore, there is a necessity to convert the desired end-effector position (and velocity) trajectory to the desired joint motion trajectory.

In order to visualize the effect of backlash in the motion of the rotary actuator, a sinusoidal position trajectory (Figure 4.1) was used as the Cartesian position trajectory. So that the corresponding velocity trajectory may be obtained as a derivative of the position trajectory. The sinusoidal wave described by equation (4.9) was generated by a time-based sine wave generator with a frequency of 1 rad/s, amplitude of 10 degrees and a bias of 12 degrees to allow the oscillation of the controlled object (arm) about the 12 degrees, since the motion of the actuator is only limited to positive angles only. That is, if the offset were not included, the oscillating motion would be performed about the zero degree position of the actuator shaft, meaning that the amplitude of the motion trajectory would have to go between ± 10 degrees, which would not be feasible due to the mechanical constraint on the motion of the actuator.

$$\theta(t) = 10° sin(1t + 0) + 12° \tag{4.9}$$

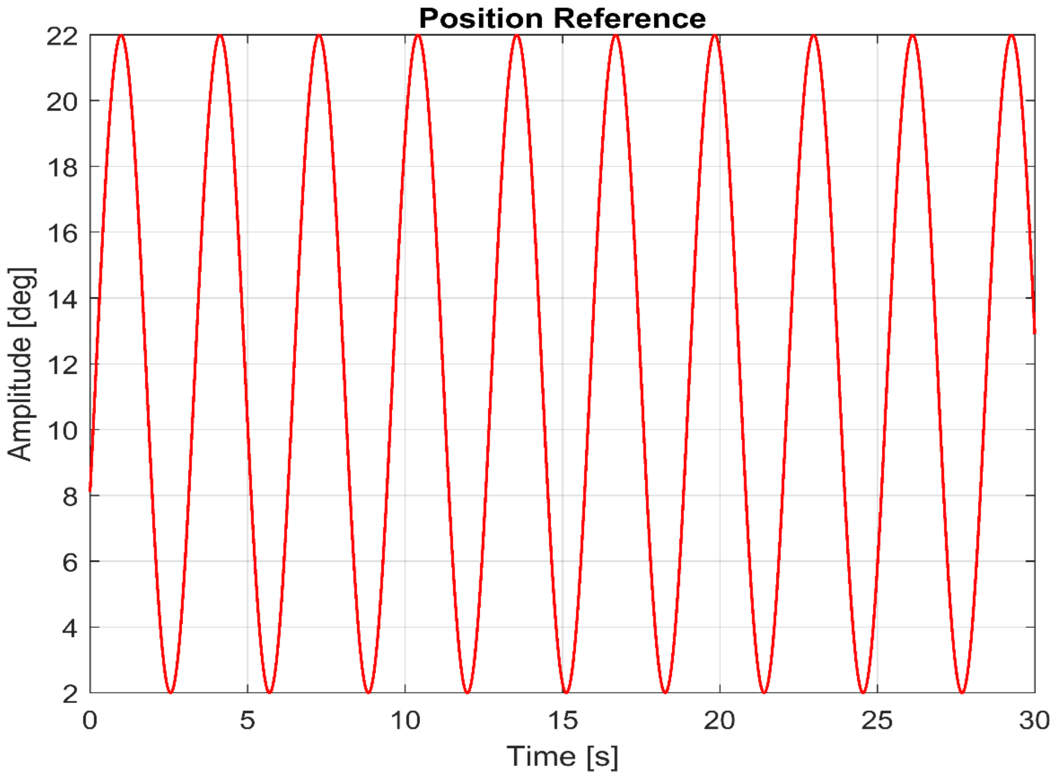

Figure 4.1. *Desired sinusoidal position trajectory.*

4.4 Experimental Results

With PID controller, the manipulator was driven through the described sinusoidal trajectory, followed by the VDC controller without and with backlash compensation, respectively. The tuned parameters applied in the three separate control approaches are presented in Table 4.1, where λ is the VDC position feedback gain, which is a parameter discussed in section 2.7.3 and described thoroughly in (Zhu 2010, p.50), and Γ_N is the backlash inverse parameter adaptation step size and K_{AG} is an adaptive gain (Tao and Kokotovic 1996).

Table 4.1. *PID and VDC/ BSI Controllers Parameters.*

PID Controller	VDC Controller	VDC Controller with Backlash Inverse Compensation
$k_P = 0.100$	$k_x = 2 \times 10^{-2}$	$k_x = 2 \times 10^{-2}$
$k_I = 0.005$	$k_{fp} = 6 \times 10^{-8}$	$k_{fp} = 6 \times 10^{-8}$
$k_D = 0.001$	λ= 5	λ= 0.6
		$K_{AG} = 0.5$
		$\Gamma_N = ([0.02, 0.02, 0.02])$

4.4.1 PID Controller

Using the given PID controller gains, measured position trajectory of the end effector is plotted on the same axes with the desired sinusoidal position trajectory (Figure 4.1) as shown in Figure 4.2 (a). A zoomed view of the same plot is presented in Figure 4.2 (b) to reveal the dual effects of backlash, which are the loss of information at the turning points (that is, where there are a changes of direction) of the motion as well as extra delayed system response. Attempts to increase the PID gains further results in noisy system response.

The loss of information is shown by the flatness at the top of the measured position trajectory, which corresponds to the instances when there were input signal without corresponding motion output on the actuator output shaft. As expected, it has been demonstrated that in the presence of backlash, the control accuracy of the linear PID controller is not impressive as revealed by the position tracking error of this motion (Figure 4.3), and as would be demonstrated numerically subsequently.

Other measured system data under the PID control approach are presented in Appendix C. The data presented include those of the normalized valve control signals, pressure signals (supply pressure and chambers A and B pressures) as well as measured arm velocity (deg. /s).

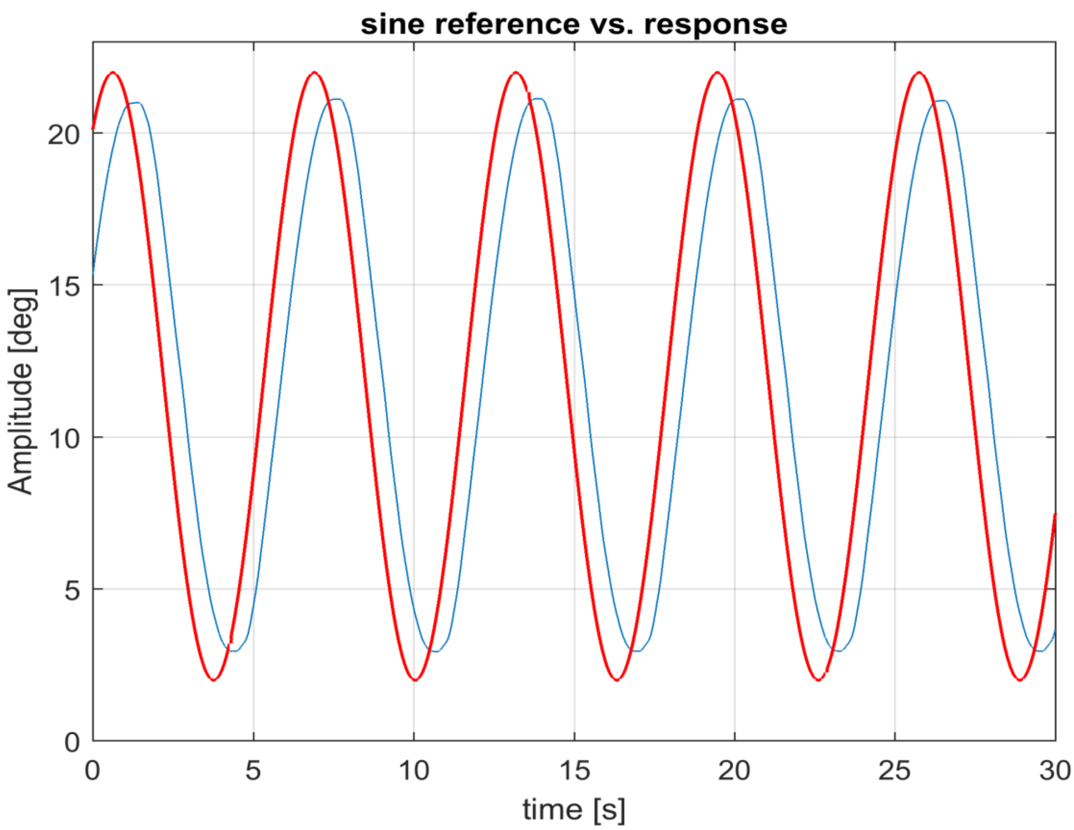

(a)

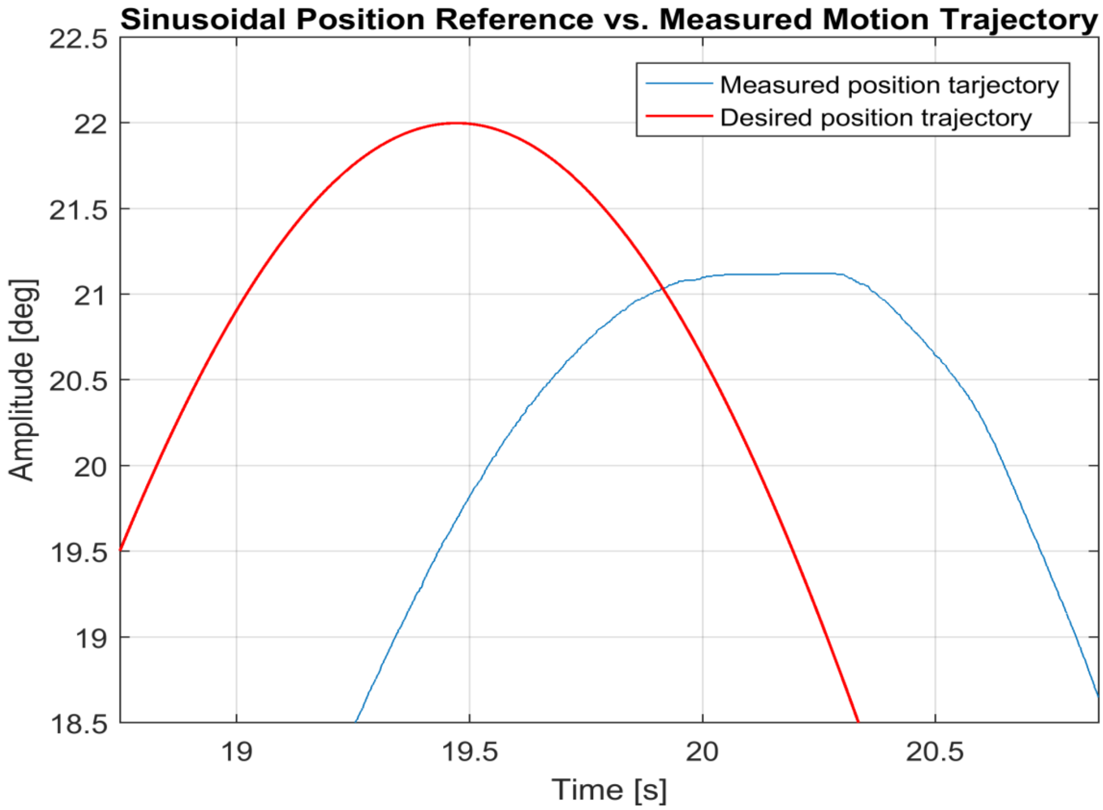

(b)

Figure 4.2: *(a) Measured position trajectory vs. sinusoidal position trajectory under PID controller (b) Zoomed view of (a).*

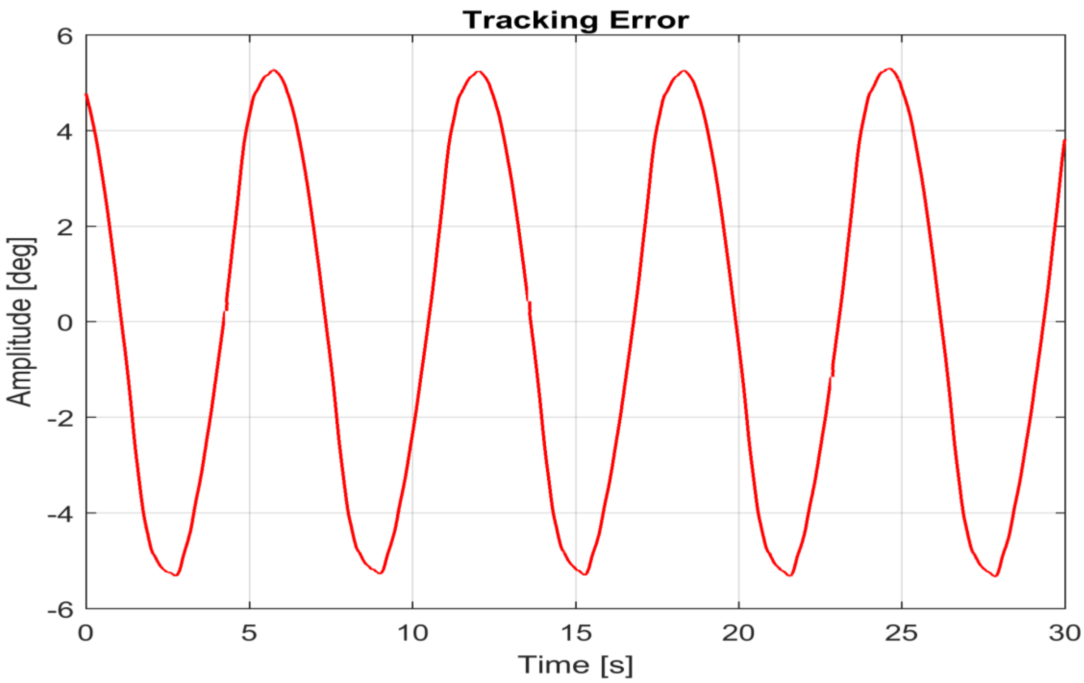

Figure 4.3. *Position tracking error under PID control.*

4.4.2 VDC Controller without Backlash Compensation

In this section, the VDC control equations designed and presented in Chapter three are implemented on the target system using the dSpace real-time environment. The system was commanded with the same sinusoidal position reference signal as done in the PID experimentation presented in the preceding sub-section.

The angular position trajectory of the end effector was captured and compared with the reference signal. The desired angular position trajectory and the measured position trajectory are as shown in Figure 4.4 (a) and likewise as in the case of PID controller, a zoomed view of the lower portion of the plot is given in Figure 4.4 (b). It is glaring from Figure 4.4 (b) that the backlash nonlinearity introduce some strange movements at the extremums of the end effector motion, probably due to the attempt of the non-linear controller to maintain good reference tracking, despite the backlash dynamics. The deviation of the actual motion trajectory from the desired (that is, position tracking error) is plotted in Figure 4.5. Other measurement data under this controller are also presented as plots in Appendix C.

As may be deduced from a comparison of Figures 4.2 (a and b) and 4.4 (a and b), despite the effects of backlash on reference tracking (in this case, the performance of the nonlinear model-based controller (that is, VDC) without consideration for backlash compensation is all ready visibly better than that of the linear PID controller. The superiority of the VDC controller without backlash compensation over the PID controller is also justified mathematically below. However, this controller performance is still quite unacceptable, for example, in applications that require very high precision control as in robotics.

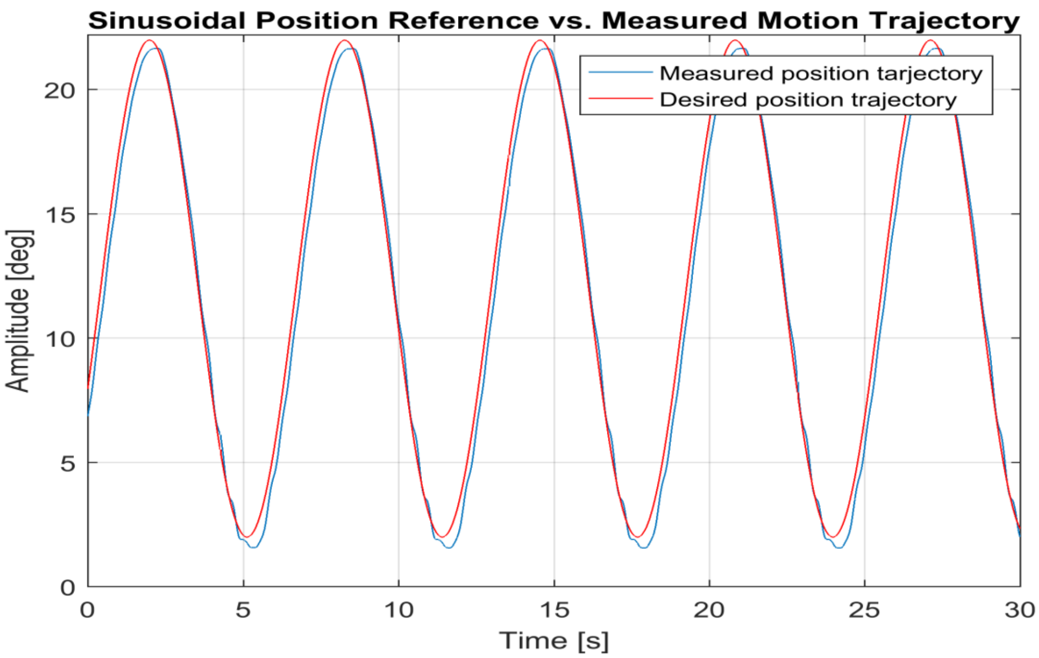

(a)

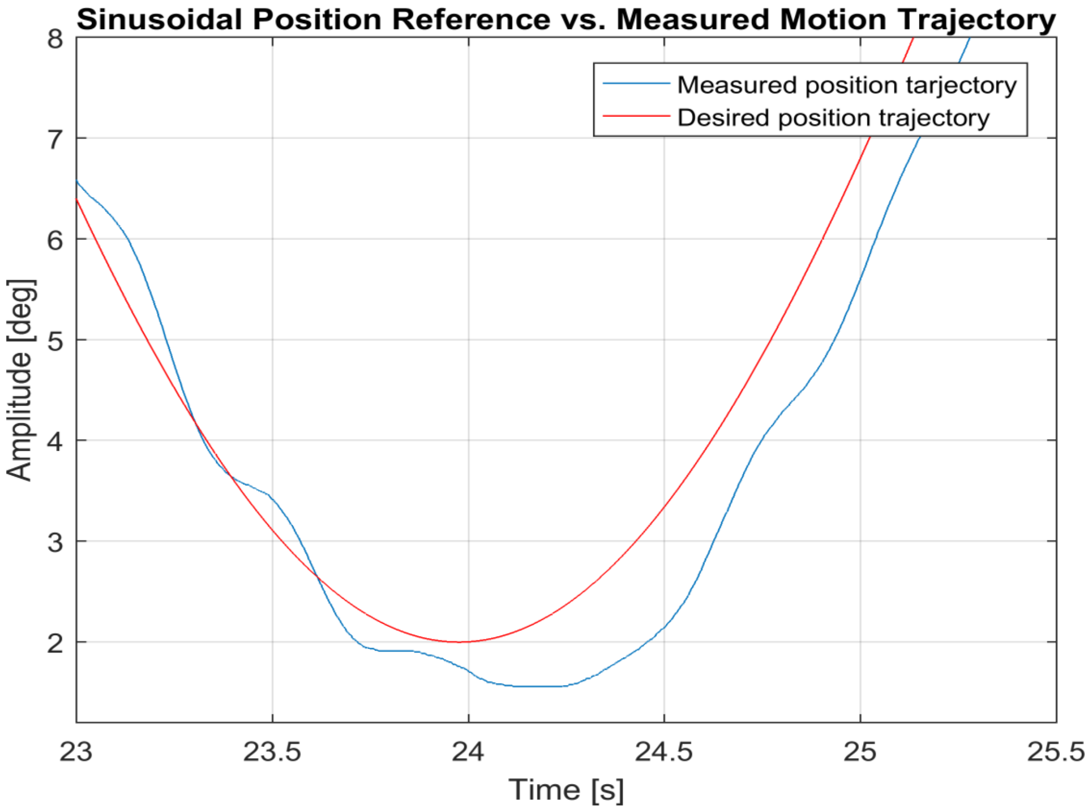

(b)

Figure 4.4. *(a) Measured position trajectory vs. sinusoidal position trajectory under VDC controller. (b) Zoomed view of (a).*

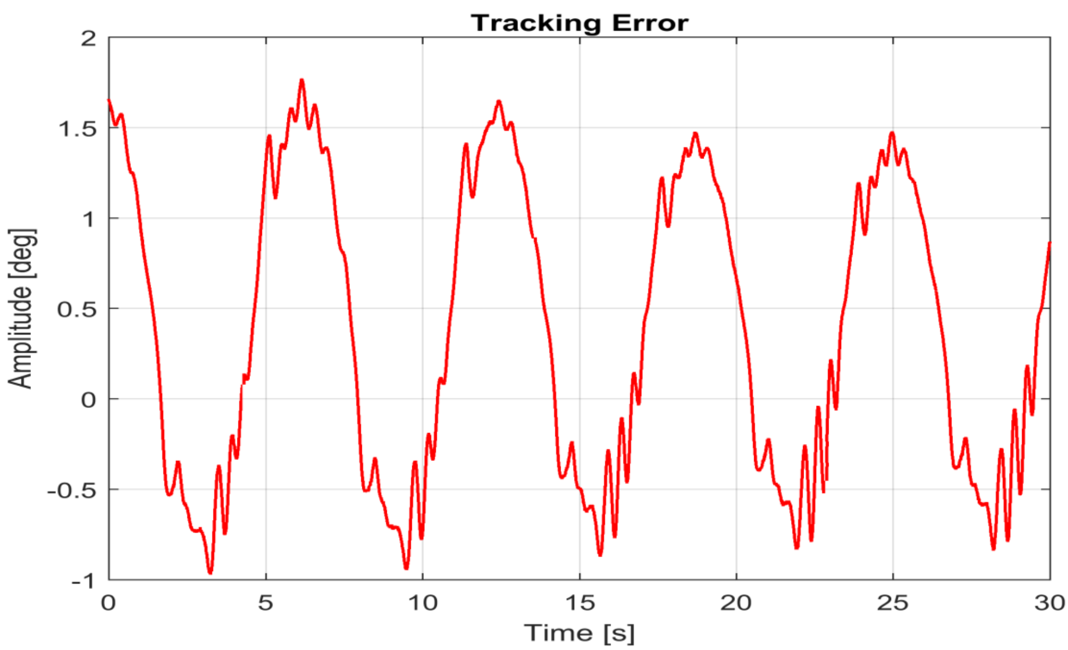

Figure 4.5: *Position tracking error under VDC controller without backlash compensation.*

According to (Mattila et al. 2016), a good universal metric for evaluating the performances of different n-degree of freedom manipulators is the performance indicator μ, which was introduced in Zhu and Piedboeuf (2005), Zhu and Vukovich (2005), and Zhu et al. (2013). The performance indicator, in normalized form, is given as

$$\mu = \frac{\max(|\boldsymbol{\theta}_{\mathrm{des}} - \boldsymbol{\theta}|)}{\max(|\dot{\boldsymbol{\theta}}|)} = \frac{|e|_{\max}}{|\dot{\boldsymbol{\theta}}|_{\max}} \tag{4.8}$$

where $\boldsymbol{\theta}_{\mathrm{des}}$ is the desired angular position vector and $\boldsymbol{\theta}$ is the actual measured angular position vector. The metric μ is such that the smaller its value, the better the performance of a particular controller. It quantifies the trajectory tracking capability of a manipulator, and the justification for its appeal is that high velocities in the task space correspond to big accelerations and consequently large position tracking errors. (Mattila et al. 2016.)

For the two controllers implemented above, the performance indicator μ are computed, respectively to be *0.0931 s* $\left(\text{that is, } \frac{|-5.3319|\ deg}{|57.2958|\frac{deg}{s}}\right)$ and *0.0309 s* $\left(\text{that is, } \frac{1.7732\ deg}{57.2958\frac{\mathrm{deg}}{\mathrm{s}}}\right)$ for PID and VDC. As also deduced from the comparison of the error plots for the two controllers, the μ value obtained for the VDC controller is significantly (about 66%) lower than that obtained for the linear controller.

However, the maximum tracking error of the VDC controller is still relatively big. Therefore, it became imposing to incorporate backlash compensation into the VDC controller implementation using the approach presented in Tao and Kokotovic (1996) and described in Chapter 2 of this thesis. From Figure 4.4, it may be inferred that when the dual effects of backlash are nearly neutralized (or possibly completely eliminated), by an appropriately parametrized and initialized adaptive inverse scheme, the performance of the VDC controller would be even further greatly enhanced, and the maximum tracking error can be significantly reduced.

4.4.2 VDC Controller with Backlash Compensation

The manufacturer's datasheet of the hydraulic rotary actuator used in the target system gives an estimate of backlash in the actuator to be maximum of $20'$. As stated in Ahmed and Khorrami (1999), this value serves as a preliminary value for parametrization of the backlash dynamics according to the model presented in Chapter 2. That is, the parameters c_r and c_l, respectively have maximum absolute value of $\frac{1}{3^{\circ}}$. Even though the actual values may be very far away from this value (depending on the operating conditions), its knowledge prevents wild guesses and enables appropriate initialization of the adaptive backlash inverse compensator.

The total backlash of the actuator may be assumed to comprise that between the output shaft and the piston, as well as the one between the piston and the housing mounted ring.

In addition, there may exist hydraulic backlash resulting from the compression of hydraulic oil in the actuator. However, the main assumption in this thesis about the backlash nonlinearity is that the dominant backlash of the hydraulic manipulator is the mechanical backlash, which exists between the rigid bodies. Furthermore, for simplicity, the total backlash nonlinearity has been lumped to the connection between the actuator output shaft and the piston.

The adaptive backlash inverse controller was constructed and implemented into the real-time environment. Starting with initial estimates of 0.2° and 0.2° for $\hat{c}_r$ and $\hat{c}_l$, respectively, and using a value of 0.25 as the backlash slope estimate $\hat{m}$, that is the backlash inverse parameter estimation vector was initialized as $\theta_b = (0.05\ 0.25\ 0.05)$. Based on the adaptive backlash inverse control algorithm, the backlash parameter vector θ_b finally converged to $(0.006946, 0.34594, -0{,}005205)$ after a simulation time of about 120 s. These values correspond approximately to the values $1.206'$ and $-0.9'$ for c_r and c_l, respectively.

Figure 4.6 (a) gives a graphical view of the elements of θ_b during the first 120 s of the simulation run, while Figure 4.6 (b) depicts the steady state plot of the same elements. Similarly, a graphical representation of the elements of the adaptive backlash inverse regressor vector ω_b during the first 120 s of simulation run is presented in Figure 4.7 (a), while Figure 4.7 (b) presents the steady state graph of the same elements.

As can be seen in Figures 4.8 and 4.9, the position tracking performance of the manipulator with a reference signal of amplitude 10° and bias 12° improved significantly with the incorporation of backlash compensation, despite the fact that VDC's parameter adaptation law has not been implemented. The maximum steady state tracking error reduced from $1.7732°$ for VDC controller without backlash compensation to about $0.02761°$ when the backlash compensation is factored in. The parameters of the adaptive backlash inverse compensation were selected such that, as presented in Table 4.1, the adaptive step size matrix $\Gamma_N = diag(\Omega_1, \Omega_2, \Omega_3)$ where $\Omega_1 = \Omega_2 = 0.02$, and $\Omega_3 = 0.02$. The adaptive gain $K_{AG} = 0.5$. (Tao and Kokotovic 1996.)

Appendix D presents the C-codes used in implementing the adaptive backlash inverse compensation algorithm.

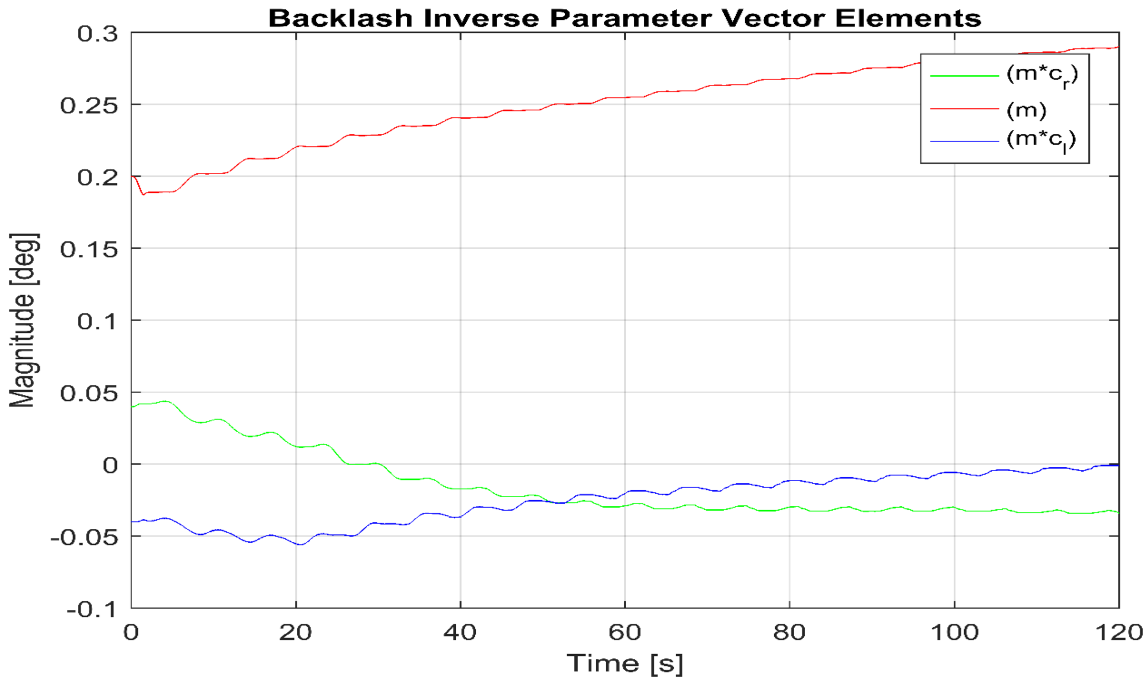

(a)

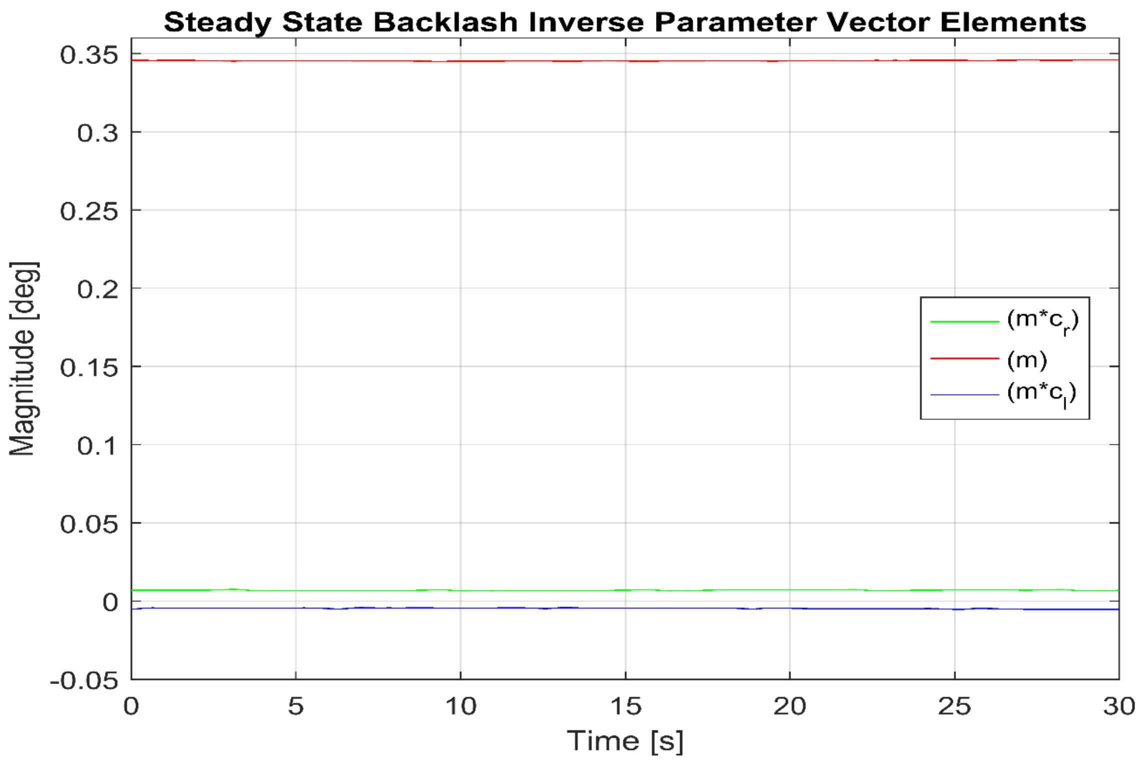

(b)

Figure 4.6. *(a) Transient values of the adaptive backlash inverse parameter vector (θ_b) elements during simulation run. (b) Steady state values of the BSI parameter vector.*

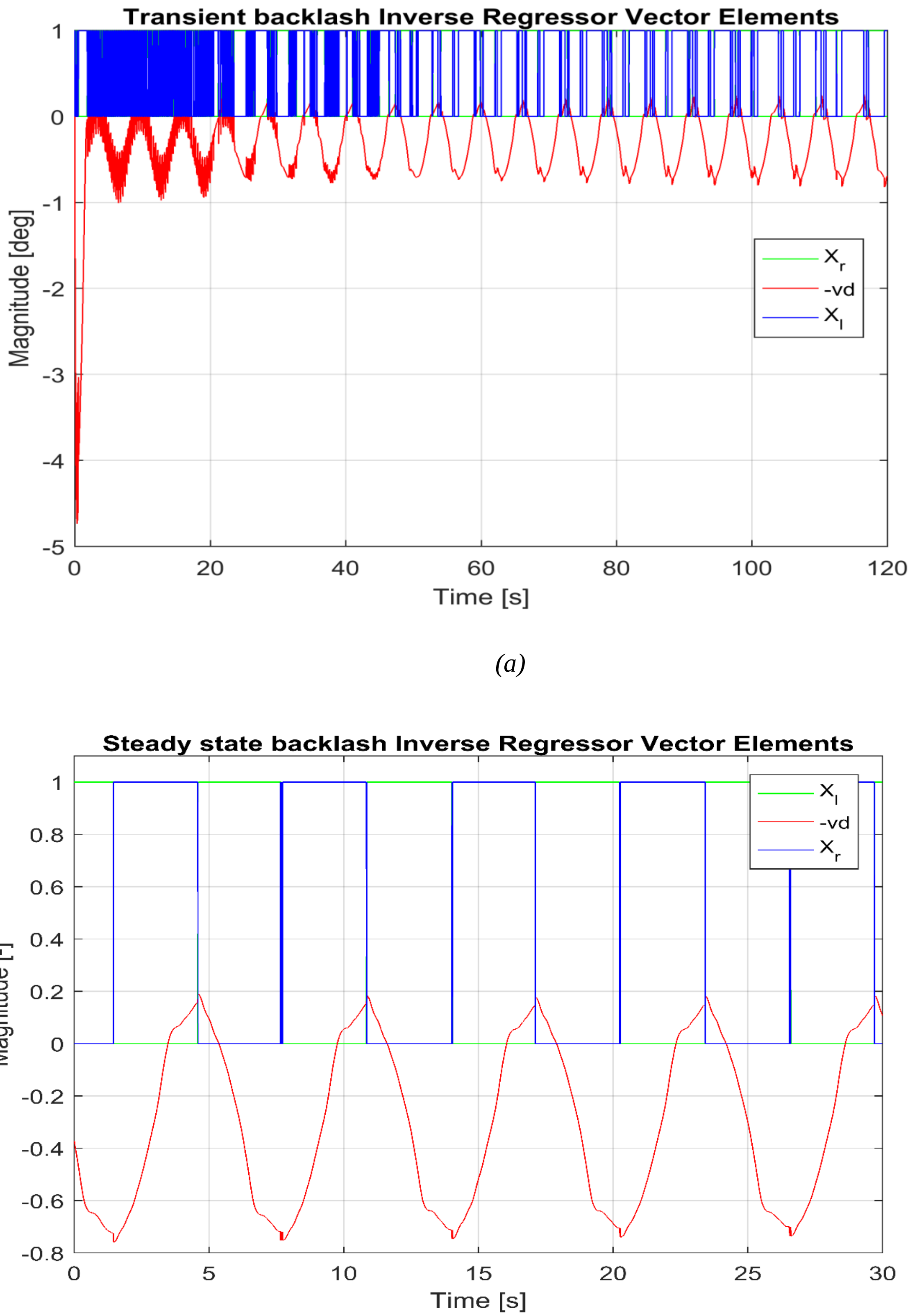

(a)

(b)

Figure 4.7. *Steady state plot of the parametrized backlash inverse regressor vector elements during simulation run.*

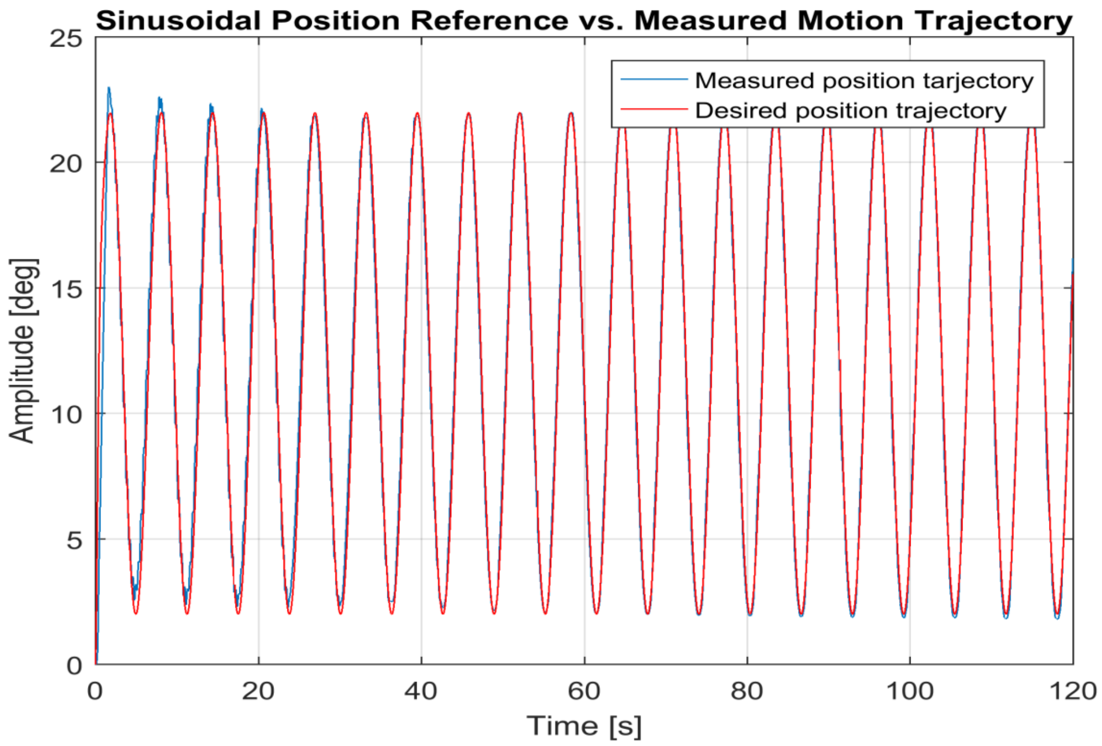

(a)

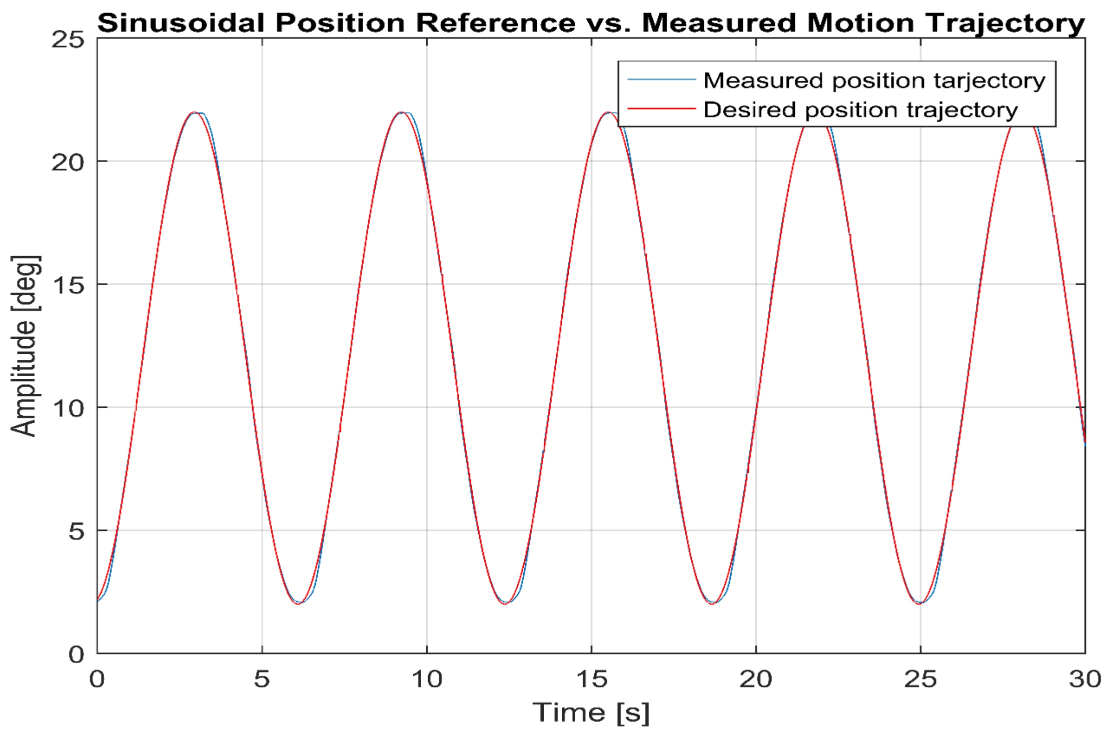

(b)

Figure 4.8. *Position trajectory with backlash inverse compensated VDC vs. sinusoidal reference trajectory (a) Transient (b) Steady state.*

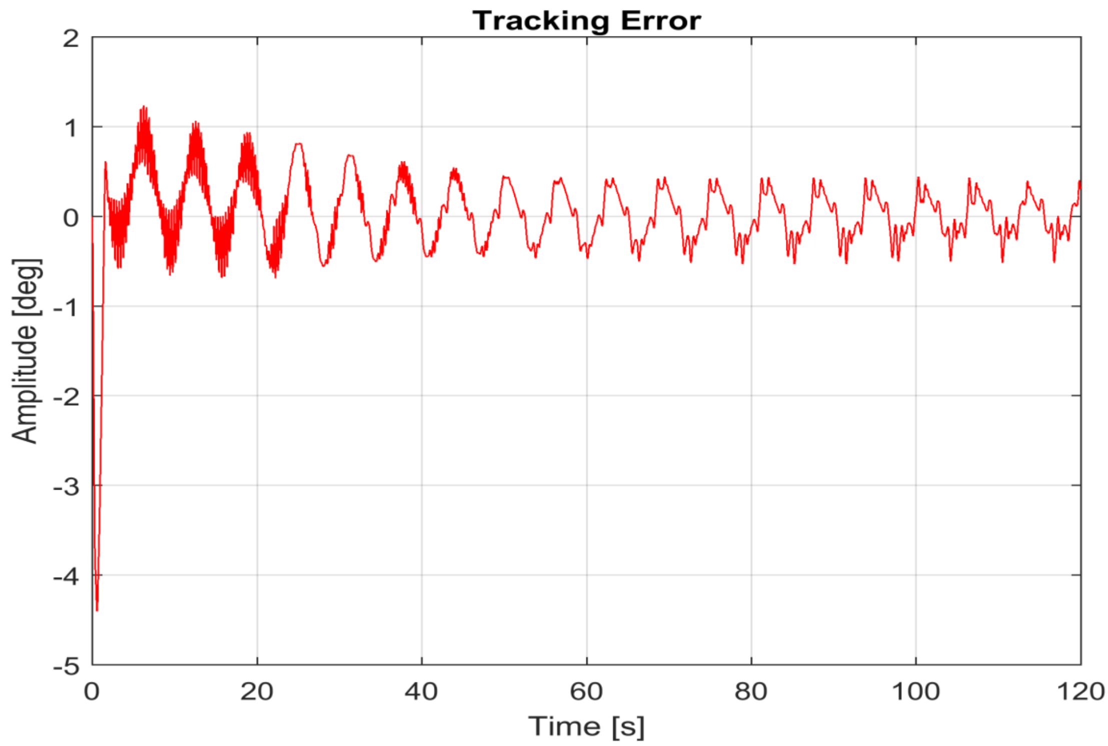

(a)

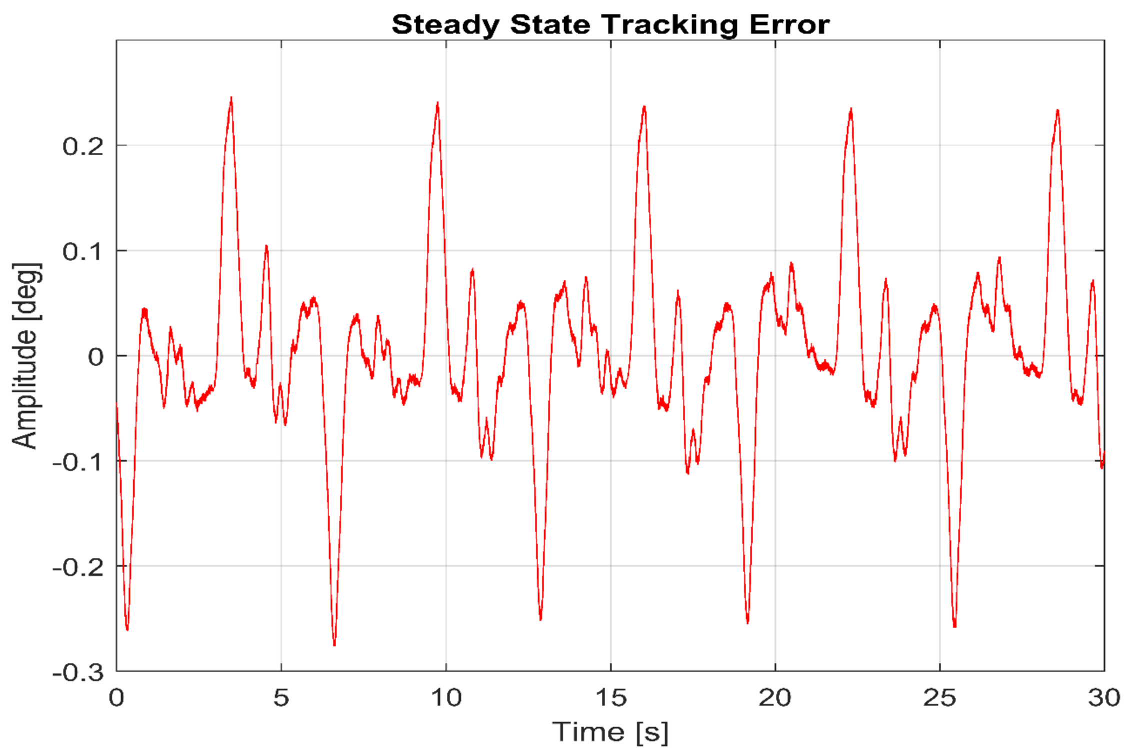

(b)

Figure 4.9. *Position tracking error with adaptive backlash inverse compensated VDC implemented. (a) Transient (b) Steady state.*

Other system data, including the measured velocity trajectory, measured during the steady state run of the adaptive backlash inverse compensated VDC controller are presented in Appendix C. From the measured velocity trajectory data available in Appendix C, the maximum absolute value was obtained as 57.2958 deg./s and from Figure 4.9 (b) and its data, the maximum absolute steady state tracking error is |-0.2761 deg.|. Therefore, in line with equation (4.8), the normalizing performance index μ may be calculated as *0.0048 s*.

In comparison, the system position tracking errors obtained under the three controller algorithms implemented have been co-plotted in Figure 4.10. This plot shows the differences in the three controllers at a glance. The ineptitude of the PID controller to maintain good reference tracking in contrast with either of the two non-linear controller algorithms is clearly visible.

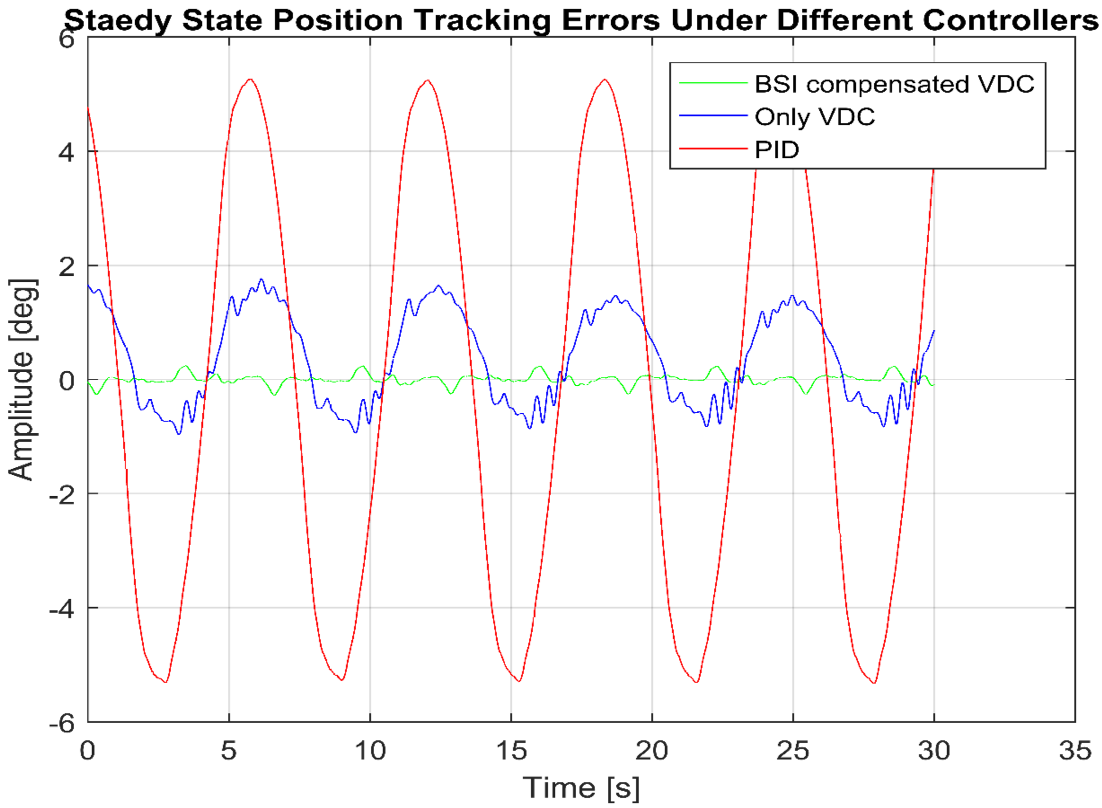

Figure 4.10. *A comparison of the position tracking errors under the three tested control algorithms.*

Even further improved system performance may be achieved by implementing the parameter adaption component of the VDC controller as described in Chapter 2 and available in (Zhu 2010). By so doing, the stress and long time involved in manual parameter tuning may be eliminated.

5. CONCLUSION, RECOMMENDATIONS AND FUTURE STUDIES

The conclusion of this research, as well as the recommendations for future studies are put forward in this chapter.

5.1 Conclusion

The theory of virtual decomposition control has been applied to a one DOF hydraulic manipulator, which is actuated by a helical spline type hydraulic rotary actuator. The hydraulic manipulator is installed at the heavy machinery laboratory of AUT/ TUT. The main objectives of the research were to design a VDC controller for the target system, and then incorporate the adaptive backlash inverse control algorithm into the designed VDC controller. Other objectives were to mathematically establish the stability of the entire robotic system under the control of the designed algorithm, and finally conduct experiments to show the possibility of implementing the designed controller in real-time environment.

Virtual decomposition of the hydraulic manipulator was conducted, leading to the development of stability guaranteed control equations for the studied system, and the effect of backlash was taken into account by incorporating the backlash inversion law into the main VDC compensator. The stability of the resulting overall controller (comprising the VDC and backlash compensators) was guaranteed in view of the convergence of the backlash inverse controller parameters when initialization and parametrization are appropriate done.

After satisfactory off-line simulation results were obtained in Simulink environment, real-time experimentations were performed on the target system. A small amplitude sinusoidal trajectory was planned for the manipulator under different controller schemes. The choice of the sinusoidal position reference was made in order to obtain the effect of backlash on a repetitive basis. Firstly, the PID controller was applied in controlling the manipulator to follow the defined trajectory, followed by using the VDC controller without and with backlash inversion compensation algorithm incorporated.

The system performances obtained for the three different controller structures were compared by using the performance indicator μ, defined as the ratio of maximum position tracking error to the maximum velocity. Under Cartesian position control using PID controller, the performance indicator for the manipulator was computed to be *0.0931 s*, while under the designed VDC controller without and with adaptive backlash inverse compensation algorithm, the value of μ were obtained to be *0.0048 s* and *0.0309 s*, respectively, even in the absence of VDC parameter adaptation implementation.

Therefore, the performance results, deducible from the error plots and the values of μ, from the different controller has demonstrated the significant supremacy of the nonlinear model-based controller, with and without backlash compensation, over the PID controller even when the parameter adaptation law has not been incorporated.

5.2 Recommendations and Future Work

The results obtained from various experimentations have demonstrated the potential of the designed VDC controller in effectively controlling systems with backlash non-smooth nonlinear characteristic even without parameter adaption law, which is a key component of the effectiveness of VDC theory.

Therefore, in order to reveal the full potential of the VDC in controlling systems with backlash nonlinearities, it is recommended that future works should look at implementing the parameter adaptation laws detailed in Chapter 3 of this thesis.

Furthermore, it would be scientifically interesting to apply the controller algorithm presented in this thesis to multi-DOF robotic system having backlash characteristics, so that the desirability of the introduced controller over other full system dynamics-based nonlinear controllers may be more clearly revealed. This is in view of the fact that the main idea of VDC theory is to deal with systems with large number of DOF.

Finally, it would be remarkable to compare the results obtained from this research with those obtainable with other nonlinear controller when used to control the target system of study.

REFERENCES

(Ahmed and Khorrami 1999) N.J. Ahmad, F. Khorrami: Adaptive Control of System with Backlash Hysteresis at the input. Proc. American. Control Conf. 3018-3022 (1999).

(Alleyne et al. 1999) A. Alleyne and R. Liu, “On the limitations of force tracking control for hydraulic servosystems,” ASME J. Dyn. Syst., Meas., Control, vol. 121, no. 2, pp. 184–190, 1999.

(An et al. 1988) C.H. An, C.G., Atkeson, J. Hollerbach: Model-based control of a robot manipulator. MIT Press, Cambridge (1988).

(Atkins and Escudier 2013) T. Atkins, M. Escudier: A dictionary of mechanical Engineering. Oxford University Press, Oxford (2013).

(Bonitz and Hsia 1994) R.G. Bonitz, T.C. Hsia: Internal force-based impedance control of rigid link flexible-joint robots with redundant joint actuators. IEEE Trans. Syst. Man Cybern. 24(7), 961-970 (1994).

(Canudas de Wit 1996) C. Canudas de Wit, B. Siciliano, G. Bastin: Theory of robot control. Springer, Berlin (1996).

(Chartrand 1985) G. Chartrand, Directed Graphs as Mathematical Models. In: Introductory Graph Theory, pp. 16-19. Courier Dover Publications, New York (1985).

(Craig 1986) J.J. Craig, Introduction to Robotics: Mechanics and Control. Addison-Wesley, Reading (1986).

(Drago 1998) R.J. Drago: Fundamentals of Gear Design. Butterworth Publishers, Stoneham (1988).

(Edge 1997) K. Edge, “The control of fluid power systems – responding to the challenges,” Proc IMechE, Part I: J. Syst. Control Eng., vol. 211, no. 2, pp. 91 – 110, 1997.

(Gorineysky et al. 1997) D.M. Gorineysky, A.M. Formalsky, A.Y. Schneider: Force control of robotics systems. CRC Press, Boca Raton (1997).

(Harrison and Stoten 1995) A.J.L. Harrison, D.P. Stoten: Generalized finite difference method for optimal estimation of derivatives in real-time control problems. Proceedings of the Institution of Mech. Engrs. Vol. 209, (pp. 67-78).

(Jouni et al. 2016) J. Mattila, J. Koivumäki, Darwin G. Caldwell and C. Semini: A survey on control of hydraulic robotic manipulators with projection to future trends. IEE/ASME Trans. Mechtr. (2016)

(Merritt 1976) H.E. Merritt: Hydraulic control systems. Wiley, New York (1976).

(Parker, 2015) Hy03-1800-2US Catalog, Parker Pneumatic, Oct 2015. Available: https://www.parker.com/literature/Literature%20Files/pneumatic/.../HY03-1800-2.pdf.

(Royden 1988) H. Royden: Real analysis. Prentice-Hall, Englewood Cliffs (1988).

(Sirouspour & Salcudean 2001) M.R. Sirouspour, S.E. Salcudean: Nonlinear control of hydraulic robots. IEEE Trans. Robot. Automat. 17 (2), 173-182 (2001).

(Slotine and Li 1987) J.J.E. Slotine, W.P. Li: On the adaptive control of robot manipulators. Int. J. Robot. Res. 6(3), 49-59 (1987).

(Slotine and Li, 1988) J.J.E. Slotine, W.P. Li: Adaptive manipulator control: a case study. IEEE Trans. Automat. Contr. 33(11), 995-1003 (1988).

(Slotine and Li 1991) J.J.E. Slotine, W.P. Li: Applied nonlinear control. Prentice Hall, Englewood Cliffs, (1991).

(Sohl and Bobrow 1999) G.A. Sohl, J. E. Bobrow, Experiments and simulations on the nonlinear control of a hydraulic servosystem. IEEE Trans. Control Systems Technology 7(2), 238-247(1999).

(Spong Vidyasagar 1987) M.W. Spong, Vidyasagar, M.: Robot dynamics and control. John Wiley & Sons, Chichester (1989).

(Tao and Kokotovic 1993) G. Tao, P. V. Kokotovic, “Adaptive control of Systems with backlash”, *Automatica*, vol. 29, no. 2, pp. 323-335, (1993).

(Tao and Kokotovic 1996)	G. Tao, and P.V. Kokotovic: Adaptive control of System with backlash, *Automatica, vol. 29, no. 2,* pp. 323-335, 1993.
(Truxal 1958)	J. G. Truxal: Automatic Feedback Control System Synthesis, McGraw-Hill, New York, (1958).
(Yao et al. 2000)	B. Yao, F. Bu, S.P. Chan, M. Chen: VSC coordinated control of two manipulator arms in the presence of environmental constraints. IEEE Trans. Automat. Contr. 37, 1806-1812 (1992).
(Yao et al. 2000)	B. Yao, F. Bu, and G. Chiu, “Non-linear adaptive robust control of electro-hydraulic systems driven by double-rod actuators,” Int. J. of Control, vol. 74, no. 8, pp. 761–775, 2001.
(Yao et al. 2014)	J. Yao, Z. Jiao, D. Ma, L. Yan: High-Accuracy tracking control of hydraulic rotary actuators with modelling uncertainties. IEEE/ ASME Trans. Mechtr. 19(2), 633-641 (2014).
(Yoshikawa 1990)	T. Yoshikawa: Foundations of Robotics: Analysis and control. MIT Press, Cambridge (1990).
(Zhu 2005)	W.H. Zhu: On adaptive synchronization control of coordinated multirobots with flexible/ rigid constraints. IEEE Trans. Robotics 21(3), 520-525 (2005).
(Zhu 2010)	W.H. Zhu, Virtual Decomposition Control: Toward Hyper Degrees of Freedom Robots, Springer-Verlag, Berlin Heidelberg, (2010).
(Zhu et al. 1998)	W.H. Zhu, Z. Bien, and J. De Schutter, “Adaptive motion/force control of multiple manipulators with joint flexibility based on virtual decomposition,” IEEE Trans. Autom. Control, vol. 43, no. 1, pp. 46 – 60, 1998.
(Zhu and De Schutter 1999)	W.-H. Zhu and J. De Schutter, “Adaptive control of mixed rigid/flexible joint robot manipulators based on virtual decomposition,” IEEE Trans. Robot. Autom., vol. 15, no. 2, pp. 310 – 317, 1999.
(Zhu and De Schutter 2002)	W.-H. Zhu and J. De Schutter, “Experimental verifications of virtual-decomposition-based motion/force control,” IEEE Trans. Robot. Autom., vol. 18, no. 3, pp. 379 – 386, 2002.

(Zhu and Piedboeuf 2005) W.H. Zhu and J. C. Piedboeuf. "Adaptive output force tracking control of hydraulic cylinders with applications to robot manipulators." Journal of dynamic systems, measurement, and control 127, no. 2 (2005): 206-217.

(Zhu and Vukovich 2011) W.H. Zhu and G. Vukovich. "Virtual decomposition control for modular robot manipulators." IFAC Proceedings Volumes 44.1 (2011): 13486-13491.

(Zhu et al. 2013) W.H. Zhu, T. Lamarche, E. Dupuis, D. Jameux, P. Barnard, and G. Liu, 2013. ‘‘Precision control of modular robot manipulators: the VDC approach with embedded FPGA’’. IEEE Transactions on Robotics, 29(5), pp.1162-1179.

(Ziegler and Nichols 1942) J.G. Ziegler, N.B. Nichols. Optimum settings for automatic Controllers. Transactions of ASME. Vol. 64. (pp.759-768). (1942).

icfluid.com *https://www.icfluid.com/products/rotary-actuators/e1/.* Accessed Jan. 7th 2017.

APPENDIX A: REGRESSOR MATRIX AND PARAMETER VECTOR OF AN OBJECT

According to Zhu's work, if frame A is attached to a rigid body, the regressor matrix $\boldsymbol{Y_B} \in \mathbb{R}^{\mathbf{6\times 13}}$ and the parameter vector $\boldsymbol{\theta_B} \in \mathbb{R}^{\mathbf{13}}$ as appeared in (2.23) are expressed in the Appendage.

The regressor matrix $\boldsymbol{Y_B} \in \mathbb{R}^{\mathbf{6\times 13}}$ contains both zero and non-zero elements, its non-zero elements are given as

$$y_{\boldsymbol{B}}(1,1) = \frac{d}{dt}\left({}^{\mathbf{B}}\mathbf{V}_{\mathbf{r}}\right)(1) + {}^{\mathbf{B}}\mathbf{V}(5)\,{}^{\mathbf{B}}\mathbf{V}_{\mathbf{r}}(3) - {}^{\mathbf{B}}\mathbf{V}(6)\,{}^{\mathbf{B}}\mathbf{V}_{\mathbf{r}}(\mathbf{2}) + {}^{\mathbf{B}}\boldsymbol{g}(1) \quad \text{(A.1)}$$

$$y_{\boldsymbol{B}}(1,2) = -{}^{\mathbf{B}}\mathbf{V}(5)\,{}^{\mathbf{B}}\mathbf{V}_{\mathbf{r}}(5) - {}^{\mathbf{B}}\mathbf{V}(6)\,{}^{\mathbf{B}}\mathbf{V}_{\mathbf{r}}(6) \quad \text{(A.2)}$$

$$y_{\boldsymbol{B}}(1,3) = -\frac{d}{dt}\left({}^{\mathbf{B}}\mathbf{V}_{\mathbf{r}}\right)(6) + {}^{\mathbf{B}}\mathbf{V}(5)\,{}^{\mathbf{B}}\mathbf{V}_{\mathbf{r}}(4) \quad \text{(A.3)}$$

$$y_{\boldsymbol{B}}(1,4) = \frac{d}{dt}\left({}^{\mathbf{B}}\mathbf{V}_{\mathbf{r}}\right)(5) + {}^{\mathbf{B}}\mathbf{V}(6)\,{}^{\mathbf{B}}\mathbf{V}_{\mathbf{r}}(4) \quad \text{(A.4)}$$

$$y_{\boldsymbol{B}}(2,1) = \frac{d}{dt}\left({}^{\mathbf{B}}\mathbf{V}_{\mathbf{r}}\right)(2) + {}^{\mathbf{B}}\mathbf{V}(6)\,{}^{\mathbf{B}}\mathbf{V}_{\mathbf{r}}(1) - {}^{\mathbf{B}}\mathbf{V}(4)\,{}^{\mathbf{B}}\mathbf{V}_{\mathbf{r}}(3) + {}^{\mathbf{B}}\boldsymbol{g}(2) \quad \text{(A.5)}$$

$$y_{\boldsymbol{B}}(2,2) = \frac{d}{dt}\left({}^{\mathbf{B}}\mathbf{V}_{\mathbf{r}}\right)(6) + {}^{\mathbf{B}}\mathbf{V}(4)\,{}^{\mathbf{B}}\mathbf{V}_{\mathbf{r}}(5) \quad \text{(A.6)}$$

$$y_{\boldsymbol{B}}(2,3) = -{}^{\mathbf{B}}\mathbf{V}(4)\,{}^{\mathbf{B}}\mathbf{V}_{\mathbf{r}}(4) - {}^{\mathbf{B}}\mathbf{V}(6)\,{}^{\mathbf{B}}\mathbf{V}_{\mathbf{r}}(6) \quad \text{(A.7)}$$

$$y_{\boldsymbol{B}}(2,4) = -\frac{d}{dt}\left({}^{\mathbf{B}}\mathbf{V}_{\mathbf{r}}\right)(4) + {}^{\mathbf{B}}\mathbf{V}(6)\,{}^{\mathbf{B}}\mathbf{V}_{\mathbf{r}}(5) \quad \text{(A.8)}$$

$$y_{\boldsymbol{B}}(3,1) = \frac{d}{dt}\left({}^{\mathbf{B}}\mathbf{V}_{\mathbf{r}}\right)(3) + {}^{\mathbf{B}}\mathbf{V}(4)\,{}^{\mathbf{B}}\mathbf{V}_{\mathbf{r}}(2) - {}^{\mathbf{B}}\mathbf{V}(5)\,{}^{\mathbf{B}}\mathbf{V}_{\mathbf{r}}(1) + {}^{\mathbf{B}}\boldsymbol{g}(3) \quad \text{(A.9)}$$

$$y_{\boldsymbol{B}}(3,2) = -\frac{d}{dt}\left({}^{\mathbf{B}}\mathbf{V}_{\mathbf{r}}\right)(5) + {}^{\mathbf{B}}\mathbf{V}(4)\,{}^{\mathbf{B}}\mathbf{V}_{\mathbf{r}}(6) \quad \text{(A.10)}$$

$$y_{\boldsymbol{B}}(3,3) = \frac{d}{dt}\left({}^{\mathbf{B}}\mathbf{V}_{\mathbf{r}}\right)(4) + {}^{\mathbf{B}}\mathbf{V}(5)\,{}^{\mathbf{B}}\mathbf{V}_{\mathbf{r}}(6) \quad \text{(A.11)}$$

$$y_{\boldsymbol{B}}(3,4) = -{}^{\mathbf{B}}\mathbf{V}(4)\,{}^{\mathbf{B}}\mathbf{V}_{\mathbf{r}}(4) - {}^{\mathbf{B}}\mathbf{V}(5)\,{}^{\mathbf{B}}\mathbf{V}_{\mathbf{r}}(5) \quad \text{(A.12)}$$

$$y_{\boldsymbol{B}}(4,3) = y_{\boldsymbol{A}}(3,1) \quad \text{(A.13)}$$

$$y_{\boldsymbol{B}}(4,4) = -y_{\boldsymbol{A}}(2,1) \quad \text{(A.14)}$$

$$y_{\boldsymbol{B}}(4,6) = y_{\boldsymbol{A}}(3,3) \quad \text{(A.15)}$$

$$y_{\boldsymbol{B}}(4,7) = -y_{\boldsymbol{A}}(2,4) \quad \text{(A.16)}$$

$$y_{\boldsymbol{B}}(4,8) = y_{\boldsymbol{A}}(3,2) \tag{A.17}$$

$$y_{\boldsymbol{B}}(4,9) = -y_{\boldsymbol{A}}(2,2) \tag{A.18}$$

$$y_{\boldsymbol{B}}(4,10) = {}^{\mathbf{B}}\mathbf{V}(6)\,{}^{\mathbf{B}}\mathbf{V}_{\mathbf{r}}(6) - {}^{\mathbf{B}}\mathbf{V}(5)\,{}^{\mathbf{B}}\mathbf{V}_{\mathbf{r}}(5) \tag{A.19}$$

$$y_{\boldsymbol{B}}(4,11) = \frac{d}{dt}\left({}^{\mathbf{B}}\mathbf{V}_{\mathbf{r}}\right)(4) + {}^{\mathbf{B}}\mathbf{V}(5)\,{}^{\mathbf{B}}\mathbf{V}_{\mathbf{r}}(6) - {}^{\mathbf{B}}\mathbf{V}(6)\,{}^{\mathbf{B}}\mathbf{V}_{\mathbf{r}}(5) \tag{A.20}$$

$$y_{\boldsymbol{B}}(4,12) = -{}^{\mathbf{B}}\mathbf{V}(6)\,{}^{\mathbf{B}}\mathbf{V}_{\mathbf{r}}(5) \tag{A.21}$$

$$y_{\boldsymbol{B}}(4,13) = {}^{\mathbf{B}}\mathbf{V}(5)\,{}^{\mathbf{B}}\mathbf{V}_{\mathbf{r}}(6) \tag{A.22}$$

$$y_{\boldsymbol{B}}(5,2) = -y_{\boldsymbol{A}}(3,1) \tag{A.23}$$

$$y_{\boldsymbol{B}}(5,4) = y_{\boldsymbol{A}}(1,1) \tag{A.24}$$

$$y_{\boldsymbol{B}}(5,5) = -y_{\boldsymbol{A}}(3,2) \tag{A.25}$$

$$y_{\boldsymbol{B}}(5,7) = y_{\boldsymbol{A}}(1,4) \tag{A.26}$$

$$y_{\boldsymbol{B}}(5,8) = -y_{\boldsymbol{A}}(3,3) \tag{A.27}$$

$$y_{\boldsymbol{B}}(5,9) = {}^{\mathbf{B}}\mathbf{V}(4)\,{}^{\mathbf{B}}\mathbf{V}_{\mathbf{r}}(4) - {}^{\mathbf{B}}\mathbf{V}(6)\,{}^{\mathbf{B}}\mathbf{V}_{\mathbf{r}}(6) \tag{A.28}$$

$$y_{\boldsymbol{B}}(5,10) = y_{\boldsymbol{A}}(1,3) \tag{A.29}$$

$$y_{\boldsymbol{B}}(5,11) = {}^{\mathbf{B}}\mathbf{V}(6)\,{}^{\mathbf{B}}\mathbf{V}_{\mathbf{r}}(4) \tag{A.30}$$

$$y_{\boldsymbol{B}}(5,12) = \frac{d}{dt}\left({}^{\mathbf{B}}\mathbf{V}_{\mathbf{r}}\right)(5) + {}^{\mathbf{B}}\mathbf{V}(6)\,{}^{\mathbf{B}}\mathbf{V}_{\mathbf{r}}(4) - {}^{\mathbf{B}}\mathbf{V}(4)\,{}^{\mathbf{B}}\mathbf{V}_{\mathbf{r}}(6) \tag{A.31}$$

$$y_{\boldsymbol{B}}(5,13) = -{}^{\mathbf{B}}\mathbf{V}(4)\,{}^{\mathbf{B}}\mathbf{V}_{\mathbf{r}}(6) \tag{A.32}$$

$$y_{\boldsymbol{B}}(6,2) = y_{\boldsymbol{A}}(2,1) \tag{A.33}$$

$$y_{\boldsymbol{B}}(6,3) = -y_{\boldsymbol{A}}(1,1) \tag{A.34}$$

$$y_{\boldsymbol{B}}(6,5) = y_{\boldsymbol{A}}(2,2) \tag{A.35}$$

$$y_{\boldsymbol{B}}(6,6) = -y_{\boldsymbol{A}}(1,3) \tag{A.36}$$

$$y_{\boldsymbol{B}}(6,8) = {}^{\mathbf{B}}\mathbf{V}(5)\,{}^{\mathbf{B}}\mathbf{V}_{\mathbf{r}}(5) - {}^{\mathbf{B}}\mathbf{V}(4)\,{}^{\mathbf{B}}\mathbf{V}_{\mathbf{r}}(4) \tag{A.37}$$

$$y_{\boldsymbol{B}}(6,9) = y_{\boldsymbol{A}}(2,4) \tag{A.38}$$

$$y_{\boldsymbol{B}}(6,10) = -y_{\boldsymbol{A}}(1,4) \tag{A.39}$$

$$y_{\boldsymbol{B}}(6{,}11) = -\,{}^{\mathbf{B}}\mathbf{V}(5)\,{}^{\mathbf{B}}\mathbf{V}_{\mathbf{r}}(4) \tag{A.40}$$

$$y_{\boldsymbol{B}}(6{,}12) = {}^{\mathbf{B}}\mathbf{V}(4)\,{}^{\mathbf{B}}\mathbf{V}_{\mathbf{r}}(5) \tag{A.41}$$

$$y_{\boldsymbol{B}}(6{,}13) = \frac{d}{dt}\left({}^{\mathbf{B}}\mathbf{V}_{\mathbf{r}}\right)(6) + {}^{\mathbf{B}}\mathbf{V}(4)\,{}^{\mathbf{B}}\mathbf{V}_{\mathbf{r}}(5) - {}^{\mathbf{B}}\mathbf{V}(5)\,{}^{\mathbf{B}}\mathbf{V}_{\mathbf{r}}(4) \tag{A.42}$$

where $y_{\boldsymbol{B}}(j,k) \in \mathbb{R}$ denotes an element of $\boldsymbol{Y_B} \in \mathbb{R}^{\mathbf{6\times13}}$ located at row j and column k for $j \in \{1{,}6\}$ and $k \in \{1{,}13\}$**;** the three variables $\frac{d}{dt}\left({}^{\mathbf{B}}\mathbf{V}_{\mathbf{r}}\right)(j) \in \mathbb{R}$**,** ${}^{\mathbf{B}}\mathbf{V}(\mathrm{j}) \in \mathbb{R}$**,** and ${}^{\mathbf{B}}\mathbf{V}_{\mathbf{r}}(j) \in \mathbb{R}$ denote the j^{th} elements of $\frac{d}{dt}\left({}^{\mathbf{B}}\mathbf{V}_{\mathbf{r}}\right) \in \mathbb{R}^6$**,** ${}^{\mathbf{B}}\mathbf{V} \in \mathbb{R}^6$, and ${}^{\mathbf{B}}\mathbf{V}_{\mathbf{r}} \in \mathbb{R}^6$, respectively, for all $j \in \{1{,}6\}$; and ${}^{\mathbf{B}}\mathbf{g}(j) \in \mathbb{R}$ denotes the j^{th} elements of ${}^{\mathbf{A}}\mathbf{R}_{\mathbf{I}}\mathbf{g} \in \mathbb{R}^3$ with $\mathbf{g} = [0{,}0{,}9.8]^T \in \mathbb{R}^3$ for $j \in \{1{,}3\}$.

For the parameter vector $\boldsymbol{\theta_B} \in \mathbb{R}^{\mathbf{13}}$, the 13 elements are listed as:

$$\theta_{\boldsymbol{B1}} = m_{\mathbf{B}} \tag{A.43}$$

$$\theta_{\boldsymbol{B2}} = m_{\boldsymbol{B}}\mathbf{B}_{r_{mx}} \tag{A.44}$$

$$\theta_{\boldsymbol{B3}} = m_{\boldsymbol{B}}\mathbf{B}_{r_{my}} \tag{A.45}$$

$$\theta_{\boldsymbol{B}4} = m_{\boldsymbol{B}}\mathbf{B}_{r_{mz}} \tag{A.46}$$

$$\theta_{\boldsymbol{B}5} = m_{\boldsymbol{B}}\mathbf{B}_{r^2{}_{mx}} \tag{A.47}$$

$$\theta_{\boldsymbol{B}6} = m_{\boldsymbol{B}}\mathbf{B}_{r^2{}_{my}} \tag{A.48}$$

$$\theta_{\boldsymbol{B}7} = m_{\boldsymbol{B}}\mathbf{B}_{r^2{}_{mx}} \tag{A.49}$$

$$\theta_{\boldsymbol{B}8} = m_{\boldsymbol{B}}\mathbf{B}_{r_{mx}}\mathbf{B}_{r_{my}} - \mathrm{I}_{\mathbf{A}_{xy}} \tag{A.50}$$

$$\theta_{\boldsymbol{B}9} = m_{\mathbf{B}}\mathbf{B}_{r_{mx}}\mathbf{B}_{r_{mz}} - \mathrm{I}_{\mathbf{A}_{xz}} \tag{A.51}$$

$$\theta_{\boldsymbol{B}10} = m_{\mathbf{B}}\mathbf{B}_{r_{my}}\mathbf{B}_{r_{mz}} - \mathrm{I}_{\mathbf{A}_{yz}} \tag{A.52}$$

$$\theta_{\mathbf{B}11} = \mathrm{I}_{\mathbf{A}_{xx}} \tag{A.53}$$

$$\theta_{\boldsymbol{B}12} = \mathrm{I}_{\mathbf{A}_{yy}} \tag{A.54}$$

$$\theta_{\boldsymbol{B}13} = \mathrm{I}_{\mathbf{A}_{zz}} \tag{A.55}$$

where $\theta_{\boldsymbol{B}i}$ represents the i^{th} element of $\boldsymbol{\theta_B} \in \mathbb{R}^{13}$ for all $k \in \{1{,}13\}$; $m_{\boldsymbol{B}}$ is the mass**;** $\mathbf{B}_{r_m} = \left[\mathbf{B}_{r_{mx}}, \mathbf{B}_{r_{my}}, \mathbf{B}_{r_{mz}}\right]^{\boldsymbol{T}} \in \mathbb{R}^3$ depicts a vector directed from the origin of frame **B** toward the mass center and expressed in frame **B** (it is equivalent to $\mathbf{B}_{\boldsymbol{r}_{\boldsymbol{AB}}}$ in (2.20) - (2.22)), and $\mathrm{I}_{\boldsymbol{A}_{xx}}$, $\mathrm{I}_{\boldsymbol{A}_{yy}}$, $\mathrm{I}_{\boldsymbol{A}_{xy}}$, $\mathrm{I}_{\boldsymbol{A}_{xz}}$, and $\mathrm{I}_{\boldsymbol{A}_{yz}}$ are elements of $\mathbf{I}_{\boldsymbol{A}}$.

APPENDIX B: PARAMETER VECTOR OF STUDIED SYSTEM

Applied system parameter vectors are given here.

Rigid Body parameters

According to the description given in Chapter 4, the computed parameter vectors, obtained by measurements and mathematical calculations, for all the rigid bodies are as given in Table B.1.

Table B.1: *Applied rigid body parameters.*

Parameter	Rigid Body Index	
	$\{\mathbf{B_2}\}$	$\{\mathbf{B_1}\}$
$m_{\mathbf{B}}[\mathbf{kg}]$	7.66	25
$\mathbf{B}_{\boldsymbol{r}_{mx}}[\mathbf{m}]$	0.00	0.2
$\mathbf{B}_{\boldsymbol{r}_{my}}[\mathbf{m}]$	0.00	0.5
$\mathbf{B}_{\boldsymbol{r}_{mz}}[\mathbf{m}]$	0.00	0
$\mathbf{I}_{\mathbf{A}_{xx}}[\mathbf{kg.m^2}]$	0.0114	6.25
$\mathbf{I}_{\mathbf{A}_{yy}}[\mathbf{kg.m^2}]$	0.0114	2.34
$\mathbf{I}_{\mathbf{A}_{zz}}[\mathbf{kg.m^2}]$	0.0174	3.55
$\mathbf{I}_{\mathbf{A}_{xy}}[\mathbf{kg.m^2}]$	0.00	0.00
$\mathbf{I}_{\mathbf{A}_{xz}}[\mathbf{kg.m^2}]$	0.00	0.00
$\mathbf{I}_{\mathbf{A}_{yz}}[\mathbf{kg.m^2}]$	0.00	0.00

Valve Flow Coefficient Parameter Vector

The parameter vector $\boldsymbol{\theta_v} \in \mathbb{R}^4$ given in (3.54) contains four elements, which are the flow coefficient parameters for each of the control notch of the used valve. Firstly, estimates fantastically of the valve flow coefficients were first extracted from the manufacturer's datasheet, and subsequently adjusted to suit good controller performance.

The elements of the applied control valve parameter vector $\boldsymbol{\theta}_v \in \mathbb{R}^4$ are as given in Table B.2.

Table B.2. *Valve flow coefficients.*

Parameter	Applied value $\left[\frac{m^3}{s.V.\sqrt{Pa}}\right]$
c_{p1}	3.564×10^{-8}
c_{n1}	3.564×10^{-8}
c_{p2}	3.564×10^{-8}
c_{n1}	3.564×10^{-8}

Cylinder Control Parameter Vector

The elements of $\boldsymbol{\theta}_c \epsilon\ \mathbb{R}^3$, that is, cylinder control parameter vector are the effective bulk modulus of the cylinder β, area of chamber A of the cylinder ($\mathrm{A_A}$), and area of the chamber B ($\mathrm{A_B}$). The used values of the parameters are presented in Table B.3.

Table B.3. *Cylinder control parameter vector elements.*

Parameter	Applied value
$\boldsymbol{B}\ [\boldsymbol{MPa}]$	1200
$\mathbf{A_A}\ [\boldsymbol{m^2}]$	0.0113
$\mathbf{A_B}\ [\boldsymbol{m^2}]$	0.0133

APPENDIX C: MEASURED SIGNAL DATA UNDER PID AND VDC CONTROLLERS

Some measured data under different controller algorithms are presented in this Appendix.

Firstly, the normalized [-1 1] valve control signals, pressure signals (supply pressure and chambers A and B pressures) and measured arm velocity (deg. /s) are presented under PID controller. Thereafter, the same sets of data acquired under the control of a VDC control without backlash compensation are presented. Finally, some interesting system data obtained when a backlash inverse compensated VDC controller is applied to control the manipulator are presented.

Measured Data under PID Controller

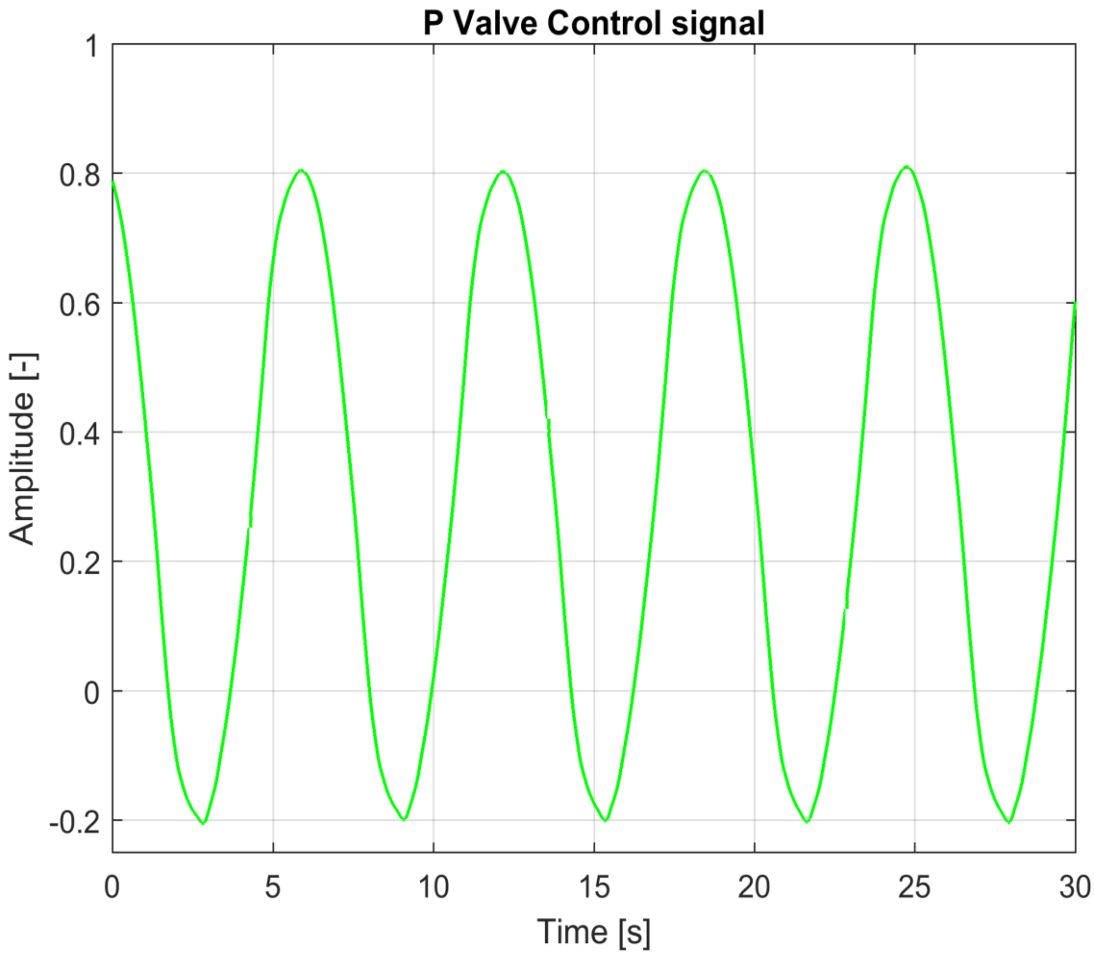

Figure C.1*: Valve control signal under PID controller.*

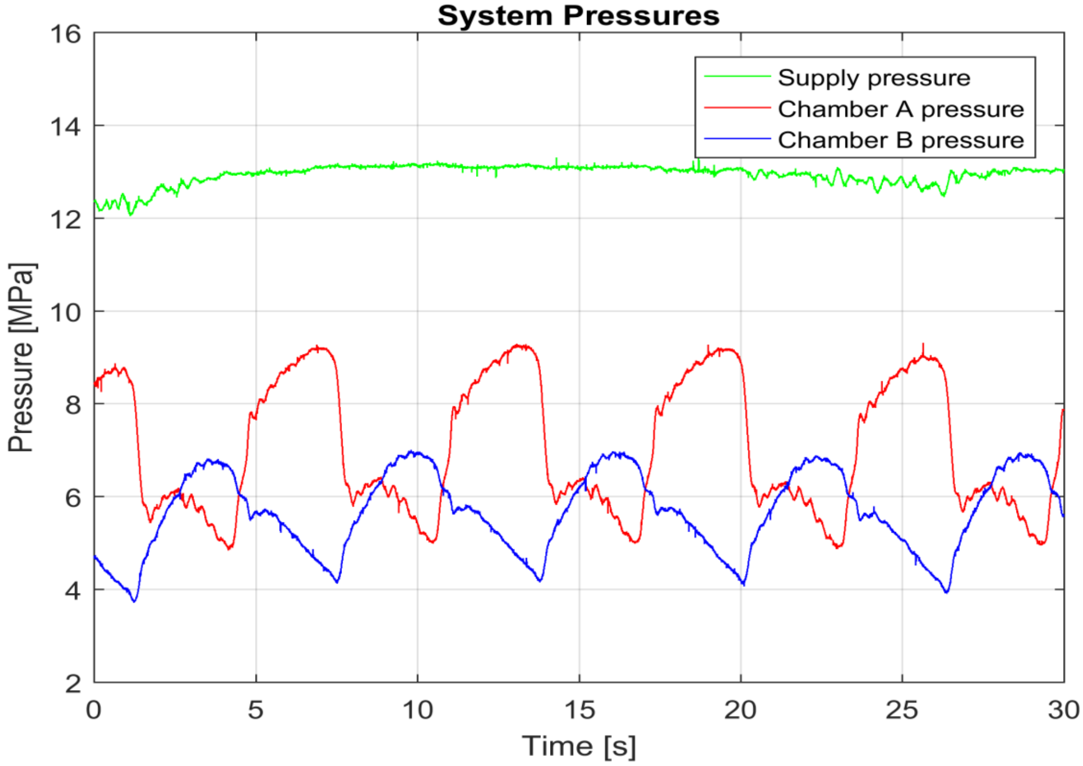

Figure C.2: *System pressure signals under the PID controller position control.*

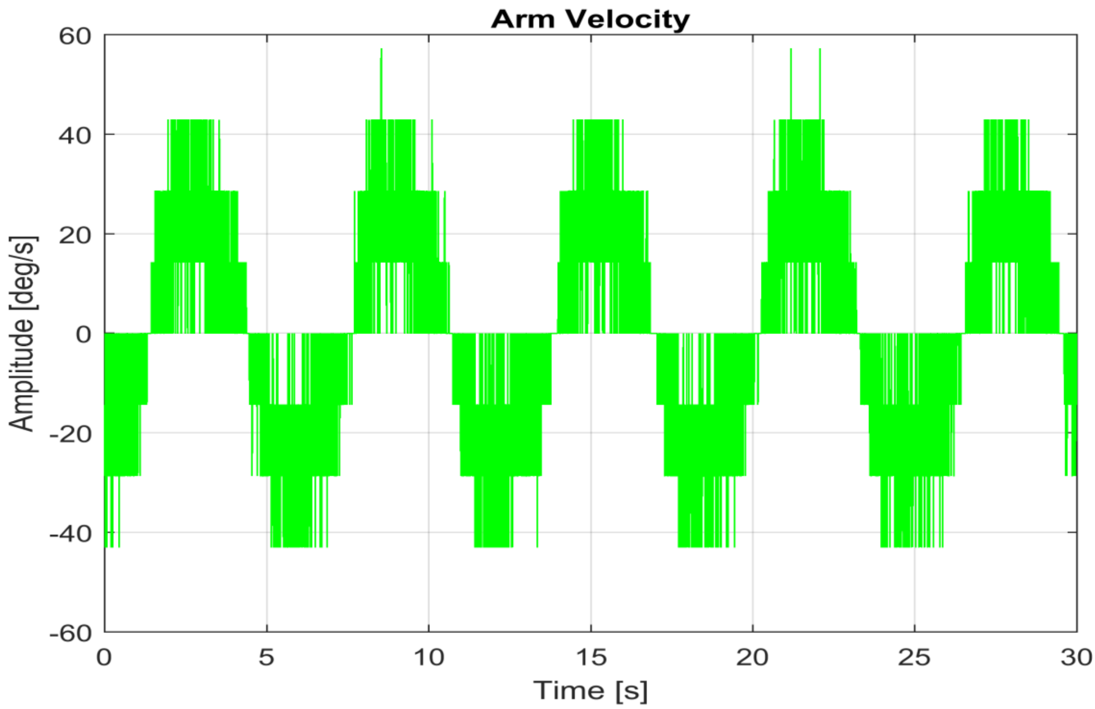

Figure C.3: *Measured velocity trajectory of the end effector (arm) with the PID controller.*

Measured Data under Pure VDC Controller

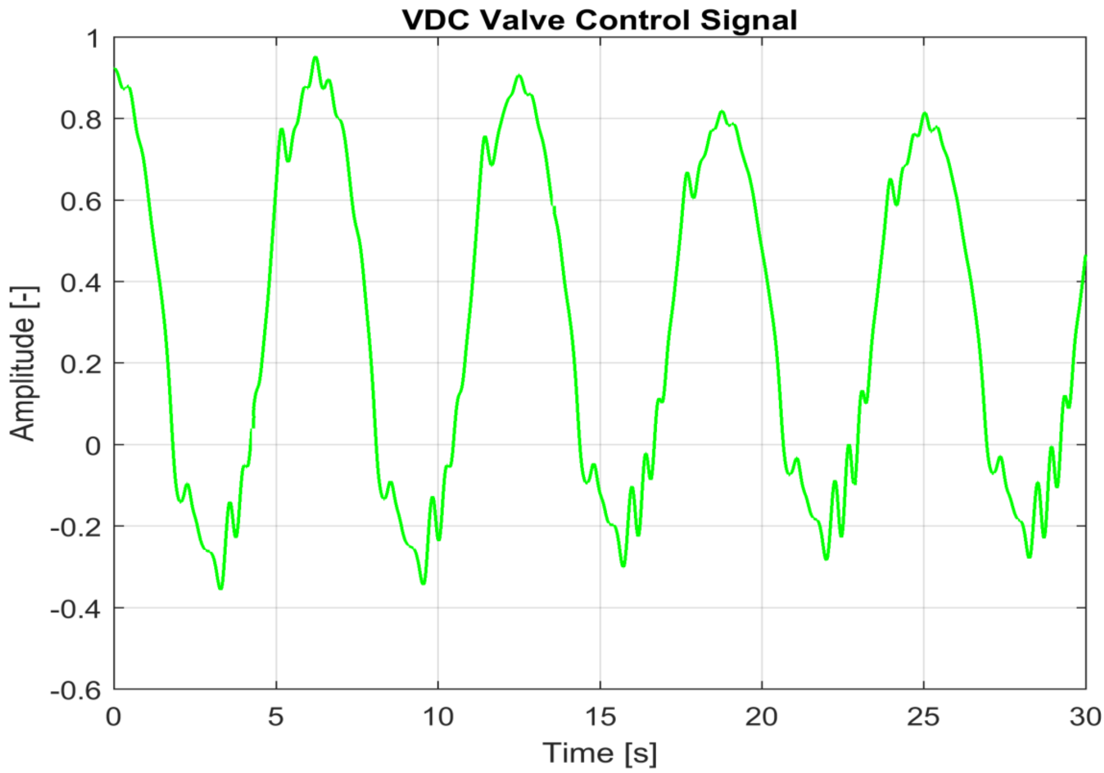

***Figure C.4**: Valve control signal under VDC controller without backlash compensation.*

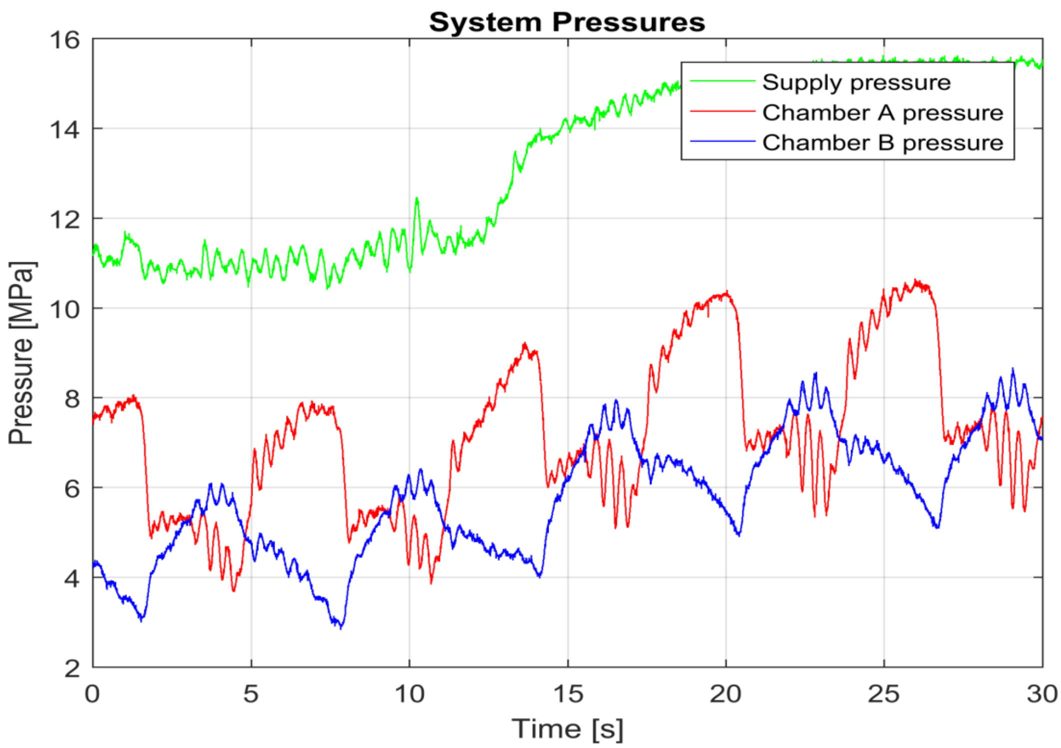

***Figure C.5**: System pressure signals under the VDC controller position control.*

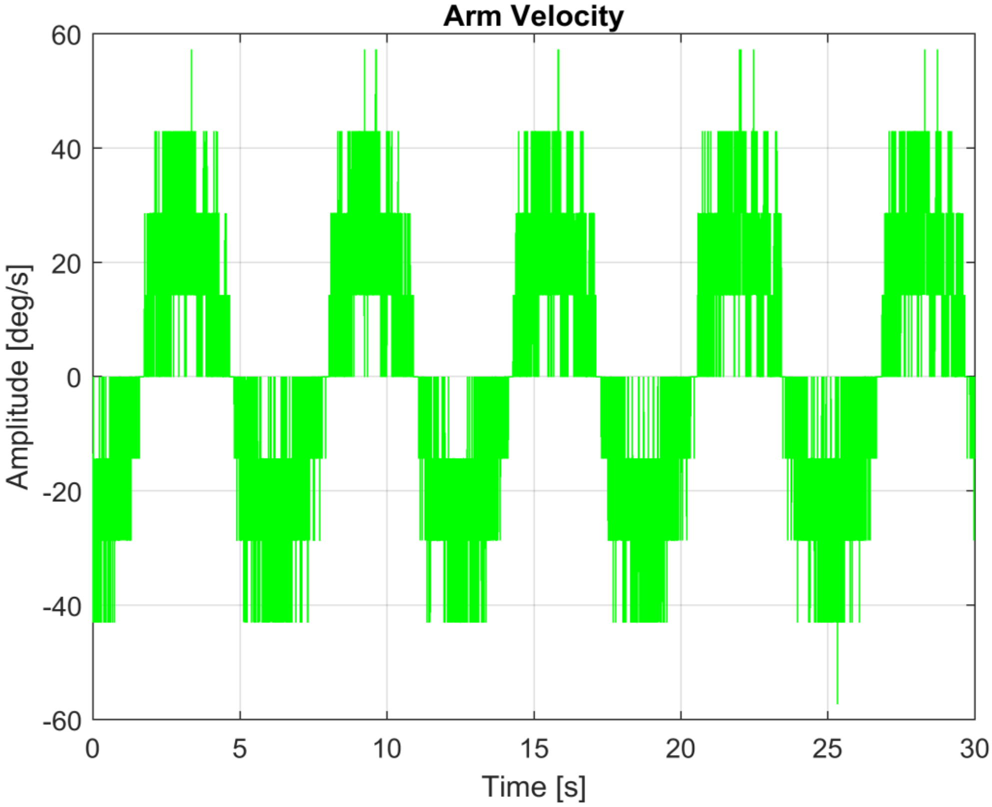

Figure C.6: *Velocity trajectory of the end effector (arm) under the VDC controller.*

Measured Data under Backlash Inverse Compensated VDC Controller

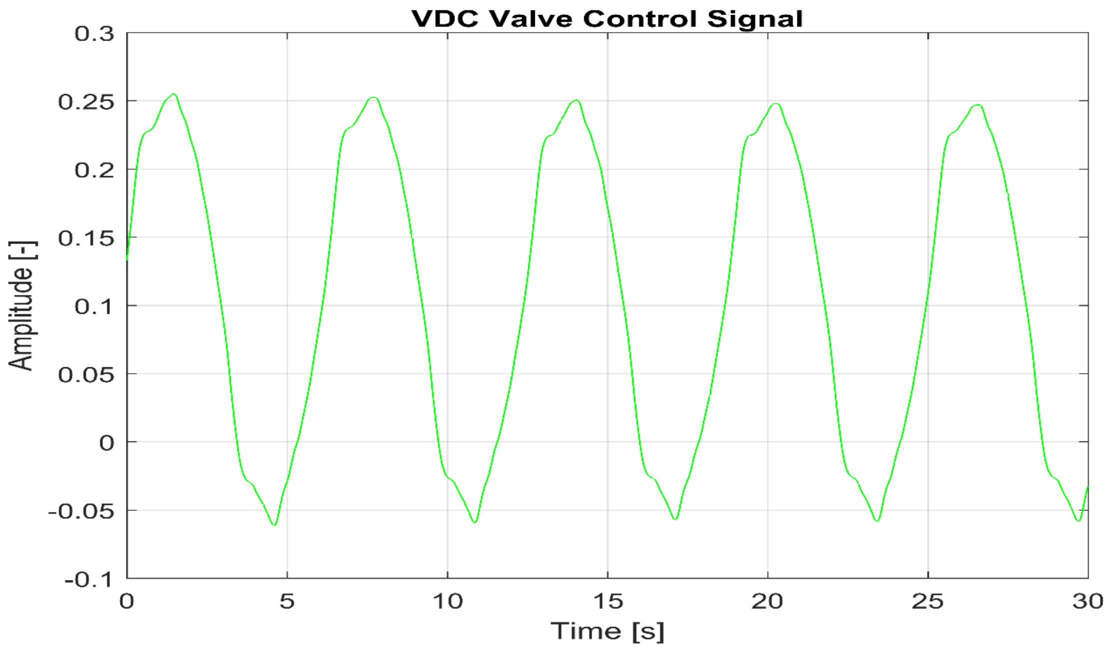

Figure C.7: *Valve control signal generated by the VDC controller only (Serving as the input to the adaptive backlash inverse controller when BSI compensation is implemented.*

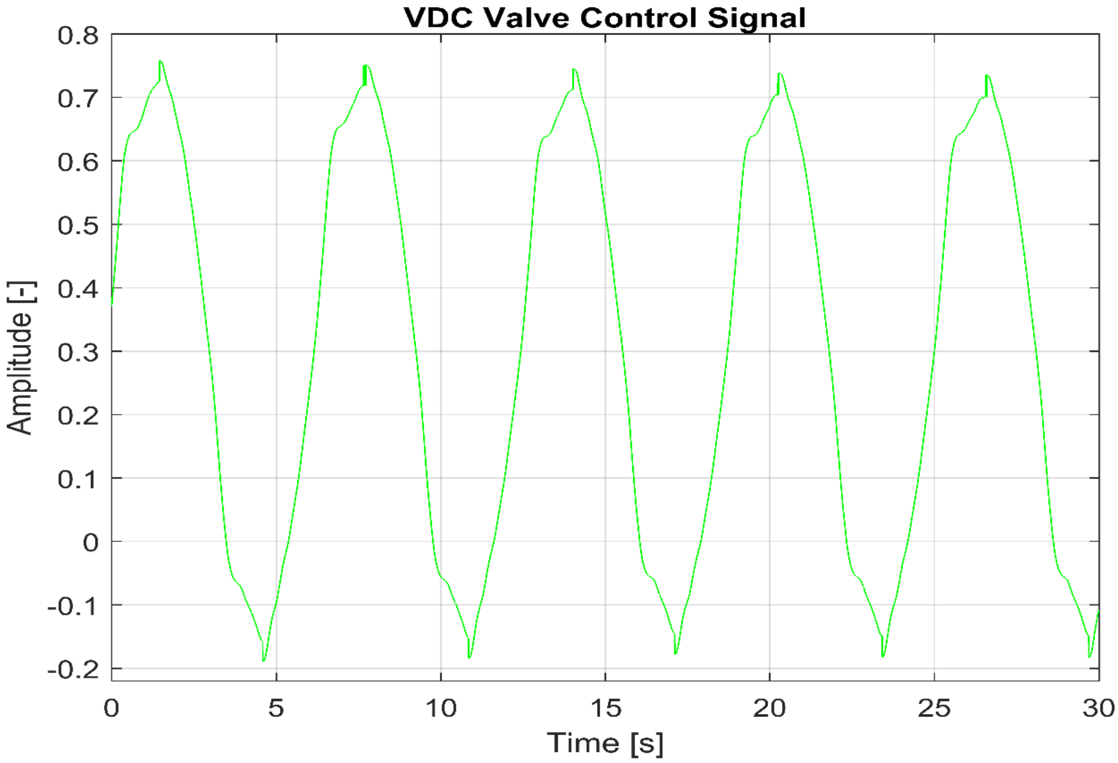

***Figure C.8**: Valve control signal generated by the BSI compensated VDC controller (the output of the adaptive backlash inverse controller).*

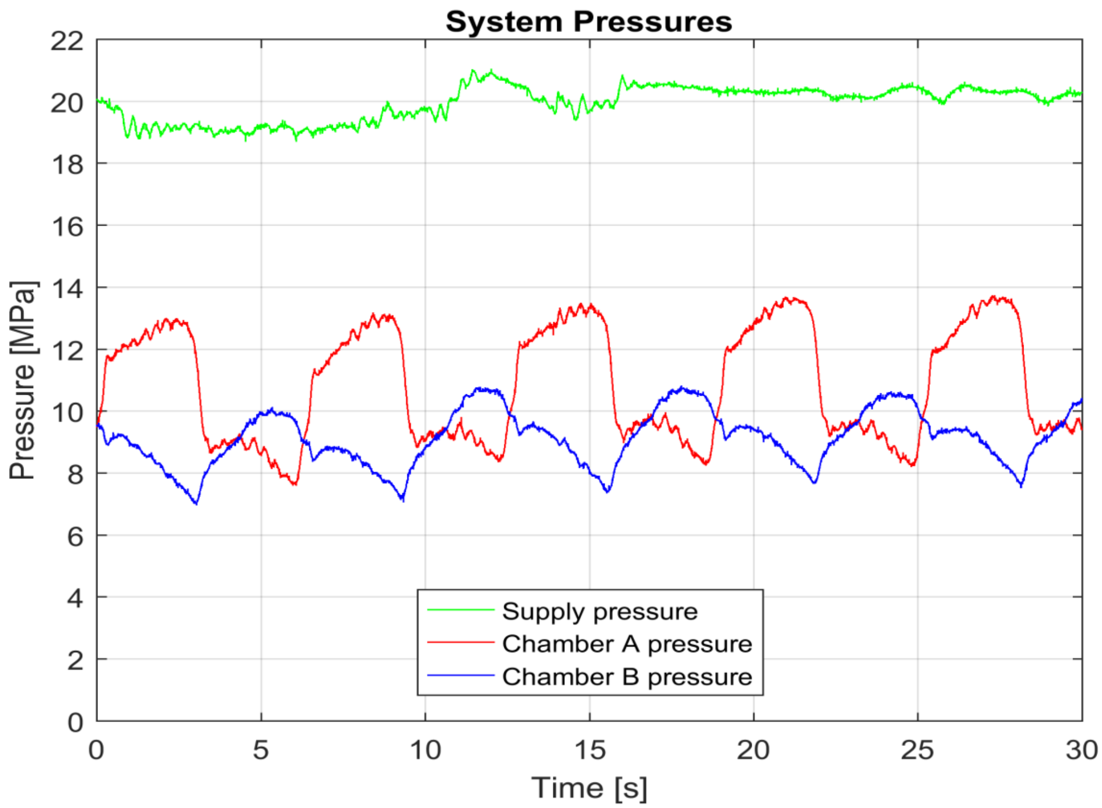

Figure C.9: System pressure signals under the *BSI compensated VDC controller*

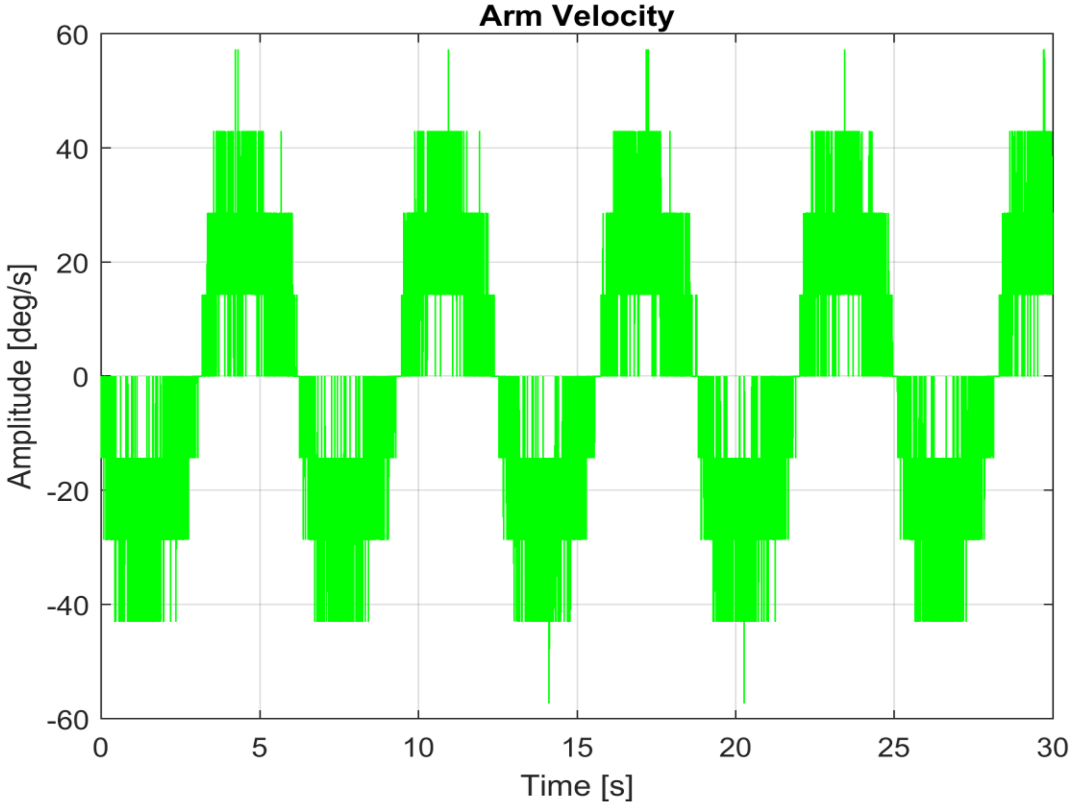

Figure C.10: *Steady state velocity trajectory of the end effector (arm) under the BSI compensated VDC controller.*

APPENDIX D: C-CODE FOR IMPLEMENTING THE ADAPTIVE BACKLASH INVERSE MODEL

```
/*
 * File: sfun_backlash_invs2.c
 *
  *
  *   --- THIS FILE GENERATED BY S-FUNCTION BUILDER: 3.0 ---
  *
  *   This file is an S-function produced by the S-Function
  *   Builder which only recognizes certain fields.  Changes made
  *   outside these fields will be lost the next time the block is
  *   used to load, edit, and resave this file. This file will be
overwritten
  *   by the S-function Builder block. If you want to edit this file
by hand,
  *   you must change it only in the area defined as:
  *
  *        %%%-SFUNWIZ_defines_Changes_BEGIN
  *        #define NAME 'replacement text'
  *        %%% SFUNWIZ_defines_Changes_END
  *
  *   DO NOT change NAME--Change the 'replacement text' only.
  *
  *   For better compatibility with the Simulink Coder, the
  *   "wrapper" S-function technique is used.  This is discussed
  *   in the Simulink Coder's Manual in the Chapter titled,
  *   "Wrapper S-functions".
  *
  *  -----------------------------------------------------------------
---------
  * | See matlabroot/simulink/src/sfuntmpl_doc.c for a more detailed
template |
  *  -----------------------------------------------------------------
---------
* Created: Tue Mar 21 20:39:10 2017(c) Adeleke Adeyemi (No reproduc-
tion is permitted
 *without the express approval of the author
*/
#define S_FUNCTION_LEVEL 2
#define S_FUNCTION_NAME sfun_backlash_invs2
/*<<<<<<<<<<<<<<<<<<<<<<<<<<<<<<<<<<<<<<<<<<<<<<<<<<<<<<<<<<<<<<<<*/
/* %%%-SFUNWIZ_defines_Changes_BEGIN --- EDIT HERE TO _END */
#define NUM_INPUTS          4
/* Input Port  0 */
#define IN_PORT_0_NAME      ud
#define INPUT_0_WIDTH       1
#define INPUT_DIMS_0_COL    1
#define INPUT_0_DTYPE       real_T
#define INPUT_0_COMPLEX     COMPLEX_NO
#define IN_0_FRAME_BASED    FRAME_NO
#define IN_0_BUS_BASED      0
#define IN_0_BUS_NAME
#define IN_0_DIMS           1-D
#define INPUT_0_FEEDTHROUGH 1
#define IN_0_ISSIGNED        0
#define IN_0_WORDLENGTH      8
```

```
#define IN_0_FIXPOINTSCALING 1
#define IN_0_FRACTIONLENGTH  9
#define IN_0_BIAS            0
#define IN_0_SLOPE           0.125
/* Input Port  1 */
#define IN_PORT_1_NAME      Qest
#define INPUT_1_WIDTH       3
#define INPUT_DIMS_1_COL    1
#define INPUT_1_DTYPE       real_T
#define INPUT_1_COMPLEX     COMPLEX_NO
#define IN_1_FRAME_BASED    FRAME_NO
#define IN_1_BUS_BASED      0
#define IN_1_BUS_NAME
#define IN_1_DIMS           1-D
#define INPUT_1_FEEDTHROUGH 1
#define IN_1_ISSIGNED        0
#define IN_1_WORDLENGTH      8
#define IN_1_FIXPOINTSCALING 1
#define IN_1_FRACTIONLENGTH  9
#define IN_1_BIAS            0
#define IN_1_SLOPE           0.125
/* Input Port  2 */
#define IN_PORT_2_NAME      ud_old
#define INPUT_2_WIDTH       1
#define INPUT_DIMS_2_COL    1
#define INPUT_2_DTYPE       real_T
#define INPUT_2_COMPLEX     COMPLEX_NO
#define IN_2_FRAME_BASED    FRAME_NO
#define IN_2_BUS_BASED      0
#define IN_2_BUS_NAME
#define IN_2_DIMS           1-D
#define INPUT_2_FEEDTHROUGH 1
#define IN_2_ISSIGNED        0
#define IN_2_WORDLENGTH      8
#define IN_2_FIXPOINTSCALING 1
#define IN_2_FRACTIONLENGTH  9
#define IN_2_BIAS            0
#define IN_2_SLOPE           0.125
/* Input Port  3 */
#define IN_PORT_3_NAME      vd_old
#define INPUT_3_WIDTH       1
#define INPUT_DIMS_3_COL    1
#define INPUT_3_DTYPE       real_T
#define INPUT_3_COMPLEX     COMPLEX_NO
#define IN_3_FRAME_BASED    FRAME_NO
#define IN_3_BUS_BASED      0
#define IN_3_BUS_NAME
#define IN_3_DIMS           1-D
#define INPUT_3_FEEDTHROUGH 1
#define IN_3_ISSIGNED        0
#define IN_3_WORDLENGTH      8
#define IN_3_FIXPOINTSCALING 1
#define IN_3_FRACTIONLENGTH  9
#define IN_3_BIAS            0
#define IN_3_SLOPE           0.125

#define NUM_OUTPUTS          3
/* Output Port  0 */
#define OUT_PORT_0_NAME      v
#define OUTPUT_0_WIDTH       1
#define OUTPUT_DIMS_0_COL    1
```

```
#define OUTPUT_0_DTYPE         real_T
#define OUTPUT_0_COMPLEX       COMPLEX_NO
#define OUT_0_FRAME_BASED      FRAME_NO
#define OUT_0_BUS_BASED        0
#define OUT_0_BUS_NAME
#define OUT_0_DIMS             1-D
#define OUT_0_ISSIGNED          1
#define OUT_0_WORDLENGTH        8
#define OUT_0_FIXPOINTSCALING 1
#define OUT_0_FRACTIONLENGTH   3
#define OUT_0_BIAS              0
#define OUT_0_SLOPE             0.125
/* Output Port  1 */
#define OUT_PORT_1_NAME        Q
#define OUTPUT_1_WIDTH         3
#define OUTPUT_DIMS_1_COL      1
#define OUTPUT_1_DTYPE         real_T
#define OUTPUT_1_COMPLEX       COMPLEX_NO
#define OUT_1_FRAME_BASED      FRAME_NO
#define OUT_1_BUS_BASED        0
#define OUT_1_BUS_NAME
#define OUT_1_DIMS             1-D
#define OUT_1_ISSIGNED          1
#define OUT_1_WORDLENGTH        8
#define OUT_1_FIXPOINTSCALING 1
#define OUT_1_FRACTIONLENGTH   3
#define OUT_1_BIAS              0
#define OUT_1_SLOPE             0.125
/* Output Port  2 */
#define OUT_PORT_2_NAME        w
#define OUTPUT_2_WIDTH         3
#define OUTPUT_DIMS_2_COL      1
#define OUTPUT_2_DTYPE         real_T
#define OUTPUT_2_COMPLEX       COMPLEX_NO
#define OUT_2_FRAME_BASED      FRAME_NO
#define OUT_2_BUS_BASED        0
#define OUT_2_BUS_NAME
#define OUT_2_DIMS             2-D
#define OUT_2_ISSIGNED          1
#define OUT_2_WORDLENGTH        8
#define OUT_2_FIXPOINTSCALING 1
#define OUT_2_FRACTIONLENGTH   3
#define OUT_2_BIAS              0
#define OUT_2_SLOPE             0.125

#define NPARAMS                0

#define SAMPLE_TIME_0          INHERITED_SAMPLE_TIME
#define NUM_DISC_STATES        0
#define DISC_STATES_IC         [0]
#define NUM_CONT_STATES        0
#define CONT_STATES_IC         [0]

#define SFUNWIZ_GENERATE_TLC 1
#define SOURCEFILES "__SFB__"
#define PANELINDEX             6
#define USE_SIMSTRUCT          0
#define SHOW_COMPILE_STEPS     0
#define CREATE_DEBUG_MEXFILE 0
#define SAVE_CODE_ONLY         0
#define SFUNWIZ_REVISION       3.0
```

```
/* %%%-SFUNWIZ_defines_Changes_END --- EDIT HERE TO _BEGIN */
/*<<<<<<<<<<<<<<<<<<<<<<<<<<<<<<<<<<<<<<<<<<<<<<<<<<<<<<<<<<<<<<<<<<<<*/
#include "simstruc.h"

extern void sfun_backlash_invs1_Outputs_wrapper(const real_T *ud,
            const real_T *Qest,
            const real_T *ud_old,
            const real_T *vd_old,
            real_T *v,
            real_T *Q,
            real_T *w);

/*====================*
 * S-function methods *
 *====================*/
/* Function: mdlInitializeSizes
===============================================
 * Abstract:
 *   Setup sizes of the various vectors.
 */
static void mdlInitializeSizes(SimStruct *S)
{
    DECL_AND_INIT_DIMSINFO(inputDimsInfo);
    DECL_AND_INIT_DIMSINFO(outputDimsInfo);
    ssSetNumSFcnParams(S, NPARAMS);
     if (ssGetNumSFcnParams(S) != ssGetSFcnParamsCount(S)) {
     return; /* Parameter mismatch will be reported by Simulink */
     }

    ssSetNumContStates(S, NUM_CONT_STATES);
    ssSetNumDiscStates(S, NUM_DISC_STATES);


    if (!ssSetNumInputPorts(S, NUM_INPUTS)) return;
    /*Input Port 0 */
    ssSetInputPortWidth(S,  0, INPUT_0_WIDTH); /* */
    ssSetInputPortDataType(S, 0, SS_DOUBLE);
    ssSetInputPortComplexSignal(S,  0, INPUT_0_COMPLEX);
    ssSetInputPortDirectFeedThrough(S, 0, INPUT_0_FEEDTHROUGH);
    ssSetInputPortRequiredContiguous(S, 0, 1); /*direct input signal
access*/

    /*Input Port 1 */
    ssSetInputPortWidth(S,  1, INPUT_1_WIDTH); /* */
    ssSetInputPortDataType(S, 1, SS_DOUBLE);
    ssSetInputPortComplexSignal(S,  1, INPUT_1_COMPLEX);
    ssSetInputPortDirectFeedThrough(S, 1, INPUT_1_FEEDTHROUGH);
    ssSetInputPortRequiredContiguous(S, 1, 1); /*direct input signal
access*/

    /*Input Port 2 */
    ssSetInputPortWidth(S,  2, INPUT_2_WIDTH); /* */
    ssSetInputPortDataType(S, 2, SS_DOUBLE);
    ssSetInputPortComplexSignal(S,  2, INPUT_2_COMPLEX);
    ssSetInputPortDirectFeedThrough(S, 2, INPUT_2_FEEDTHROUGH);
    ssSetInputPortRequiredContiguous(S, 2, 1); /*direct input signal
access*/

    /*Input Port 3 */
    ssSetInputPortWidth(S,  3, INPUT_3_WIDTH); /* */
```

```
    ssSetInputPortDataType(S, 3, SS_DOUBLE);
    ssSetInputPortComplexSignal(S,  3, INPUT_3_COMPLEX);
    ssSetInputPortDirectFeedThrough(S, 3, INPUT_3_FEEDTHROUGH);
    ssSetInputPortRequiredContiguous(S, 3, 1); /*direct input signal
access*/


    if (!ssSetNumOutputPorts(S, NUM_OUTPUTS)) return;
    /* Output Port 0 */
    ssSetOutputPortWidth(S, 0, OUTPUT_0_WIDTH);
    ssSetOutputPortDataType(S, 0, SS_DOUBLE);
    ssSetOutputPortComplexSignal(S, 0, OUTPUT_0_COMPLEX);
    /* Output Port 1 */
    ssSetOutputPortWidth(S, 1, OUTPUT_1_WIDTH);
    ssSetOutputPortDataType(S, 1, SS_DOUBLE);
    ssSetOutputPortComplexSignal(S, 1, OUTPUT_1_COMPLEX);
    /* Output Port 2 */
    ssSetOutputPortWidth(S, 2, OUTPUT_2_WIDTH);
    ssSetOutputPortDataType(S, 2, SS_DOUBLE);
    ssSetOutputPortComplexSignal(S, 2, OUTPUT_2_COMPLEX);

    ssSetNumSampleTimes(S, 1);
    ssSetNumRWork(S, 0);
    ssSetNumIWork(S, 0);
    ssSetNumPWork(S, 0);
    ssSetNumModes(S, 0);
    ssSetNumNonsampledZCs(S, 0);

    //ssSetSimulinkVersionGeneratedIn(S, "8.7");

    /* Take care when specifying exception free code - see
sfuntmpl_doc.c */
    ssSetOptions(S, (SS_OPTION_EXCEPTION_FREE_CODE |
                     SS_OPTION_USE_TLC_WITH_ACCELERATOR |
             SS_OPTION_WORKS_WITH_CODE_REUSE));
}

# define MDL_SET_INPUT_PORT_FRAME_DATA
static void mdlSetInputPortFrameData(SimStruct  *S,
                                     int_T      port,
                                     Frame_T    frameData)
{
    ssSetInputPortFrameData(S, port, frameData);
}
/* Function: mdlInitializeSampleTimes
=========================================
 * Abstract:
 *    Specifiy  the sample time.
 */
static void mdlInitializeSampleTimes(SimStruct *S)
{
    ssSetSampleTime(S, 0, SAMPLE_TIME_0);
    ssSetModelReferenceSampleTimeDefaultInheritance(S);
    ssSetOffsetTime(S, 0, 0.0);
}

#define MDL_SET_INPUT_PORT_DATA_TYPE
static void mdlSetInputPortDataType(SimStruct *S, int port, DTypeId
dType)
{
```

```
    ssSetInputPortDataType( S, 0, dType);
}
#define MDL_SET_OUTPUT_PORT_DATA_TYPE
static void mdlSetOutputPortDataType(SimStruct *S, int port, DTypeId
dType)
{
    ssSetOutputPortDataType(S, 0, dType);
}

#define MDL_SET_DEFAULT_PORT_DATA_TYPES
static void mdlSetDefaultPortDataTypes(SimStruct *S)
{
  ssSetInputPortDataType( S, 0, SS_DOUBLE);
 ssSetOutputPortDataType(S, 0, SS_DOUBLE);
}
/* Function: mdlOutputs
=======================================================
 *
*/
static void mdlOutputs(SimStruct *S, int_T tid)
{
    const real_T   *ud  = (const real_T*) ssGetInputPortSignal(S,0);
    const real_T   *Qest  = (const real_T*) ssGetInputPortSignal(S,1);
    const real_T   *ud_old  = (const real_T*) ssGetInputPortSig-
nal(S,2);
    const real_T   *vd_old  = (const real_T*) ssGetInputPortSig-
nal(S,3);
    real_T        *v  = (real_T *)ssGetOutputPortRealSignal(S,0);
    real_T        *Q  = (real_T *)ssGetOutputPortRealSignal(S,1);
    real_T        *w  = (real_T *)ssGetOutputPortRealSignal(S,2);

    real_T cr = 0;
    real_T cl = 0;
    real_T vd = 0;
    real_T Xr = 0;
    real_T Xl = 0;

    // Calculate break points cr and cl
    if( Qest[1] == 0 ) {
        cr = 0;
        cl = 0;
    } else {
        cr = Qest[0]/Qest[1];
        cl = Qest[2]/Qest[1];
    }
    // Backlash inverse. Calculate compensated control signal vd
    if( ud[0] > ud_old[0] ) {
        if( Q[1] == 0 ) {
            vd = 0;
        } else {
            vd = (ud[0] + Qest[0])/Qest[1];
        }
    } else if( ud[0] < ud_old[0] ) {
        if( Q[1] == 0 ) {
            vd = 0;
        } else {
            vd = (ud[0] + Qest[2])/Qest[1];
        }
    } else {
        vd = vd_old[0];
    }
```

```
    // Backlash inverse regressor
    if( vd == (ud[0] + Qest[0])/Qest[1] ){
        Xr = 1;
    } else {
        Xr = 0;
    }
    if( vd == (ud[0] + Qest[2])/Qest[1] ) {
        Xl = 1;
    } else {
        Xl = 0;
    }
    // Update regressor
    w[0] = Xr;
    w[1] = -vd;
    w[2] = Xl;

    // Update backlash inverse parameters
    Q[0] = Qest[0];
    Q[1] = Qest[1];
    Q[2] = Qest[2];

    // Update compensated control signal
    v[0] = vd;

    //sfun_baclash_inverse_Outputs_wrapper(ud, Qest, ud_old, vd_old,
v, Q, w);

}



/* Function: mdlTerminate
=====================================================
 * Abstract:
 *    In this function, you should perform any actions that are neces-
sary
 *    at the termination of a simulation.  For example, if memory was
 *    allocated in mdlStart, this is the place to free it.
 */
static void mdlTerminate(SimStruct *S)
{

}

#ifdef  MATLAB_MEX_FILE    /* Is this file being compiled as a MEX-
file? */
#include "simulink.c"      /* MEX-file interface mechanism */
#else
#include "cg_sfun.h"       /* Code generation registration function */
#endif
```